KfK 4164
November 1986

Comparative Calculations and Validation Studies with Atmospheric Dispersion Models

J. Päsler-Sauer
Institut für Neutronenphysik und Reaktortechnik
Projekt Nukleare Sicherheit

Kernforschungszentrum Karlsruhe

KERNFORSCHUNGSZENTRUM KARLSRUHE
Institut für Neutronenphysik und Reaktortechnik
Projekt Nukleare Sicherheit

KfK 4164

Comparative Calculations and Validation Studies with Atmospheric Dispersion Models

J. Päsler-Sauer

Kernforschungszentrum Karlsruhe GmbH, Karlsruhe

Die diesem Bericht zugrunde liegenden Arbeiten wurden vom Bundesminister des Innern gefördert. Der Bundesminister des Innern übernimmt keine Gewähr für die Richtigkeit, die Genauigkeit, Vollständigkeit der Angaben, sowie für die Beachtung privater Rechte Dritter.

Kernforschungszentrum Karlsruhe GmbH
Postfach 3640, 7500 Karlsruhe 1

ISSN 0303-4003

Abstract

This report presents the results of an intercomparison of different mesoscale dispersion models and measured data of tracer experiments. The types of models taking part in the intercomparison are Gaussian-type, numerical Eulerian, and Lagrangian dispersion models. They are suited for the calculation of the atmospherical transport of radionuclides released from a nuclear installation.

For the model intercomparison artificial meteorological situations were defined and corresponding arithmetical problems were formulated.

For the purpose of model validation real dispersion situations of tracer experiments were used as input data for model calculations; in these cases calculated and measured time-integrated concentrations close to the ground are compared. Finally a valuation of the models concerning their efficiency in solving the problems is carried out by the aid of objective methods.

Vergleichsrechnungen und Validierungsuntersuchungen mit atmosphärischen Ausbreitungsmodellen

Kurzfassung

In diesem Bericht werden die Ergebnisse vorgestellt, die aus einem Vergleich verschiedener mesoskaliger Ausbreitungs-Rechenmodelle untereinander und mit experimentellen Meßergebnissen hervorgehen. Bei den Modellen handelt es sich um Gauß-artige, numerische Euler- und Lagrange-Dispersionsmodelle, die für die Berechnung des atmosphärischen Radionuklidtransports nach Freisetzungen aus kerntechnischen Anlagen geeignet sind. Zum Vergleich der Modelle wurden einerseits künstliche meteorologische Situationen definiert und als Rechenaufgaben formuliert; andererseits wurden zum Zweck der Modellvalidierung echte Ausbreitungssituationen von Tracerexperimenten als Aufgaben gestellt. In diesen Fällen waren die berechneten und die gemessenen bodennahen Konzentrationen zu vergleichen. Abschließend erfolgt eine Bewertung der Modelle nach ihrer Leistungsfähigkeit mit Hilfe objektiver Methoden.

Table of Contents

1. Introduction

This report presents findings of the research project St.Sch.909 sponsored by the Federal Minister of the Interior,

"Release and Dispersion Characteristics of Radioactive Pollutants: Consequences for the Optimisation of Measures for the Protection of the Public in Case of Nuclear Accidents".

The investigations and results reported here refer to the sub-project "Application of Mathematical Models in Determining Atmospheric Dispersion, Deposition, and Damaging Effects of Released Radionuclides", with particular regard to the "Detection of Uncertainties and Errors in the Gaussian Dispersion Model and Decisions Concerning the value of Complex Numerical Dispersion Models in Different Atmospheric Conditions".

A comparative evaluation of several dispersion models followed by a comparison between dispersion models and tracer dispersion experiments (comparative calculations and validation studies) was assumed to be the best way to tackle the problem. This meant that mathematical problems had to be defined for typical atmospheric dispersion conditions and interested partners had to be found for the comparative calculations.

Karlsruhe Nuclear Research Center (KfK) therefore asked a number of users and authors of dispersion models both in West Germany and abroad to participate in the comparative evaluation of dispersion models. The preliminary discussions took place in Winter 1983/84.

The first meeting of interested parties was held in Karlsruhe on 12 April 1984. Details of the problems and modes of procedure were discussed. Table 1 presents the participants, institutions, and models.

PARTICIPANT	INSTITUTION	TYPE OF MODEL	NAME
Dunst	Hamburg Univ. (FRG)	Huang plume model	-
Dunst	Hamburg Univ. (FRG)	Eulerian grid model	-
Gassmann	EIR (Switzerland)	semi-Gaussian strata model	FOG
Jones	NRPB (U.K.)	Gaussian plume model	ADMARC
Mikkelsen Thykier-N.	Risø (Denmark)	Gaussian puff model	RIMPUFF
Möllmann	KFA-Jülich (FRG)	Gaussian volume-source model	MUSEMET
Päsler-S.	KfK (FRG)	Gaussian plume model	DOSI
Schnatz, Rohbock	Battelle-Inst. (FRG)	Eulerian grid model	TRANSLOC
Schorling	IABG (FRG)	Lagrangian random walk model	-
Ulrich*	Munich Univ. (FRG)	Eulerian grid model	-

Tab.1

*) (Mr. Ulrich attended the first two AVVA meetings and prepared his model for the calculations. Unfortunately, timing and manpower problems made it impossible for him to carry out the calculations.)

The following advisory meteorologists took part in the meetings of the AVVA working group: Mrs. Nitsche (Deutscher Wetterdienst),
Mr.S.Vogt (KfK),
Mr.K.Nester (KfK).

The next meeting of the AVVA ("Arbeitskreis Vergleichsrechnungen und Validierungsuntersuchungen mit atmosphärischen Ausbreitungsmodellen") was held on 12 July 1984; first results of the comparative calculations were discussed, and new calculation problems were prepared for the validation studies.

Evaluation of the submitted data tapes was continued at KfK through 1984. Due to some errors and misunderstandings, recalculation by the users was necessary in some instances. This, together with timing problems of some participants, caused a considerable delay. The third meeting, scheduled for November 1984, at which the results were to be discussed, had to be adjourned until 27/28 February 1985, since only a fraction of the results was available at the first date. The final evaluation could not take place until after the third meeting in February 1985 at which also the methods of evaluation were agreed upon. Graphical and numerical evaluations were finished in November 1985.

The author should like to thank Dr.H.J.Panitz for his help in the initial processing of the submitted data (coordinate transformations and plots) and in the processing of the data calculated by the Lagrangian model.

2. Objectives of the comparative calculations and validation studies

The comparative calculations are intended to reveal the characteristic features of the various dispersion models.

This task requires relatively simple mathematical problems allowing, e.g., typical divergences between the results of complex numerical models and Gaussian-type models to become obvious. It also requires unambiguously defined variables and parameters that describe the source term and the meteorological and topographic features of the dispersion situation. For example, atmospheric stability was defined not only by the stability classes but also by the wind profile and the vertical temperature gradient and the Monin-Obukhov length (see annex).

The problems of Batch 1 describe various situations of linear, steady dispersion. Emission heights, wind velocities, the stability of atmospheric stratification, the surface roughness length, and the wind profile exponent determined by the roughness length are given. What is to be defined is the field of time-integrated activity concentration at ground level below the emitted plume. Specific features of the various models can be determined by systematic variation of input values, and the general uncertainty in the modelling of simple atmospheric dispersion situations can be assessed.

More complex dispersion situations (shear of wind direction and inversion situations) are described by the Batch II problems. These problems are to determine the efficiencies of numerical dispersion models as compared with the Gaussian plume model.

The validation problems are the central element in the comparison between realistic dispersion experiments and computer models, although the comparison between the surface concentrations measured in a specific experiment and the theoretical results of a model cannot be the sole criterion of validation. The reproducibility of atmospheric dispersion experiments is limited, owing to the statistical character of the turbulent fluctuations and to the fact that not all boundary conditions can be fixed experimentally; in consequence, series of experiments made in one site can only be similar and never completely identical. The researcher must therefore take into account not only the turbulence related scatter but also a certain scatter depending on the experimental parameters and on the quantity and quality of the measuring instruments.

Limited time and manpower made it impossible to carry out and evaluate more than four dispersion experiments of different laboratories (KFA, KfK, Cabauw, Risø). In spite of this, attempts were made to determine the typical experimental scatter. This was possible with experiments which were similar to others of the same measuring campaign with regard to the prevailing meteorological conditions. The experimental scatter could then be determined by comparing the measured concentration distributions.

Originally, the validation studies were to include not only dispersion on flat terrain but also dispersion on terrains with a more complex topography, conditions of gentle breeze, releases at ground level,and unsteady dispersion. In view of the problems mentioned above, this was impossible altough it would surely have been profitable to have these problems treated by the experienced group of experts.

3. Modelling of atmospheric dispersion processes

This section gives a brief outline of the dispersion models used in the comparative study and their way of modelling atmospheric transport by wind currents (advection) and turbulent diffusion.

In principle, atmospheric dispersion of airborne substances (aerosols, gases) can be described by the continuity equation

$$\frac{\partial \varrho}{\partial t} + \vec{\nabla} \cdot \vec{j} = 0 \qquad \text{(Equation 1)}$$

In this equation, ϱ is the density of the airborne material and $\vec{j}$ the current density which comprises an advection component and a diffusion component:

$$\vec{j} = \vec{j}_A + \vec{j}_D \qquad \text{(Equation 2a)}$$

$$= \varrho \cdot \vec{v} - \mathbb{K} \cdot \vec{\nabla} \varrho \qquad \text{(Equation 2b)}$$

$\vec{v}$ is the wind velocity vector, $\mathbb{K}$ the second-stage diffusion tensor which is diagonal if the atmospheric turbulence is described by independent vertical, transversal, and longitudinal components. Equation 1 and Equation 2b yield the diffusion/advection equation

$$\frac{\partial \varrho}{\partial t} + \vec{\nabla}(\varrho \cdot \vec{v}) - \vec{\nabla}(\mathbb{K} \cdot \vec{\nabla} \varrho) = 0 \qquad \text{(Equation 3)}$$

There are several analytical solutions for specific forms and approximations of this equation, as well as a multitude of numerical solutions. For example, for stationary conditions $\left(\frac{\partial \varrho}{\partial t} = 0\right)$ and a constant wind vector field $\vec{v} = (\bar{u},0,0)$, diffusion independent of height and location, and negligible longitudinal diffusion ($K_x=0$) we obtain the equation

$$\bar{u} \cdot \frac{\partial \varrho}{\partial x} = K_y \cdot \frac{\partial^2 \varrho}{\partial y^2} + K_z \cdot \frac{\partial^2 \varrho}{\partial z^2} \qquad \text{(Equation 4)}$$

with the analytical solution

$$\varrho(\vec{x}) = \frac{\dot{Q}}{4\pi x \sqrt{K_y K_z}} \exp\left[-\frac{\bar{u}}{4x}\left(\frac{y^2}{K_y} - \frac{(z-h_s)^2}{K_z}\right)\right] \qquad \text{(Equation 5)}$$

The result corresponds to the density distribution on the leeside of a point source with a continuous emission Q at a height h_s for dispersion in x direction.

The so-called Gaussian model is quite similar, except that empirically determined σ parameters from the statistical theory of turbulence are used instead of the diffusion constant K:

$$\varrho(\vec{x}) = \frac{\dot{Q}}{2\pi \bar{u} \sigma_y(x) \sigma_z(x)} \exp\left[-\left(\frac{y^2}{2\sigma_y^2} - \frac{(z-h_s)^2}{2\sigma_z^2}\right)\right] \qquad \text{(Equation 6)}$$

The Gaussian volume source model and Gaussian puff model are based on similar solutions.

Finite difference solutions of the DA equation (Equation 3) are calculated using Eulerian grid models. These can take account of time-dependent wind fields and realistic vertical profiles of the wind velocity $\vec{v}(z)$ and the diffusion $K_z(z)$.

In contrast, Lagrangian models of atmospheric dispersion processes do not apply analytical or numerical integration of the diffusion/advection equation but track the trajectories of many individual emitted particles in consideration of the statistical

scatter of wind velocity (Random Walk Method). For this purpose, the model of the Brownian motion is used. The equation of motion of one particle (Langevin equation) is:

$$\frac{d\vec{v}}{dt} = \vec{a}(t) - c \cdot \vec{v}$$

$\vec{a}$ is the random acceleration of the particle while $-c.\vec{v}$ is a friction term.

4. Short descriptions of the models

4.1. Gaussian model DOSI (KfK)

This is a stationary Gaussian plume model assuming reflection from the ground and the inversion layer; the concentration at ground level is described by

$$\chi(x,y,0) = \frac{\dot{Q}}{\pi \bar{u} \sigma_y(x) \sigma_z(x)} \cdot e^{-\frac{y^2}{2\sigma_y^2}} \cdot e^{-\frac{h_s^2}{2\sigma_z^2}} \cdot f_{refl}(h_s, h_{mix}, \sigma_z) \qquad \text{(Equation 7)}$$

The wind vector is constant in time and space:

$$\vec{v} = (\bar{u},0,0) \;, \qquad \bar{u} = \frac{1}{\Delta h} \int_{h_s-\sigma_z}^{h_s+\sigma_z} u(z)\,dz \qquad \text{(Equation 8)}$$

$\bar{u}$ is the wind velocity averaged over height and time of dispersion.

Diffusion is described by σ parameters $\sigma_y(x)$ and $\sigma_z(x)$ which describe the standard deviations of the concentration distribution within the plume and are determined by the stability class (which characterizes the stability of stratification).

Two different sets of $\sigma_{y,z}$ parameters were used in the DOSI model calculations: First, the height-dependent "Karlsruhe-Jülich" parameters for a roughness length $z_o \geq 1m$ /Ge 81, Th 81/; secondly, a set of parameters for a smaller z_o value: $\langle\sigma\rangle$.

4.2. Gaussian model ADMARC (NRPB)

ADMARC is identical with DOSI in most respects, except that $\bar{u}=u_{10}$ (wind velocity at height 10 m) is used as transport velocity. Roughness-dependent σ parameters according to Smith and Hosker /Cl 79/ are used.

4.3. Huang model (Meteorological Institute, Hamburg University)

Like the Gaussian model, this model applies an analytical solution of the steady-state DA equation. Specific, stability-dependent power equations are assumed for the height dependence of the wind velocity u(z) and the diffusion $K_z(z)$:

$$u(z) = u_{10} \cdot \left(\frac{z}{10m}\right)^p$$

$$K_z(z) = K_z(h_s) \cdot \left(\frac{z}{h_s}\right)^n$$

In these equations, p is the wind profile exponent determined by stability and roughness; $K_z(h_s)$, too, is calculated as a function of stability on the basis of similarity theory according to Dyer /Dy 74/. The concentration at ground level is described by

$$\varrho(x,y) = \frac{Q \cdot A}{\sqrt{2\pi}\ \sigma_y(x)\ x^\beta} \cdot \exp\left(-\frac{y^2}{2\sigma_y^2}\right) \cdot \exp\left(-\frac{h_s}{B}\right)$$

where A and B are functions of u_{10}, h_s, $K_z(h_s)$, p, n, and x /Hi 84/.

Horizontal diffusion is modelled by suitable σ_y parameters.

The power equations for u(z) and especially for $K_z(z)$ apply only within the Prandtl layer. In cases of stable stratification, the Huang model can only be applied with release heights relatively close to the ground.

4.4. Gaussian strata model FOG (EIR)

This model was originally developed for cooling tower plumes, but it can be used as a dispersion model for dry, non-thermal releases.

The strata structure of this model permits calculations of vertical profiles of wind velocity and diffusion.

Vertical diffusion is simulated by a convolution integral with a strata-dependent Gaussian kernel; horizontal diffusion is calculated using σ_y parameters /Ga 81/. The model can be classified as a stationary Gaussian model with height-dependent wind velocity and diffusion.

4.5. Gaussian volume source model MUSEMET (KFA Jülich)

This model calculates concentrations by assuming, in subsequent moments, the volume elements of the preceding concentration distribution as point sources for superposition of the following distribution. From this concept, a Gaussian model is derived which takes account of changes in wind directions and diffusion categories within a pre-selectable clock rate /St 81/.

The transport velocity $\bar{u}$ is the wind velocity at source height h_s. Diffusion is described by suitable parameters, e.g. the Karlsruhe-Jülich σ parameters with $\sigma_x=\sigma_y$, or by σ parameters determined by calculation from measured $\sigma_{\theta,\phi}$ -data.

4.6. Gaussian puff model RIMPUFF (Risø)

In puff models, the dispersion of time-dependent atmospheric releases is described by a series of discretely released puffs whose superposition pattern approximates the concentration distribution of a continuous plume /Mi 84/.

Each puff represents an ellipsoidal spatial concentration distribution which corresponds to the 3-fold Gaussian solution of a momentaneous point emission:

$$\varrho_p(\vec{x},t) = \frac{Q}{(2\pi)^{3/2}\sigma_x(t)\,\sigma_y(t)\,\sigma_z(t)} \exp\left[-\frac{1}{2}\cdot\left(\left(\frac{x-ut}{\sigma_x}\right)^2 - \left(\frac{y-vt}{\sigma_y}\right)^2 - \left(\frac{z-h_s}{\sigma_z}\right)^2\right)\right]$$

where $\vec{v} = (u,v,0)$ is the wind vector at source height h_s. Each puff is tracked along its individual trajectory, which permits dispersion calculations taking into account time and space-dependent meteorological conditions (e.g. wind fields).

The radial growth of puffs during dispersion as a result of "internal turbulence" is described by σ parameters for short sampling times, e.g. by the Pasquill σ parameters /Gi 76/. The total width of a plume is derived from the contribution of the low-frequency fluctuations of the wind direction σ_θ and the puff width

$$\sigma^2_{y\,\text{plume}} = \sigma^2_y(\sigma_\theta) - \sigma^2_{y\,\text{puff}}$$

If σ_θ -data are not available, the puffs can be assumed to disperse with widths corresponding to a $\sigma_{y\,\text{plume}}$ along an averaged wind direction:

$$\sigma^2_{y\,\text{plume}} = \sigma^2_{y\,\text{puff}}$$

In this case, other suitable parameters, e.g. the Karlsruhe-Jülich σ parameters can be applied.

4.7. Eulerian grid models with numerical solutions of the DA equation; Dunst model (Met.Inst.Hamburg University) and TRANSLOC (Battelle Frankfurt)

a) Dunst model

This model calculates the turbulent diffusion coefficient K_z /Du 84/ on the basis of time-dependent vertical wind profiles for advection, together with potential temperature profiles, or the Richardson number Ri and the roughness length z_o:

$$K_z(z) = k \cdot u_* \cdot f(z, z_o, h_{mix}) \cdot \exp\left[-g(Ri; z, z_o, h_{mix})\right]$$

h_{mix} : height of mixing layer
u_* : friction velocity
f and g functions, see /Du 84/.

Horizontal diffusion is assumed to be $K_x = K_y = 3 \cdot K_{z,max}$.

b) TRANSLOC

This model relies on similar input data but uses a different K_z profile:

$$K_z(z) = \sqrt{\left(\frac{\partial u}{\partial z}\right)^2 + \left(\frac{\partial v}{\partial z}\right)^2 - \frac{g}{T}\frac{\partial \theta}{\partial z}} \cdot \left(\frac{kz}{1 + kz/\lambda}\right)^2$$

k v.Karman constant = 0.4
θ = potential temperature
λ = mixing length

Horizontal diffusion is described by $K_x = K_y = 2 \cdot K_{z,max}$.

For further information see /Ha 80/.

4.8. Lagrangian model (IABG)

The meteorological input data of the random-walk Lagrangian model are vertical profiles of the wind vector $\vec{v}(z)$ and velocity variances σ_u, σ_v, σ_w in the form of 10-min averages at different heights. In addition, data on atmospheric stability are required, e.g. the Monin-Obukhov length L or the Richardson number Ri(z), and the height of the mixing layer h_{mix}.

Using the wind vector $\vec{v}$ $(\vec{x},t)$ and velocity variances $\sigma_u, \sigma_v, \sigma_w$ in subsequent time steps, the emitted particles are assigned velocities $\vec{V}_i$ (i = particle index) derived from the mean local transport velocity and a random component $\vec{v}_i'$:

$$\vec{V}_i = \bar{\vec{v}}_i + \vec{v}_i'$$

The time steps should be chosen with a view to realistic modelling of the Lagrangian autocorrelation /Ha 82/. The fundamentals of Lagrangian Random Walk models have already been discussed above (p.7).

The model is suited calculating atmospheric dispersion processes with variable meteorological conditions and source terms; the averaging time should not be shorter than 10 min. To keep the statistical scatter at an acceptable level, a dispersion calculation up to a distance $x \leq 10$ km requires $\geq 10^4$ particles. This means a computing time of about 15 min on a Siemens 7890 computer.

Part I: Comparative Calculations

5. The calculation problems

5.1. Batch I: Comparative problems; simple dispersion situations suited for Gaussian models

Batch I comprises 24 one-hour dispersion processes with constant standard emission from a point source. Each problem is characterized by four parameters: Stability (stability class) st.cl. 10m wind velocity u_{10}, source or release height h_s, and roughness length z_o. The combinations of values for stability and 10m wind velocity are:

stab.class	u_{10}
unstable (B)	2 m/s
neutral (D)	2 u.8 m/s
stable (F)	2 m/s

Tab. 2: Combinations of stability classes and wind-velocities

These four situations, each with three different source heights h_s=10m, 100m, 200m, and two roughness lengths z_o=0.1m (rural, flat), 1.0m (urban or wooldland) are combined to make a total of 24 calculation problems.

As results, concentration fields at ground level and deposited concentration fields were to be obtained as well as vertical concentration profiles at a distance up to 20 km from the source using given polar or cartesian coordinate grids.

The original problems are presented in Annex 3.

5.2. Closer specification of the problems

a) Wind profile u(z):

The power equation

$$u(z) = u_{10}\left(\frac{z}{10m}\right)^{p(st.cl.,z_o)}$$

$$u(z \geq 200m) = u(200m) \qquad \text{Equation 9}$$

is applied. According to Irwin /Ir 79/, the wind profile exponent p is a function of the stability class and the roughness length z_o:

z_o / stab.cl.	0.1m	1.0m
B	0.08	0.17
D	0.15	0.27
F	0.50	0.60

Tab. 3: wind-profile exponent p(s.c.,z_o) Irwin /Ir 79/.

b) Temperature gradient

The height-averaged values of the potential temperature gradient $\overline{\partial\theta/\partial z}$ were determined for the different stability classes as follows:

(stab.cl. B; u_{10} = 2m/s):

z [m]	0 - 50	50 - 150	> 150
[°K/100m]	-0.5	0.0	+0.3

(stab.cl. F; u_{10} = 2m/s):

z [m]	0 -100	100 -300	> 300
[°K/100m]	+2.3	+1.0	+0.3

(stab.cl. D; u_{10} = 2m/s &. 8m/s):

$$= +0.3 \ [^{\circ}K/100m]$$

c) Equivalent formulation on the basis of the similarity theory approach

Similarity theory /Mo 58/ describes the wind and temperature profiles of the surface boundary layer (Prandtl layer). As shown in the annex, the profiles were described by the Monin-Obukhov length L, the friction velocity u_*, and the roughness length z_o. Table 4 presents the pairs of values for L and u_* for the Batch I problems:

stability cl. wind	z_o [m]	L[m]	u_* [m/s]
B	0.1	-20	0.22
u_{10} = 2[m/s]	1.0	-25	0.40
F	0.1	+20	0.10
u_{10} = 2[m/s]	1.0	+25	0.13
D	0.1	|L|> 500m	0.15
u_{10} = 2[m/s]	1.0	|L|>1000m	0.30
D	0.1	|L|> 500m	0.61
u_{10} = 8[m/s]	1.0	|L|>1000m	1.30

Tab. 4 : Calculated values of L und u_*

The wind profile can be described by integrating

$$\frac{\partial u}{\partial z} = \frac{u_*}{k \cdot z} \cdot \phi_M(z,L) \qquad \text{Equation 10}$$

as shown in the annex. With the above values for L, u_*, and z_o the result obtained for the surface boundary layer is quite similar to the power profile (Equation 9). At greater heights, e.g. $z \geq 100m$, only the power profile applies.

According to similarity theory, the profile of the potential temperature gradient is as follows:

$$\frac{\partial\theta}{\partial z} = \frac{T}{g} \cdot \frac{u_*^2}{k^2} \cdot \frac{\Phi_H(z,L)}{z \cdot L} \qquad \text{Equation 11}$$

L and u_* are chosen with a view to matching $\partial\theta/\partial z$ to the above height-averaged values $\overline{\partial\theta/\partial z}$. Details are given in the annex.

d) Stability definition using the Richardson number

According to the definition presented in the annex, the Richardson number

$$Ri = \frac{g}{T} \cdot \frac{\partial\theta/\partial z}{(\partial u/\partial z)^2} = \frac{z}{L} \cdot \frac{\Phi_H(z,L)}{\Phi_M^2(z,L)} \qquad \text{Equation 12}$$

is derived from the wind and temperature gradient profiles. The values of Ri for different stabilities and roughness levels of problems in Batch I are listed in Table 5:

stability cl. wind	z_0 [m]	z [m]	Ri
B	0.1	30	-1.5
		50	-2.5
	1.0	30	-1.2
u_{10} = 2 [m/s]		50	-2.0
F	0.1	30	+0.176
		50	+0.185
	1.0	30	+0.171
u_{10} = 2 [m/s]		50	+0.182
D	0.1	50	$\|Ri\| < 0.1$
u_{10} = 2 [m/s]	1.0	50	$\|Ri\| < 0.05$
D	0.1	50	$\|Ri\| < 0.1$
u_{10} = 8 [m/s]	1.0	50	$\|Ri\| < 0.05$

Tab. 5: Calculated values of the Richardson-number Ri.

5.3. Coordinate grid

It has been agreed that concentration at ground level and deposited concentrated fields were to be represented in fields of polar coordinates (r,θ). In special cases, a cartesian grid (x,y) could be used.

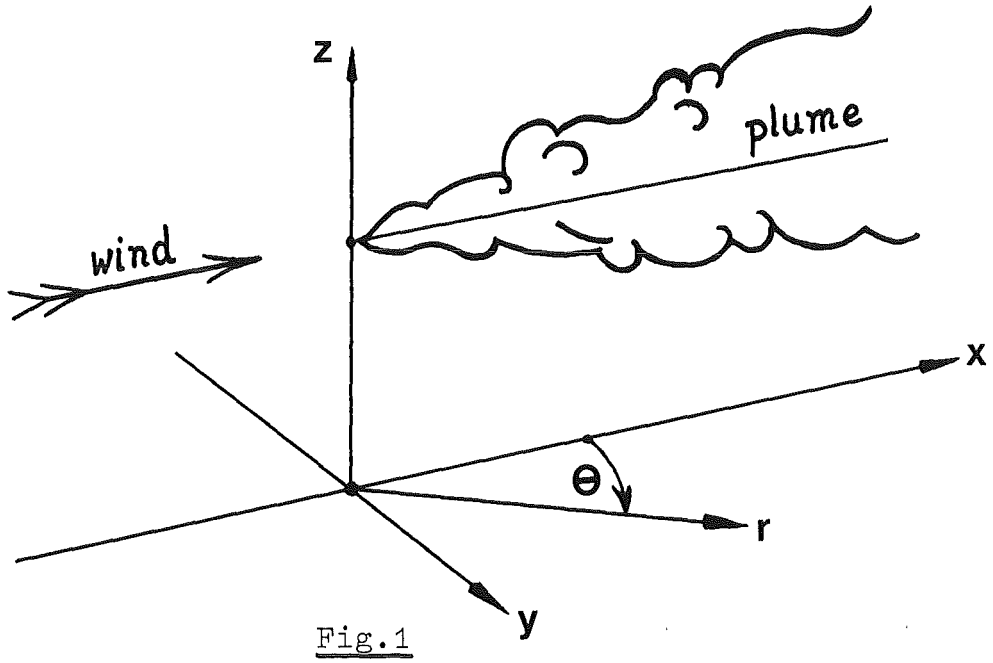

Fig.1

The angular coordinates θ_j could be chosen as required in steps of 2.5°, 5° and 10°; the fixed array of source distances r_i was

$r_i(i=1,..20) = \{200,400,800,1200,1600,2000,2400,3000,3600,4400,$
$5400, 6600, 8000,10000,12000,14000,16000,20000,$
$24000,30000\}$ m.

5.4. Data transfer to KfK

The participants were asked to write the results of their model calculations on magnetic tape according to an agreed schedule, to add their comments, and to mail the magnetic tape to Karlsruhe Nuclear Research Center.

6. Calculated results of the dispersion models for Batch I problems

6.1. Presentation of results

The results of the model calculations of Batch I are compared for the distance dependence of the time-integrated concentration at ground level (TIC) below the plume axis, and for the angular distributions of TICs at different distances from the source. Vertical concentration profiles were used as an additional control factor in the initial stage of data evaluation.

The TIC distributions of the different models are compared by graphical means; log (TIC) values are plotted against log r or Θ values.

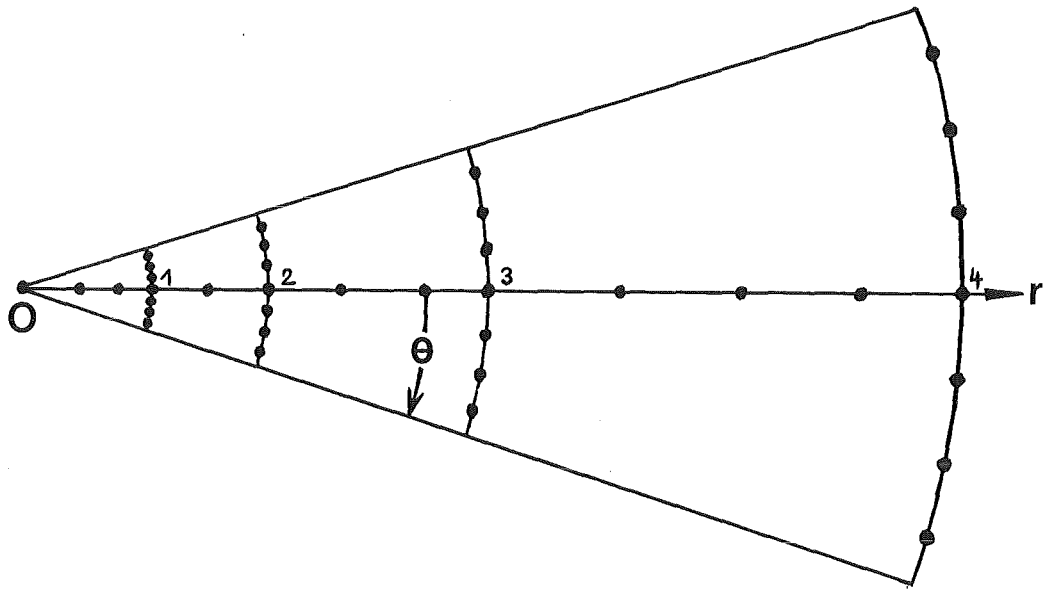

Fig.2: Points $P(r_i, \Theta_j)$ used for the representation of TIC below the plume axis $TIC(r_i, \Theta=0^{\circ})$ and the angular distribution of $TIC(r=const, \Theta_j)$; (arbitrary units).

For graphical evaluation of the TIC below the plume axis, only the roughness length z_o=1m and the wind velocity u_{10}=2m/s were considered. The release height h_s=10,100,200m and the stability st.cl.= B,D,F were varied. Of the angular distributions of the TIC, only h_s=100m was considered.

Some of the curves in the graphs are marked with a letter to identify the model or participant:

Du.....Eulerian grid model (Dunst,
H.....Huang model Univ.of Hamburg)
F.....FOG,(semi-Gaussian strata model,EIR)
Ad.....ADMARC,(Gaussian plume model,NRPB,U.K.)
R_K .....RIMPUFF,KJ-σ-par.,(Gaussian puff m.,Risø)
R_P ..... " ,Pasq.-par.,(" " " ")
M.....MUSEMET,(volume-source model,KFA-Jülich)
$D_{K\sigma}$.....DOSI,KJ-σ-par.,(Gaussian plume m.,KfK)
D<> ..... " , <σ>-par.,(" " " ")
T.....TRANSLOC,(Eulerian grid model,Battelle)
L.....Lagrangian random-walk model,(IABG)

6.2. Calculated angular distributions of TIC obtained by different models for Batch I problems

Figures 3-11 present the results of the model calculations in the following order: DOSI, MUSEMET, RIMPUFF, Huang model, Lagrangian model (Schorling), Eulerian model (Dunst), TRANSLOC, FOG.

Each figure indicates, for the three stability classes B,D, and F, the release height h_s=100m and the roughness length z_o=1m, up to four angular distributions of TIC at a distance of r=800m, 2000m, 8000m, 20000m from the source as shown in Fig.2.

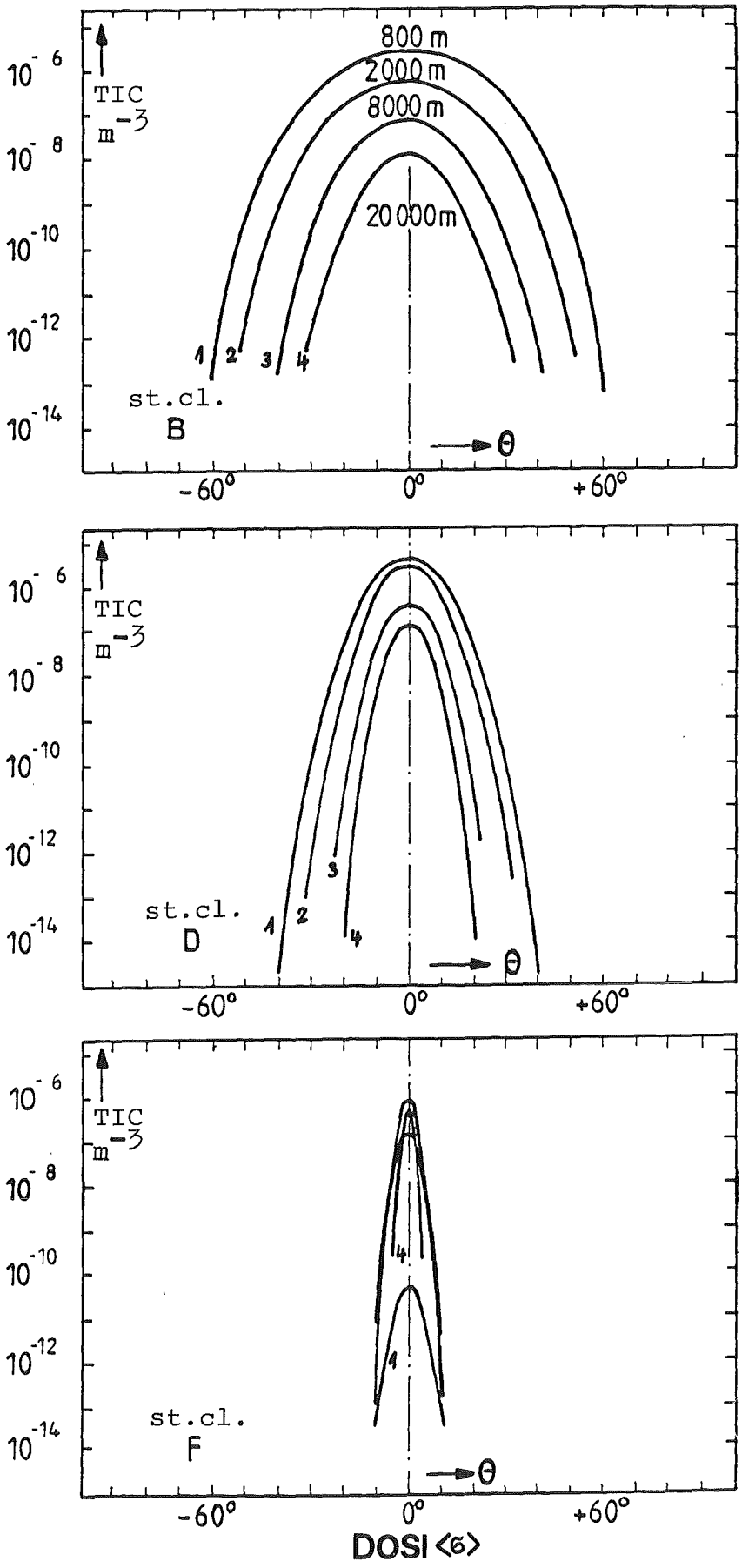

Fig.3a,b,c: Angular distributions of TIC, Batch I.

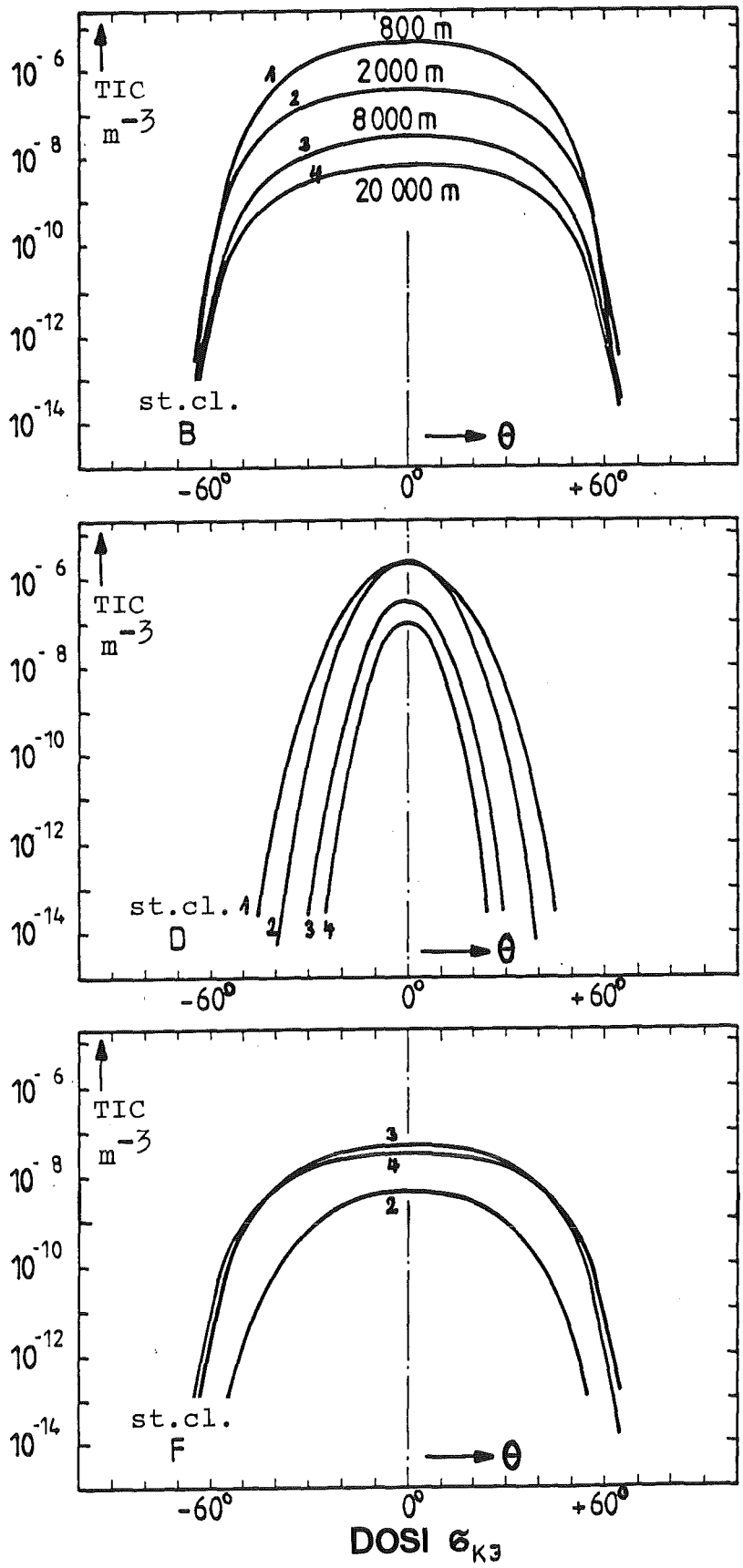

Fig.4a,b,c: Angular distributions of TIC, Batch I.

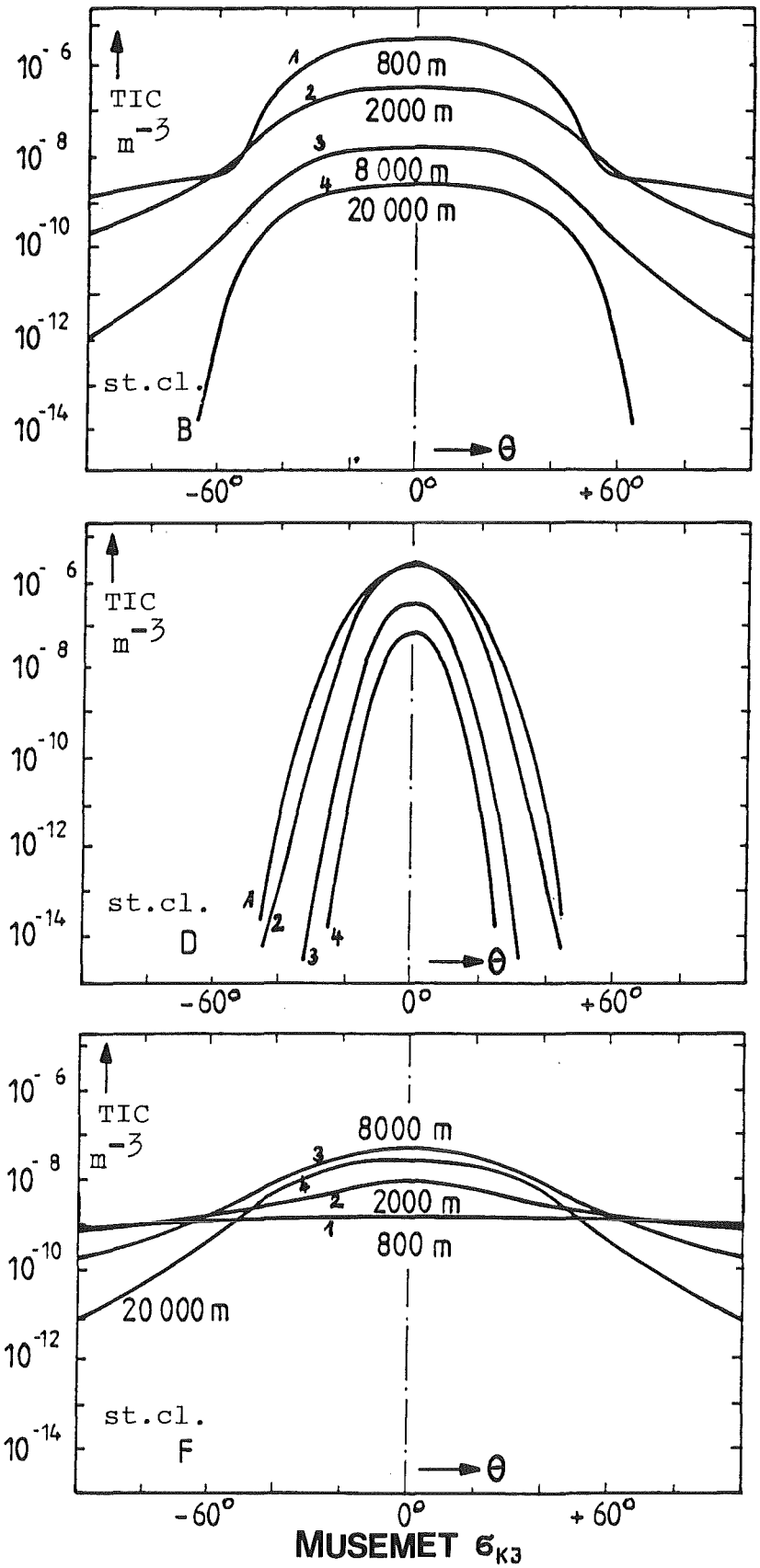

Fig.5a,b,c: Angular distributions of TIC, Batch I.

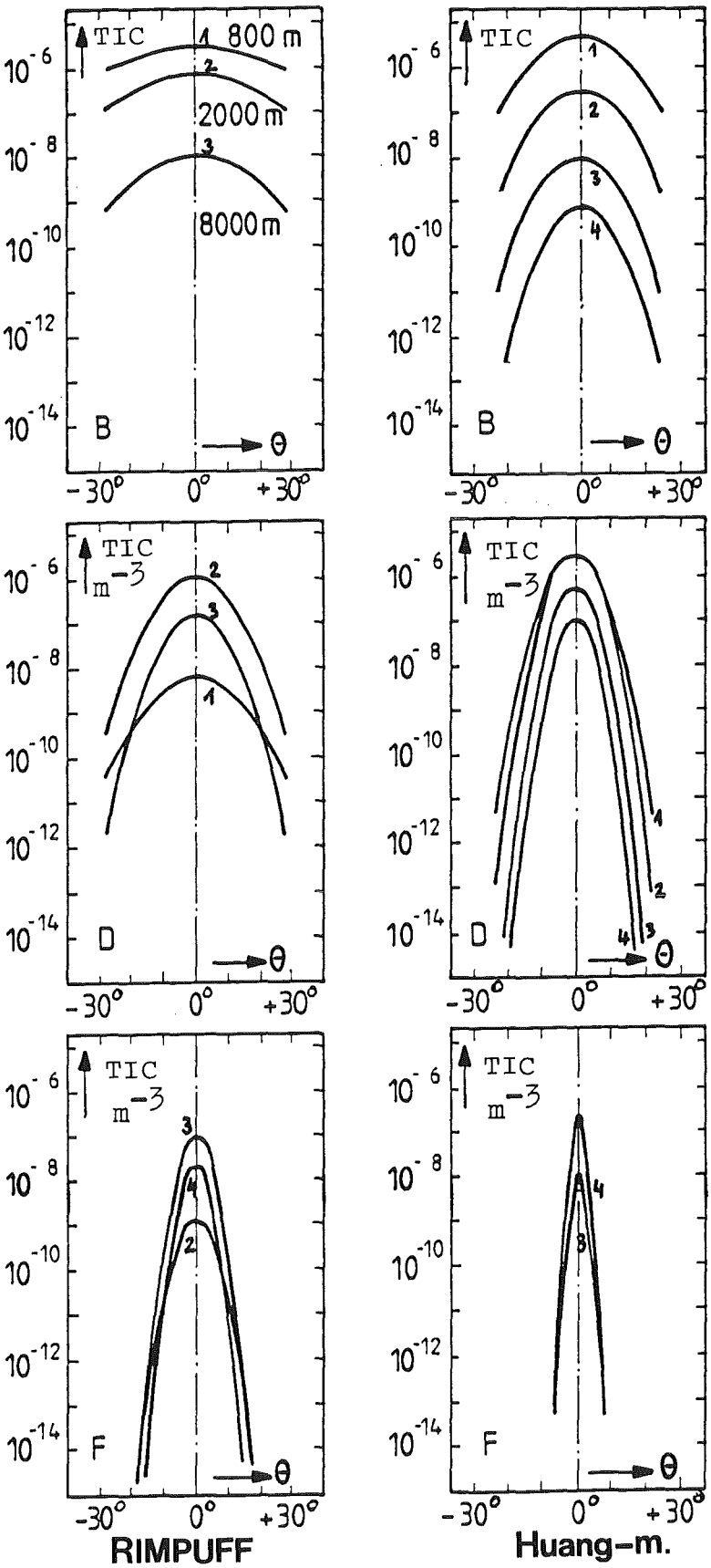

Fig.6a,b,c:
Angular distributions of TIC, Batch I

Fig.7a,b,c:

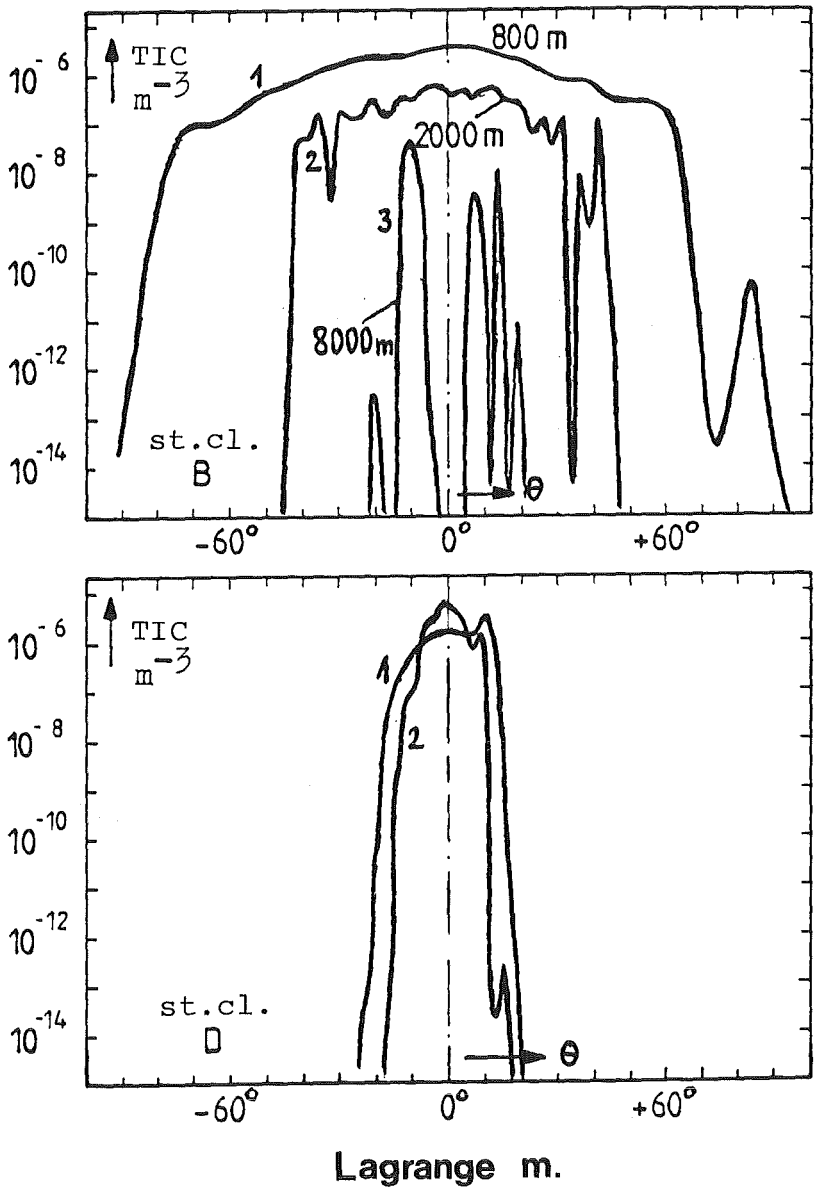

Fig.8a,b : Angular distributions of TIC, Batch I.

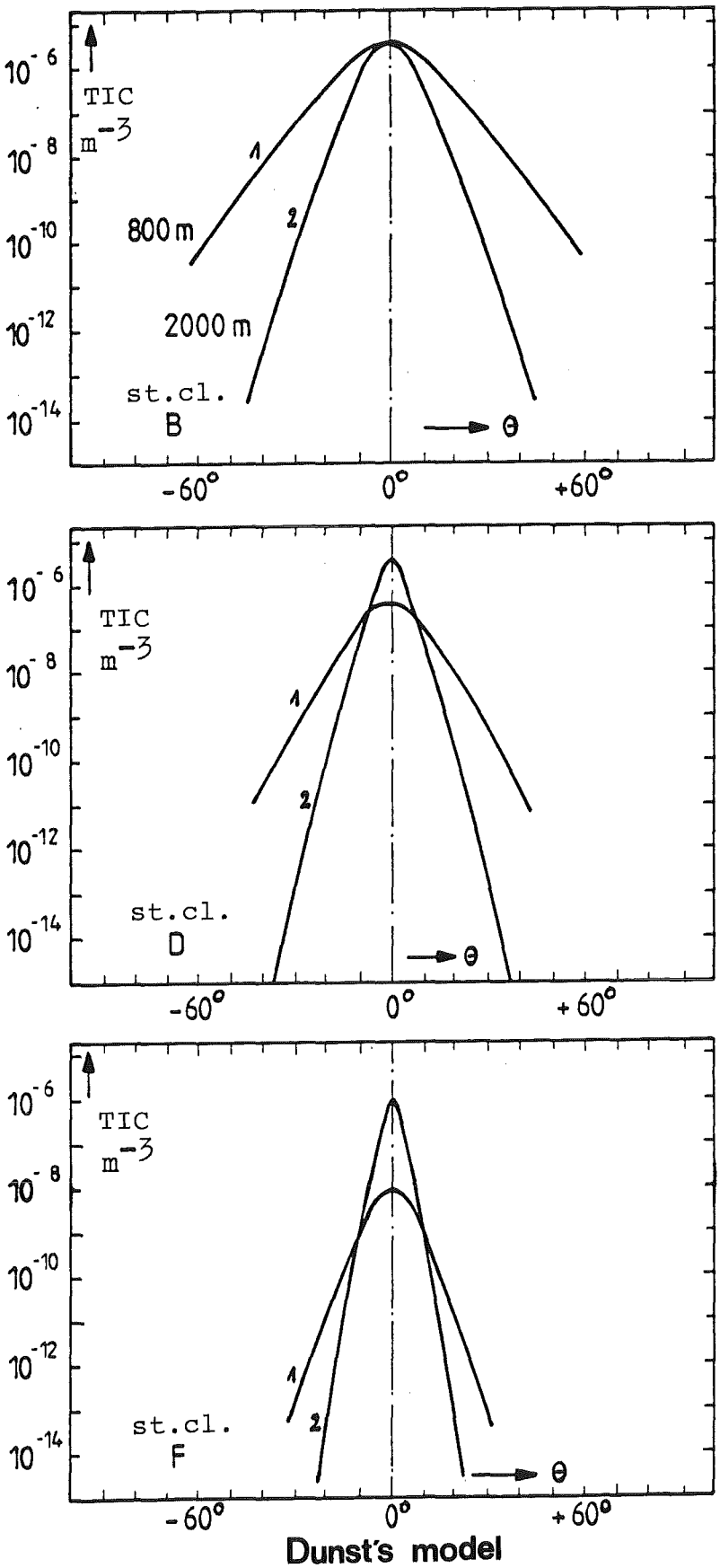

Fig.9a,b,c: Angular distributions of TIC, Batch I.

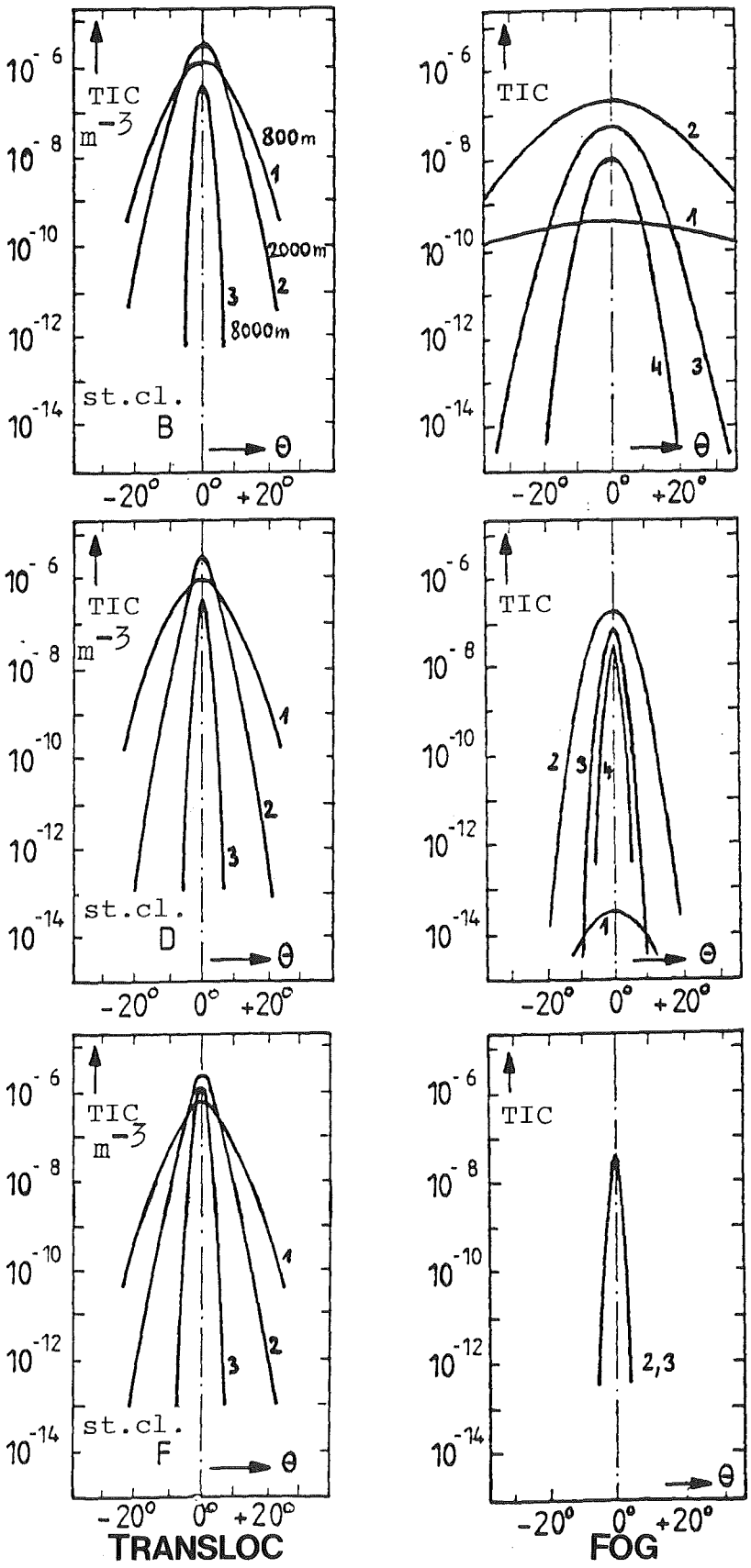

Fig.10a,b,c:
Angular distributions of TIC, Batch I

Fig.11a,b,c:

In models calculating horizontal turbulent diffusion (in y direction) by a Gaussian distribution (DOSI, MUSEMET, RIMPUFF, Huang, FOG), negative parabolas are obtained when $\lg(\exp -y^2/2\sigma_y^2)$ is plotted against y; σ_y can be derived from these parabolas. In the present manner of plotting against the angular coordinate Θ, parabolas are also obtained in the range $\pm 30^\circ$ in good approximation, and σ_y parameter curves were derived from the model calculations. The same was done with the numerical Lagrangian and Eulerian models.

6.2.1. Plume widths and σ_y parameters calculated by the models for Batch I problems

Fig.s 12a,b,c, present the distance-dependent plume widths or σ_y parameters derived from the angular distributions (Figs. 3-11). The Pasquill σ_y parameters (P) are marked with dashed lines for comparison; these parameters have been derived from 5-min averages of the wind direction for a roughness length around 0.01m (flat terrain with lawn) /Gi 76/ while the problems calculated in the present study assume hourly averages and roughness lengths of 1m. In consequence, realistic model calculations should yield plume widths larger than the Pasquill parameters $\sigma_{y\,PQ}$.

Unstable stratification (see fig. 12a):

The largest plume widths (about 4 times $\sigma_{y\,PQ}$) are assumed by the models DOSI (KJ), MUSEMET (KJ), and the Lagrangian model. These plume widths correspond to the Karlsruhe-Jülich σ_y parameter widths for a release height h_s=100m at a distance up to 5km. At longer distances, the increase of the Lagrangian plume widths is less marked.

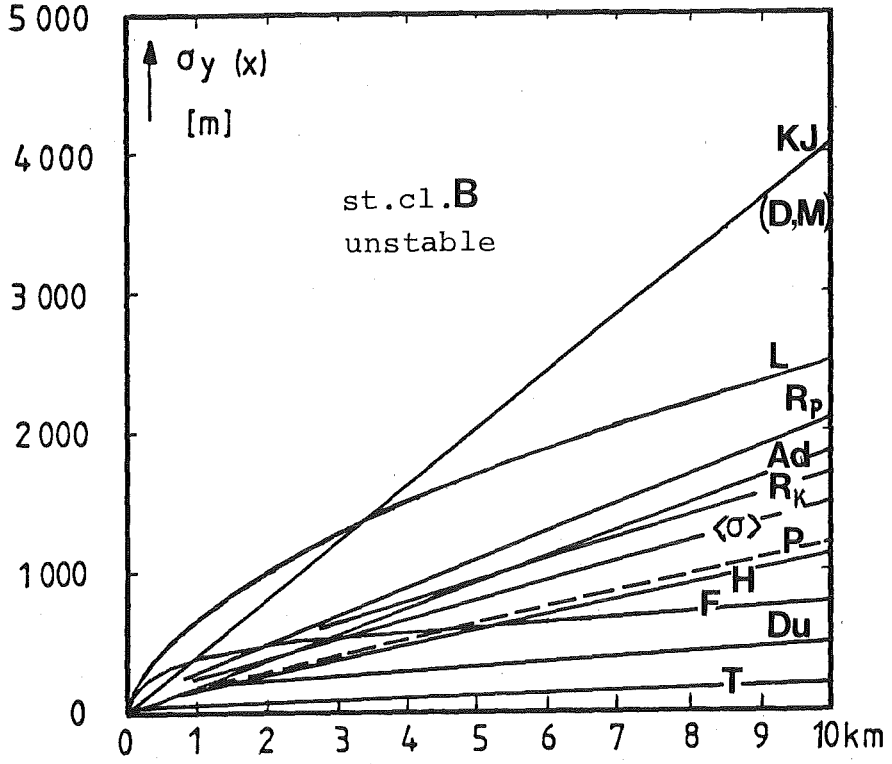

Fig.12a: Plume widths of different models; stability class B, Batch I.

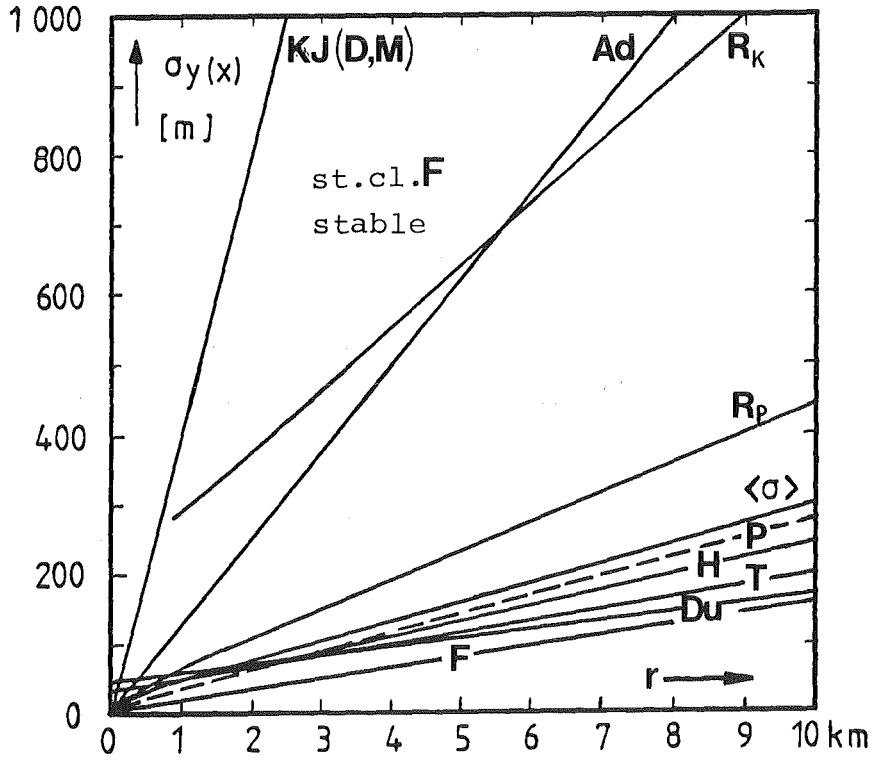

Fig.12b: like a), but stability class F.

Also the plume widths calculated by RIMPUFF (P), ADMARC, RIMPUFF (K) and DOSI $\langle\sigma\rangle$ are larger than the Pasquill plume widths. The factors are between 1.8 and 1.3 in the above order. The models therefore meet the above requirements.

TRANSLOC, FOG, Huang model and Dunst model calculate plume widths that are narrower than the Pasquill widths. In the Huang model and FOG, the deviation from σ_{yPQ} is rather small while Dunst and TRANSLOG have factors of 2.5 and 7. Huang and FOG both assume parameters of the type

$$\sigma_y(x) = \left(\frac{2\,K_y}{\bar{u}}\right)^{\frac{1}{2}} \cdot x^{\frac{1}{2}}$$

where the horizontal diffusion constant K_y is derived from the vertical diffusion constant K_z. In the case of Huang, this equation was calibrated using experiments of the Prairie Grass Series (sampling time: 10min, roughness length: 0.01m). This explains the narrow plume width.

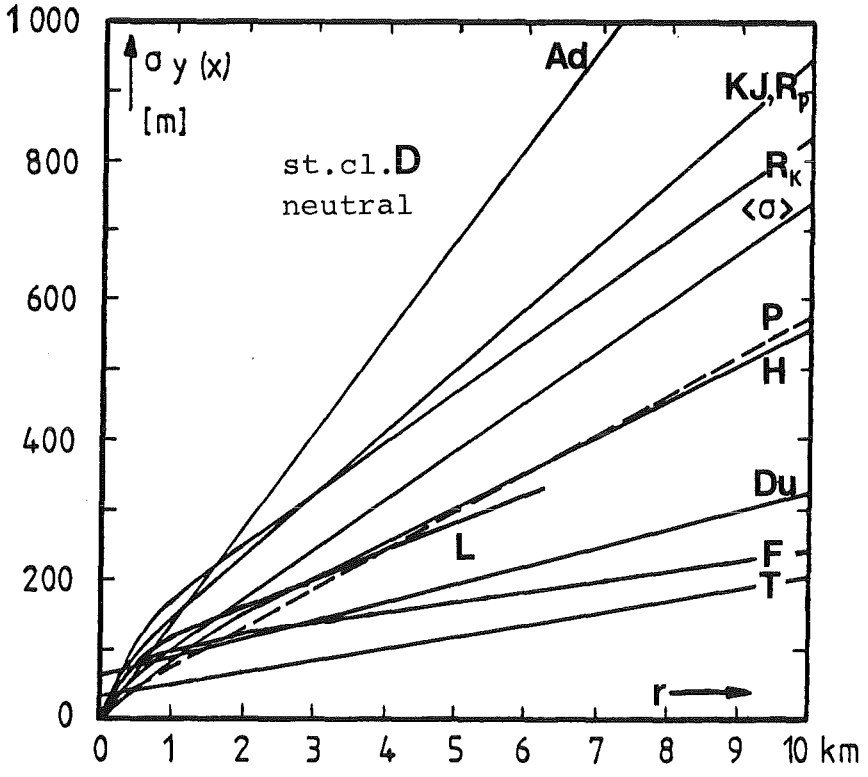

Fig.12c: like a), but stability class D.

In FOG, the vertical diffusion constant is based, among others, on the Jülich σ_θ, σ_ϕ , and $\partial T/\partial z$ measurements and on Pasquill diffusion experiments /Ga 81/. This method seems to be too indirect to provide results that are compatible with the parameters directly measured in Jülich.

The two numerical Eulerian grid models (Du, T) use only the high-frequency turbulence components (typical time measure $\tau \ll 1h$) for modelling horizontal diffusion. The low frequency components of turbulence characteristic of one-hour dispersion situations must be entered in the form of time-dependent wind direction data. This was omitted in Batch I and II problems and resulted in too narrow plume widths.

Stable stratification (see fig. 12b):

The models DOSI (KJ) and MUSEMET (KJ) give very large plume widths corresponding to σ_{yKJ} . They are wider by a factor 15 than the σ_{yPQ} parameters. The plume widths calculated by ADMARC and RIMPUFF (K) are only slightly smaller (factor ≈ 0.5).

This strong horizontal dispersion results from low frequency changes of wind direction (meandering) which may occur in stable conditions and which have been taken into account in the Karlsruhe-Jülich σ_y parameters and in the plume widths of ADMARC. RIMPUFF (P) and DOSI $\langle\sigma\rangle$ with Pasquill-Gifford σ_y parameters (with correction factor for the longer sampling time of 1h) or with $\langle\sigma_y\rangle$ parameters yield plume widths that are compatible with stable situations without meandering.

As in the unstable situations, the plume widths of the Huang model and the Dunst model, TRANSLOC and FOG are narrower than the Pasquill values although the deviations are less marked than in unstable conditions ($\lesssim$ factor 2). The reasons are the same as in the above, unstable case.

Neutral stratification (see fig. 12c):

Here, too, ADMARC, DOSI (KJ) and $\langle\sigma\rangle$, MUSEMET (KJ) and RIMPUFF (P) and (K) have large plume widths. They are larger by a factor 1.3 to 2 than the Pasquill widths.

The plume width of the Huang model corresponds to $\sigma_{y\,PQ}$. The results of the Lagrangian model are similar. The plume widths calculated by the numerical Eulerian grid models (Dunst and TRANSLOC) are narrower than $\sigma_{y\,PQ}$ by a factor 2-3. The reasons are the same as stated above.

FOG yields plume widths that are narrower than the Pasquill widths by a factor 1.5 to 2.

6.2.2. Remarks on some angular distributions

A comparison of the DOSI (KJ) results calculated for the angular distributions of the TIC with those of MUSEMET which also uses the Karlsruhe-Jülich σ parameters, shows remarkable deviations in the lateral concentration decrease in categories B and F.

In stability class B and at a distance of 800m, 2000m and 8000m, MUSEMET has concentration socles for angles $\theta \geq 50^{\circ}$ which are not found in the simple Gaussian plume model with corresponding σ parameters.

This effect in MUSEMET results from too high σ_x parameters. In MUSEMET, longitudinal diffusion is described by

$$\sigma_x(x) = \sigma_{y\,\mathrm{plume}}(x)$$

in the volume source method. With very high σ_y values comprising low-frequency meandering of the direction of dispersion, the equation $\sigma_x = \sigma_y$ is unrealistic, leading to backward diffusion of considerable concentration components over distances of several kilometers. In stability class F and with r=800 m (Fig.5c), there is even a uniform distribution of TIC in the angular range $-90^\circ < \theta < +90^\circ$. It would be better to have only the relatively high-frequency turbulence components considered in σ_x, e.g. by $\sigma_x = \sigma_{yPQ}$. The same noticeable influence of σ_x is found in the representations of TIC below the plume axis (see section 6.3).

In the angular distributions of TIC in TRANSLOC, there is a markedly narrow distribution range almost independent of the stability class.

The results of the Lagrangian model clearly show the statistical scatter of concentration curves resulting from the random walk method. As expected, the scatter is highest with low concentrations (= number of particles per unit volume at ground level) since the statistics is poor in this case. In general, these data can only be interpreted after applying smoothing interpolation methods. Alternatively, the number of emitted particles might be increased; however, four times the initial number of particles is required to reduce the mean amplitude of the statistical scatter by half. This also means four times the original computing time.

The plume widths of RIMPUFF (K) were expected to correspond to the Karlsruhe-Jülich σ_y parameters but a simple programming error resulted in reduced values (curves R_k in Fig. 12).

6.3. Calculated TIC below the plume axis - Batch I problems

Figs. 13-21 present the TIC below the plume axis for different release heights and stabilities. Each diagram contains up to ten model curves for a given diffusion category and release height. For more clearness and for a better distinction between typical effects of numerical models and Gaussian models, Gaussian families of curves have been drawn as fat lines. The term "Gaussian models" in this context refers to all models describing both horizontal and vertical turbulent diffusion by σ parameters, i.e. the models ADMARC, DOSI, MUSEMET, and RIMPUFF.

The widths of these "Gaussian regions" in Figs. 13-21 are determined almost exclusively by the use of different (σ_x), σ_y, and σ_z parameters; the treatment of the wind velocity $\bar{u}$ has a slight influence (factor ≤ 2; see section 6.5).

The behaviour of the Gaussian formula for concentrations at ground level with regard to the variation of σ_z explains the behaviour of the widths of the regions close to the source:

$$\frac{1}{\varrho} \cdot \frac{d\varrho(x,0,0)}{d\sigma_z} = \frac{1}{\sigma_z} \cdot \left(\left(\frac{h_s}{\sigma_z} \right)^2 - 1 \right)$$

At great release heights h_s and small σ_z (close to the source and especially in stable conditions), $(h_s/\sigma_z)^2 \gg 1$ is dominant. The large scatter of TIC in Gaussian models at large release heights (100m and 200m) and especially in stable conditions on

the left (source) side of the curves (Figs. 18,19,20,21; st.cl.D, F; h_s=100m and 200m) is explained almost exclusively in terms of this strong σ_z-dependence: $\sim 1/\sigma_z^3$!

Table 6 shows the 'widths' of the families of TIC curves at a distance of 1 km and 10 km from the source:

stab. cl.:	B	D	F	B	D	F
h_s						
10m	4.5	4	5	7	3.5	5
100m	5	20	2500	20	3	20
200m	4	10^5	-	18	6	2200
	x = 1 km			x = 10 km		

Tab. 6: Widths of the TIC-curve-bands of the Gaussian models at source distances of x=1 km and x=10 km.

Apart from the σ_z dependence determined by the ratio h_s/σ_z , there is the general $1/(\sigma_y(x) \cdot \sigma_z(x))$ behaviour of the TIC curves which describes the increasing dilution of concentration at large distances ($(h_s/\sigma_z(x))^2 \ll 1$). The widths of the families of curves at x=10 km (Table 6) for neutral and unstable (D and B) as well as for stable conditions at h_s = 10m are determined by the value assigned to this factor in the different models.

This means that the different σ-parameter sets alone result in TIC deviation factors between 3 and 20 for Gaussian models. In the regions near the source (defined as $(h_s/\sigma_z(x))^2 \gg 1$ these values may increase to 10^3 - 10^5.

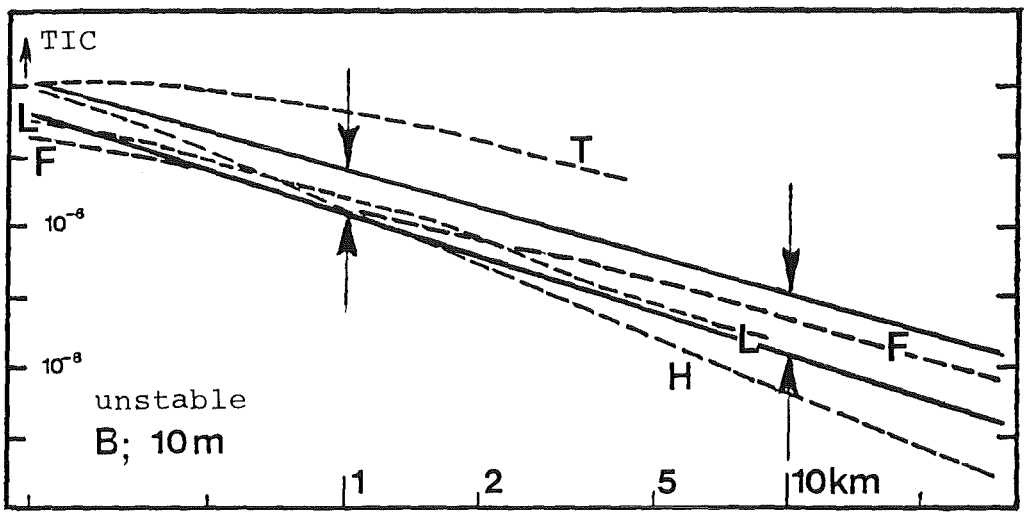

Fig.13: TIC below the plume axis; batch I.

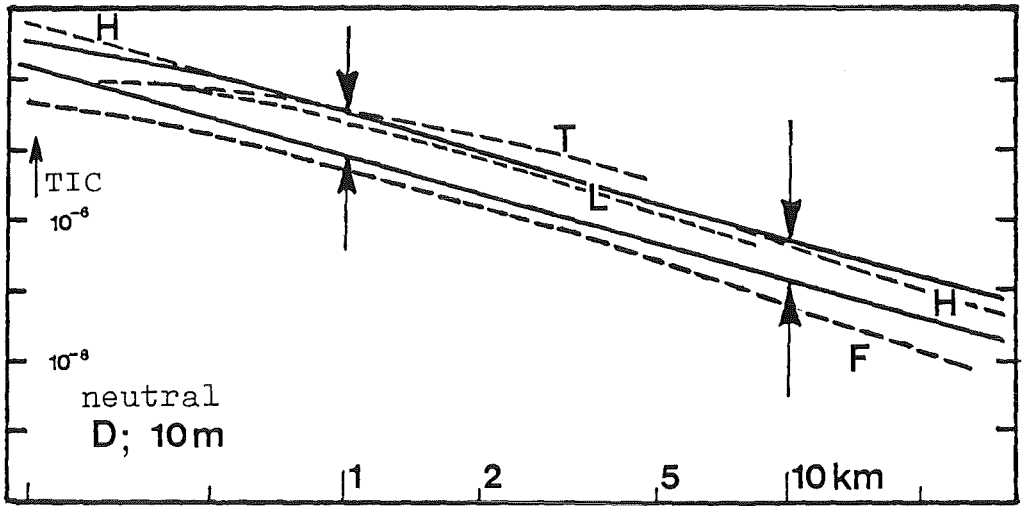

Fig.14: TIC below the plume axis; batch I.

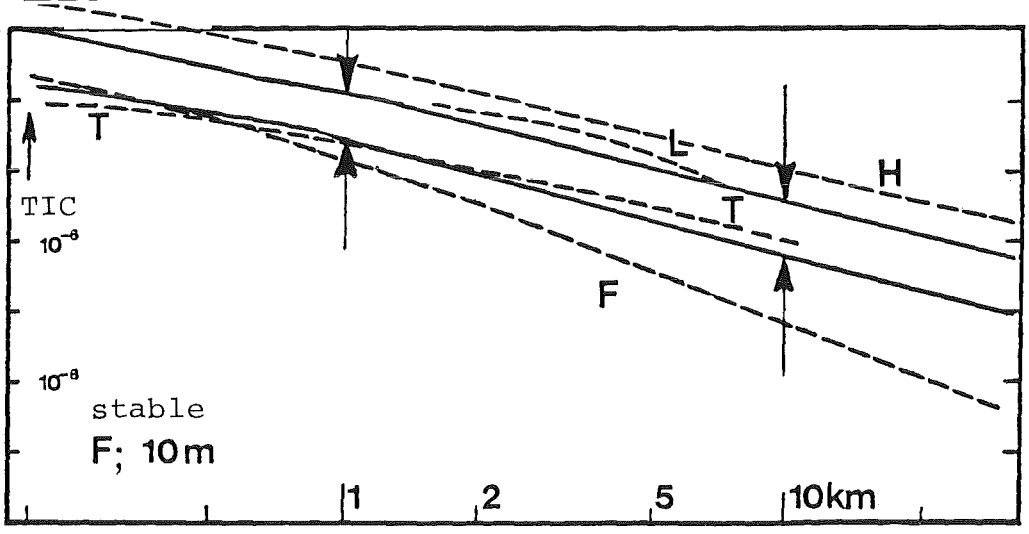

Fig.15: TIC below the plume axis; batch I.

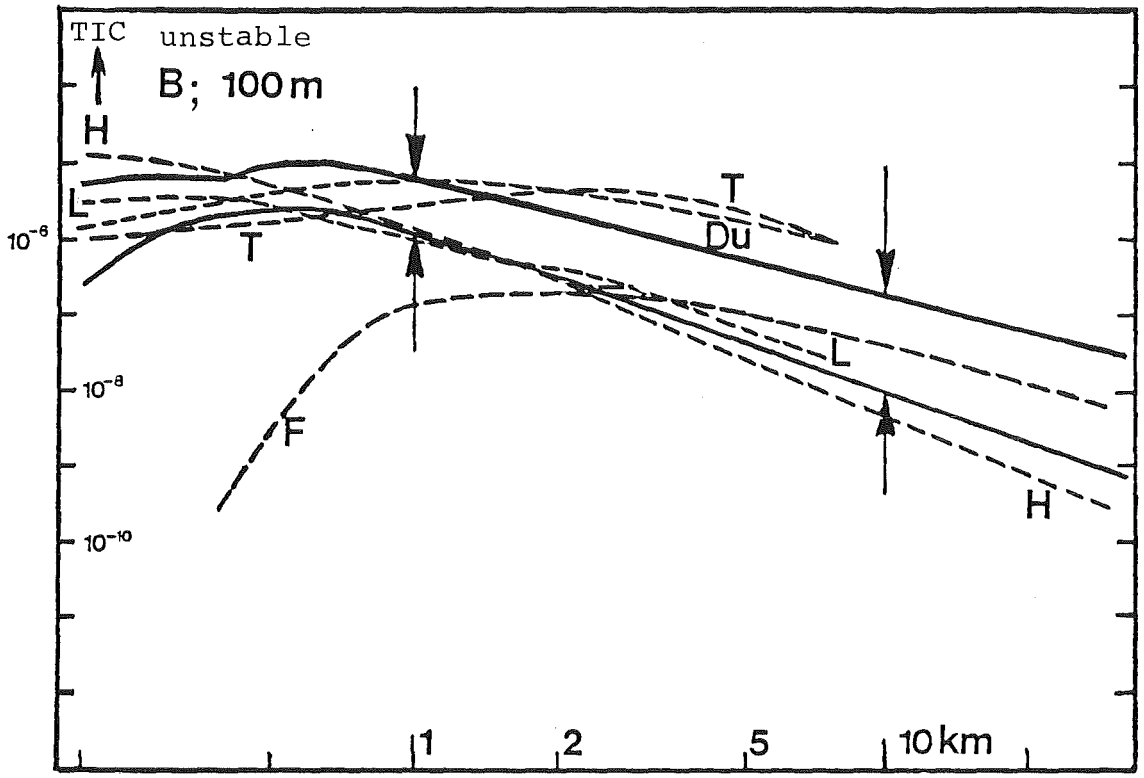

Fig.16: TIC below the plume axis; batch I.

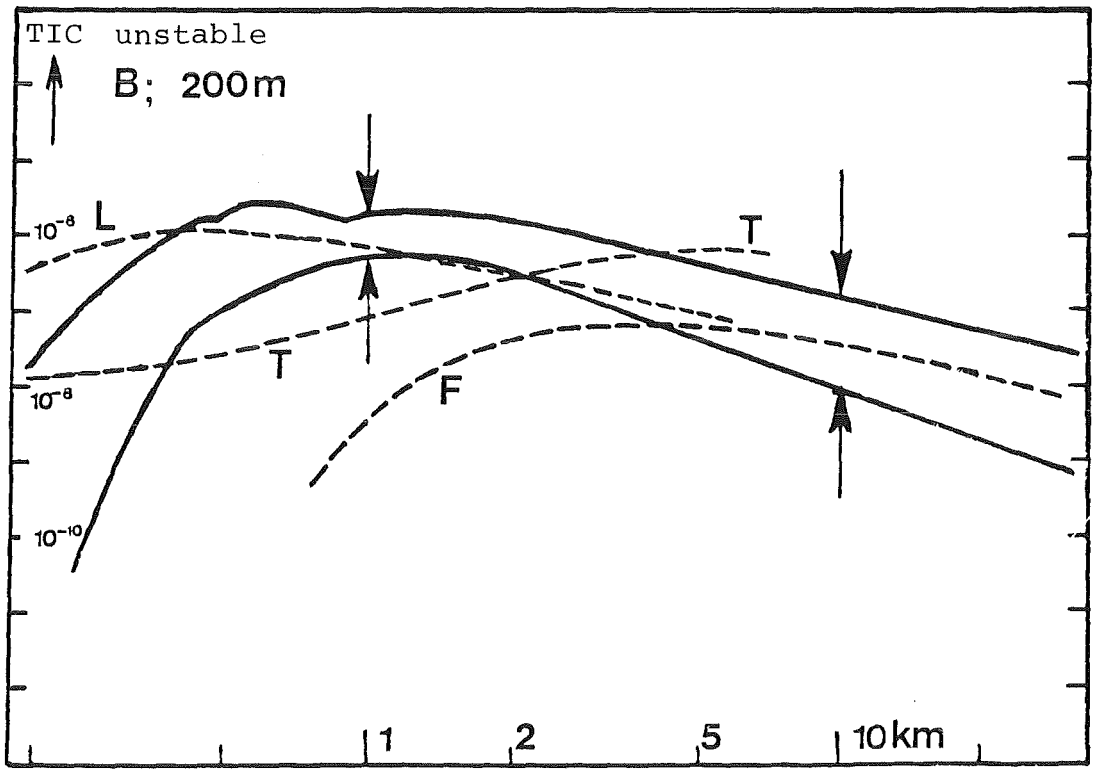

Fig.17: TIC below the plume axis; batch I.

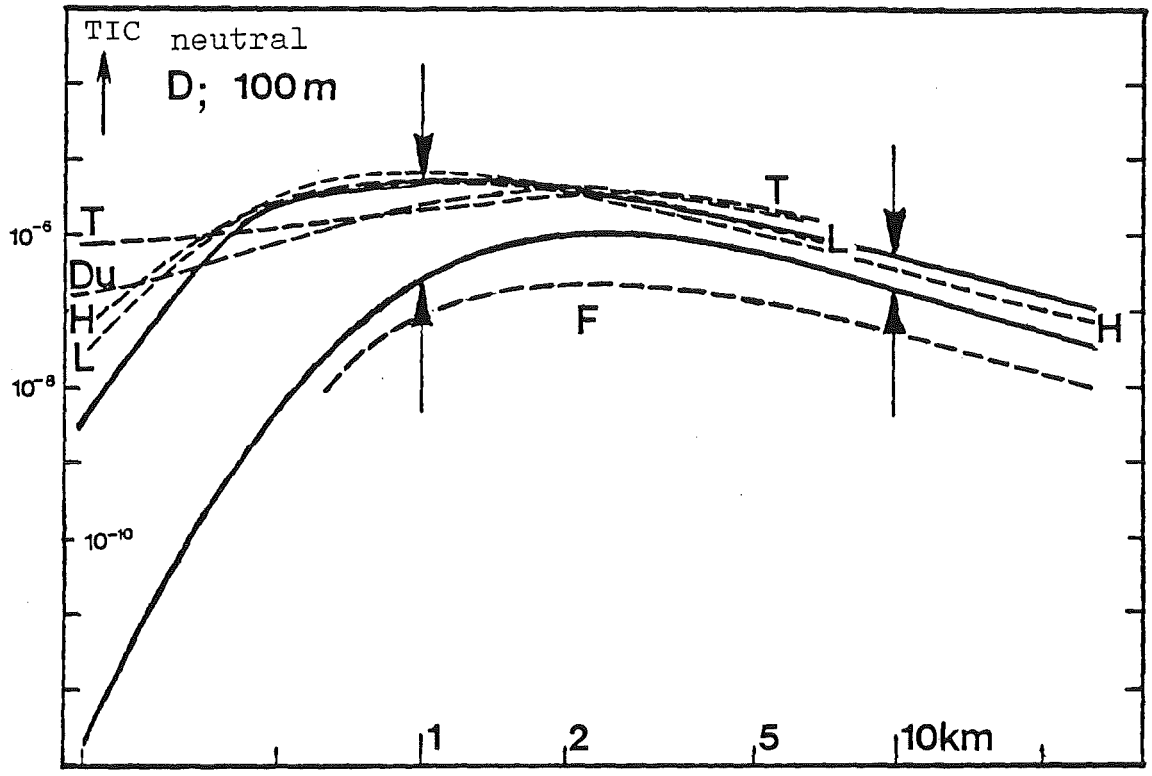

Fig.18: TIC below the plume axis; batch I.

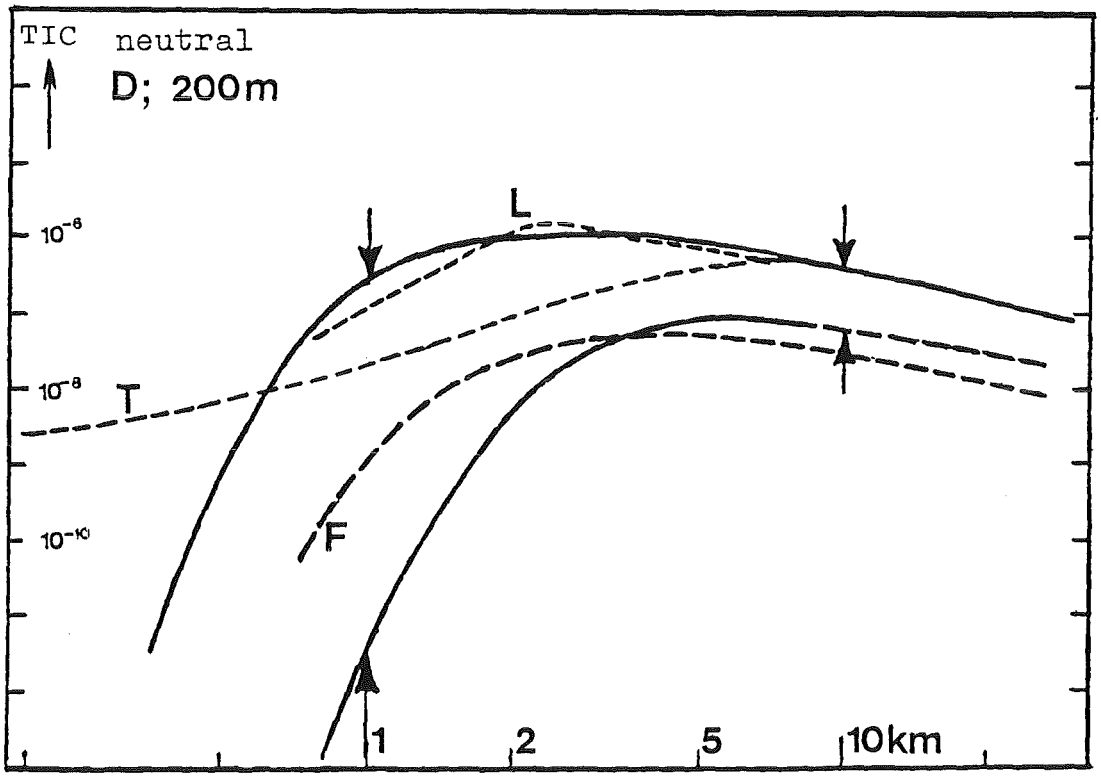

Fig.19: TIC below the plume axis; batch I.

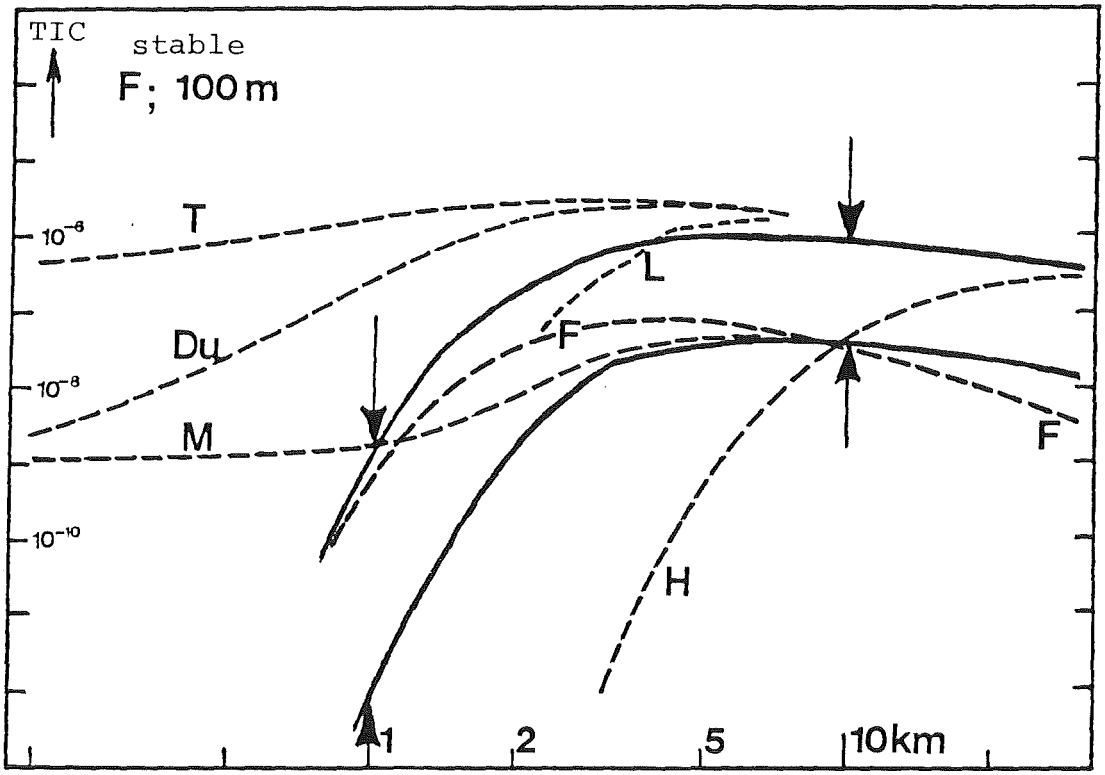

Fig.20: TIC below the plume axis; batch I.

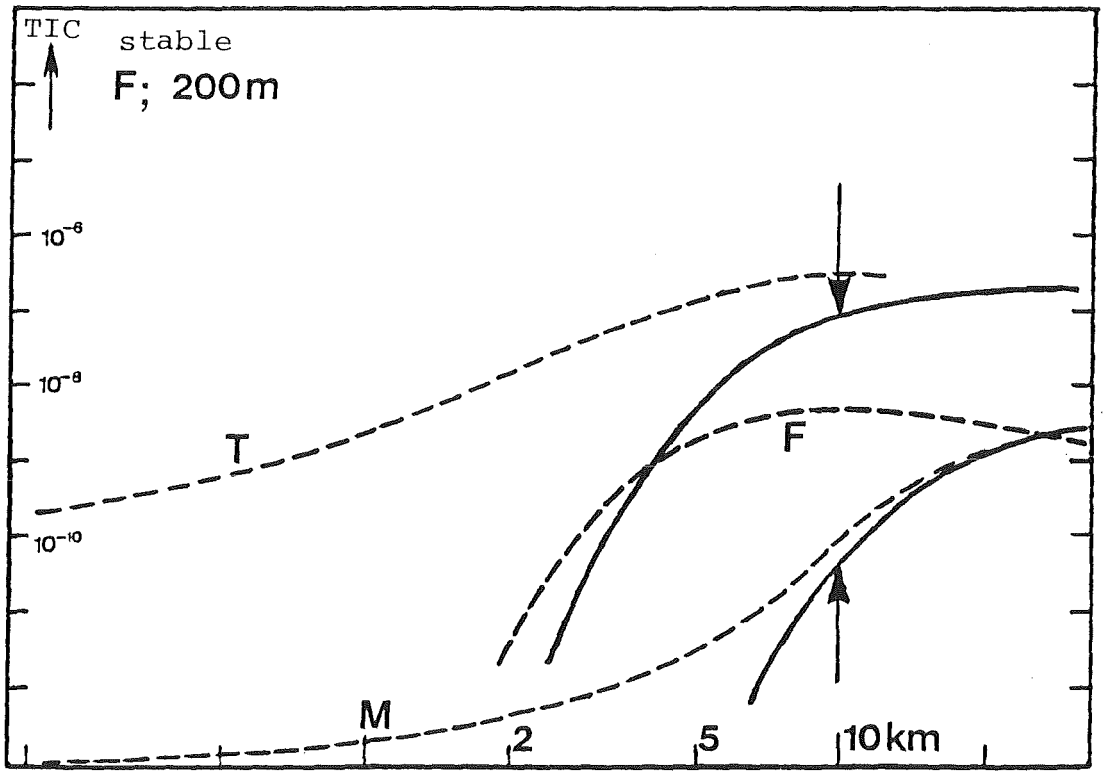

Fig.21: TIC below the plume axis; batch I.

6.3.1. Results of individual models

The Gaussian volume source model MUSEMET calculates unrealistically high surface concentrations near the source (Figs. 20,21) in stable conditions and at large release heights (stability class F, h_s=100m, 200m). As explained in the discussion of angular distributions, this error is caused by too large σ_x parameters resulting in "backward diffusion" from the concentration peak to the source. The authors of MUSEMET have remedied this error by using suitable $\sigma_{x,y}$ parameters combined with shorter time steps.

The Lagrangian Random Walk Model is similar to the Gaussian-type models in its performance. The shape and position of the TIC curves correspond in most respects to the families of curves of the Gaussian models. The undulation of concentration curves at longer distances from the source which results from the above-mentioned statistical scatter (amplitude $\approx$1 power of ten), has been suppressed by manual plotting of an averaged curve.

The Huang model applies, in principle, only to dispersion processes in the Prandtl layer (see description of the model in Section 4.3). We have therefore considered only the h_s=100m (st.cl.B,D; Figs. 16,18). The TIC curves of Huang exhibit, beyond the concentration peak, a more pronounced dependence on the stability class than the Gaussian models: For unstable stratification (st.cl.B, x=10000m), the Huang curves are lower by a power of ten than the average of the Gaussian family of curves (Fig. 13); in cases of stable stratification (st.cl.F; x=10000m), they are accordingly higher (Fig.15). No deviations are observed

with neutral stratification (st.cl.D; Fig.14). In the unstable case, vertical diffusion appears to be more enhanced and in the stable case reduced as compared with Gaussian-type models.

In TRANSLOC, there is a markedly slow gradient of the TIC curves from relatively high values near the source to the concentration peak far away. In the cases (B, 200m, Fig.17; D, 100m and 200m, Figs. 18,19; F, 100m and 200m, Figs. 20,21), this behaviour can be said to be non-compatible with physical laws. The too flat initial gradient of the curves is partly due to the too wide mesh of the lattice used in the finite difference method, and partly to the way in which vertical diffusion is modelled. TIC values at x=10000m are usually higher by a power of ten than the average values of the Gaussian-type models; one reason for this is the narrowness of the TRANSLOC plumes (see Section 6.2, Figs. 10,12).

The numerical model of Dunst was applied only to stability classes B,D,F (h_s=100m; Figs. 16,18,20) in Batch I. In all three cases, the results were similar to the TRANSLOC results with respect to high TIC near the source at release heights of 100m and 200m and the long distance to the concentration peak, although the data of Dunst are closer to the family of curves of the Gaussian-type models. The high concentrations near the source in class F (100m, Fig.20) are unrealistic.

At a source height h_s=10m and in stable conditions (F; Fig.15), the TIC curves of FOG have a much steeper slope at long distances from the source (5-20km) than the those of the Gaussian type models. At x=10 km, FOG is lower than the Gaussian family of

curves by more than a power of ten. This indicates strong dilution of the concentration of the plume. With the very small σ_y parameters of FOG, this must be mostly due to vertical diffusion. However, in the stable dispersion situation assumed here, vertical diffusion should not be dominant at all. In addition, at a distance of 20km from the source, FOG calculates smaller TIC for stable stratification than for stability class D (Fig.14). The modelling of vertical diffusion in FOG thus leads to results that are incompatible with physical laws.

At all release heights and at long distances from the source, FOG yielded smaller concentrations at ground level for stable stratification than for neutral stratification; this is against all experience.

On the whole, the TIC curves of FOG more or less match the Gaussian family of curves.

6.4. Treatment of surface roughness in the models

In the Batch I problems, the influence of the roughness length z_o on the vertical wind profile is taken into account by suitable wind profile exponents. This section investigates how the different values assigned to z_o are also reflected in the modelling of turbulent diffusion. In Gaussian-type models, the problem is reduced to the σ parameter dependence on the roughness length z_o. The Karlsruhe-Jülich σ parameters used in the models DOSI, MUSEMET and RIMPUFF are independent of z_o owing to the fact that these parameters were determined experimentally for a constant value $z_o \approx 1m$.

The same applies to the Pasquill-Gifford-Turner parameters used in RIMPUFF for small roughness lengths.

The Smith-Hosker σ parameters of the British model ADMARC are roughness-dependent and apply in the range z_o=0.03m - 1m. The $\langle\sigma\rangle$ parameters in DOSI have the same roughness dependence; the effect of a decrease in roughness length from 1m to 0.1m is shown in Table 7a. This table presents the ratio TIC(z_o=0.1m)/TIC (z_o=1.0m) for short and long distances from the source for the different stabilities and release heights.

At h_s=100m and 200m, calculated concentrations near the source before the concentration peak ($x<x_{max}$) are higher by a factor of ten while there is no difference to the roughness z_o=0.1m at longer distances from the source. The higher concentrations in the region $x<x_{max}$ result from the higher σ_z values in this region corresponding to a faster vertical diffusion from $z=h_s$ to z=0m. At h_s=10m (and stability classes B and D), only the higher initial vertical dilution becomes noticeable, as x is beyond the concentration peak even for short distances from the source: $x>x_{max}$.

The influence of surface roughness decreases with the distance from the source; the higher the degree of vertical mixing, the lower will be the influence of enhanced turbulence on concentrations at ground level.

In the Huang and Lagrangian models, the dependence on roughness length is similar to the Gaussian-type models; however, TICs lower by a factor 2 are also calculated for long distances if the given roughness length is z_o=1m instead of z_o=0.1m (Tables 7b and c). In the case of the Lagrangian model, this can be explained in terms of a horizontal plume width which is wider by this factor and results in a higher dilution of the TIC.

In the Huang model, there are no larger plume widths, and a simple explanation of the factor 2 cannot be given.

TRANSLOC (Table 7d) shows a similar behaviour close to the source at z_o=1m, but also an excessive increase of the TIC at greater source heights and longer distances (up to a factor 5!), although the plume width decreases with increasing roughness.

st.-cl.	B		D		F	
h_s	short	long	short	long	short	long
10m	1.6	1	1.5	1	0.25	1
100m	<0.1	1	<0.1	1	<0.1	1
200m	<0.1	1	<0.1	1	<0.1	1

a) ADMARC and DOSI<6>.

st.-cl.	B		D		F	
h_s	short	long	short	long	short	long
10m	2.5	2.5	1	2	0.6	1.5
100m	1	2.5	<0.1	2.5	-	-

b) Huang model.

st.-cl.	B		D		F	
h_s	short	long	short	long	short	long
10m	2	2	3	3	-	1.3
100m	1	2	<0.1	2	0.5	-
200m	0.3	2	<0.1	2	-	-

c) Lagrange model.

st.-cl.	B		D		F	
h_s	short	long	short	long	short	long
10m	2	2	2	2	1.4	1.4
100m	0.3	1	0.3	1	0.8	1
200m	<0.1	0.2	<0.1	0.2	0.5	0.8

d) TRANSLOC.

Tab.7: z_o-dependence of TIC close to the ground for different stabilities and source heights h_s. The numbers in the table are the ratios TIC (z =0.1m)/TIC (z =1.0m) at short and long source distances.

6.5. Modelling of wind velocities

Gaussian-type models, as shown in equation 6, have only one (averaged) value $\bar{u}$ for the wind velocity. The averaged value refers not only to variations in time but also in some cases to the height dependence of the wind velocity. Table 8 shows the dispersion velocities used in the different Gaussian-type models.

model	case	$\bar{u}$
ADMARC	1	$u(z = 10m)$
MUSEMET	2	$u(z = h_s)$
RIMPUFF	2	$u(z = h_s)$
DOSI	3	$1/\Delta h \int_{h_1}^{h_2} u(z)dz$ $h_2 = h_s + \sigma_z \leq 200$ m $h_1 = h_s - \sigma_z > 0$ m

Tab.8

The concentrations at ground level obtained by the different approaches differ by a factor ≈ 2. DOSI (case 3), as a result of height averaging for surface release, calculates TICs that are lower by a factor 2 than MUSEMET and RIMPUFF (case 2).

ADMARC, with u(z=10m) (case 1), yields excessive TIC in stable conditions and at $h_s > 10$m. The authors of the model consider this to be justified by the decrease of the real plume width with increasing source height /Jo 82/.

The other models, i.e. Huang, FOG, the Lagrangian model, Dunst, and TRANSLOC, use the vertical wind velocity profile u(z) given in the mathematical problems. The influence of this method of wind profile modelling cannot be separated from diffusion modelling as it is possible in the case of Gaussian-type models. The upper limit of variation of the TIC as a result of different ways of wind profile modelling is set at $u(h_s > 10m)/u(z=10m)$; real deviations are lower than this. As in the Gaussian-type models, factors of 2 are not likely to be exceeded.

7. Batch II problems

The Batch II problems were to show how the different dispersion models react to more complex atmospheric conditions than those assumed in Batch I problems.

Apart from the height-dependent wind speed, the Batch II.1 problems comprise also a marked shear of the wind direction which is characteristic of situations with stable atmospheric stratification.

The Batch II.2 problems describe an inversion situation.

For the original versions of the Batch II problems see Annex 3.

7.1. Description of the Batch II.1 problems
Shear of wind direction as a function of height

The direction of the wind vector at ground level is 0^{o} (x-direction); at a height of 200m, the wind vector is assumed to have turned to $+45^{o}$ (Fig.22).

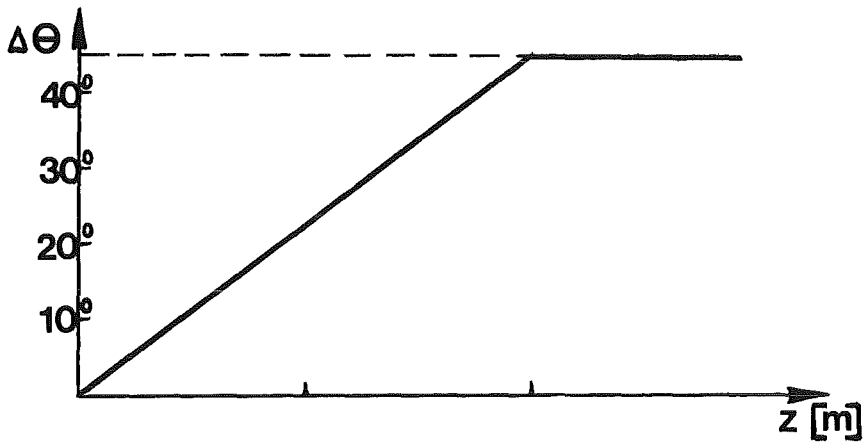

Fig.22: Directional shear $\Delta\Theta$ of the wind-vector depending on height z.

The value of the wind velocity $u(z)=|\vec{u}(z)|$ is assumed to have the same height dependence as in Batch I problems for stable stratification conditions. Problem II.1 was to be calculated for stability class F and three different release heights, i.e. 10m, 100m, 200m.

7.2. Description of Batch II.2 problems
Stationary inversion

The lower boundary of an inversion layer with a thickness of 200m is assumed at a height z=150m; the gradient of the potential temperature in the inversion layer $\partial\Theta/\partial z$ is set at +2°K/100m. Below this, unstable stratification with a gradient -0.5°K/100m corresponding to stability class B (Fig. 23) is assumed.

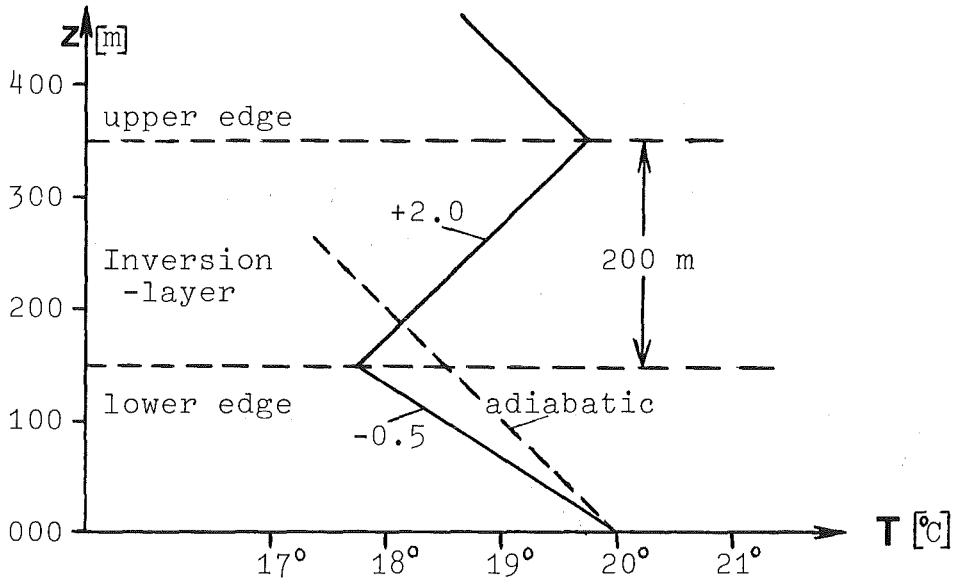

Fig.23: Inversion temperature profile T(z) of problem II.2.

The chosen vertical wind profile is identical with the vertical wind profile of the unstable stratification in Problem I,st.cl.B.

The assumed release heights are the same as in Batch I problems, i.e. 10m, 100m, and 200m.

7.3. Results of the model calculations of Batch II problems

7.3.1. Problem II.1: Shear of wind direction

For a detailed solution of this problem, models are required whose formalism takes account of height-dependent wind fields, i.e. Eulerian grid models or Lagrangian particle models. Gaussian-type models assume homogeneous wind fields in vertical direction and only one defined direction of dispersion. In consequence, the best solution to be expected of Gaussian models is one in which shear directions have been averaged suitably and the larger plume width has been taken into account by modified σ_y parameters.

RIMPUFF offers a more sophisticated solution: the "sheared puff" concept, in which the puffs (i.e. ellipsoids with x,y,z main axes corresponding to the $\sigma_{x,y}$ and σ_z parameters) are represented by ellipsoids inclined in shear direction /Mi 82/. Unfortunately, time problems prevented the calculation of problem II using RIMPUFF.

The Lagrangian model resulted in unsystematic and inaccurate data, which is probably attributed to errors in the input of wind field data; in principle, the Lagrangian model should be capable of calculating the TIC in wind fields with directional shear.

The remaining data compared here are the results of the Dunst model and TRANSLOC. Fig. 24a,b,c present the TRANSLOC results obtained for problem II.1 for the release heights h_s=10m, 100m, 200m in the form of angular distributions of TIC at a distance of x=800m, 2000m and 8000m from the source.

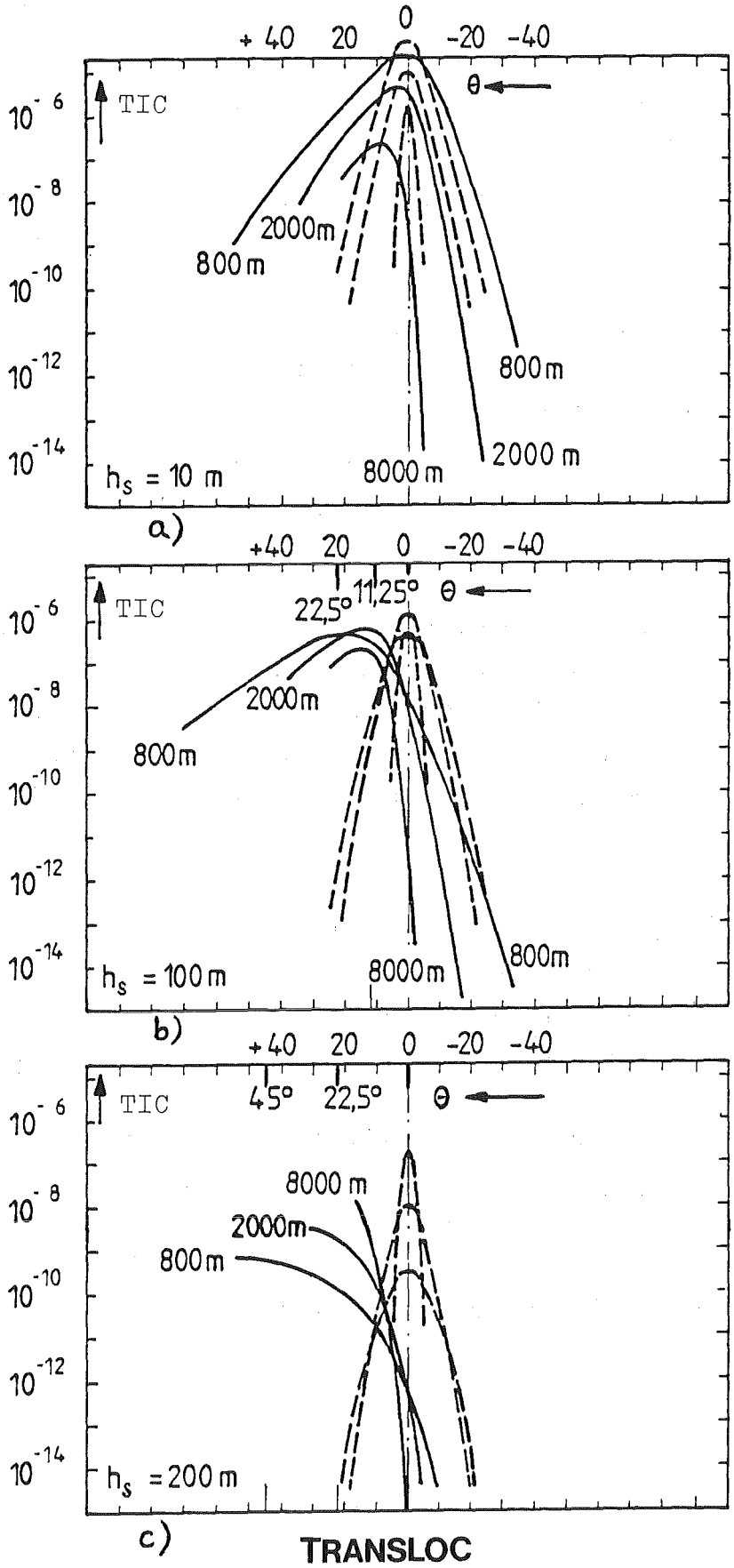

Fig.24: Angular distributions of TIC with directional wind shear (II.1):——; without dir.shear (I):---.

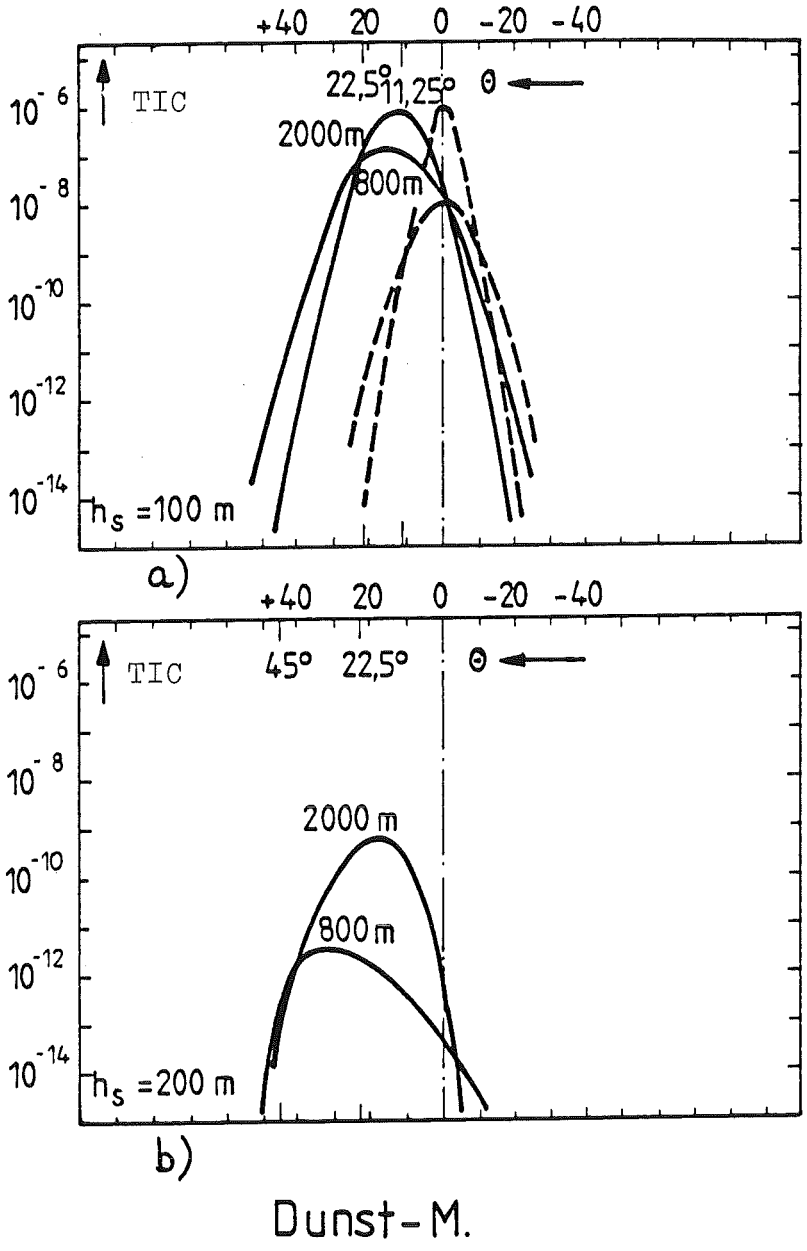

Fig.25: Angular distributions of TIC
with directional wind shear (II.1): ——;
without dir. wind shear (Batch I): ---.

At low release height (h_s=10m), the maxima of the TIC move to larger angles with increasing distance from the source r. At greater release heights, the angular maximum (at r=800m) is more or less in the wind vector direction at release level (22.5° at h_s=100m, 45° at h_s=200m). At longer distances (r=8000m), the maximum moves to mean angles between z=0 and z=h_s, i.e. to 11.25° at h_s=100m and 22.5° at h_s=200m.

This behaviour of TRANSLOC is qualitatively correct, as is the marked widening of angular distributions under the influence of vertical shear, as illustrated by a comparison with "unsheared" angular distributions.

The Dunst model yields similar results for the release heights h_s=100m and 200m; the widening of the plume is less pronounced than with TRANSLOC (Figs. 25a and b).

7.3.2. Problem II.2: Stationary inversion

7.3.2.1. Gaussian-type models:

In Gaussian-type models, the influence of a strong inversion layer at height $h_i > h_s$ on the vertical concentration distribution can be modelled by multiple reflection of the plume between the ground and the lower edge of the inversion layer. Fig.26 gives an illustration. At a point near the source, x_1, with a relatively narrow plume width in vertical direction, the concentration distribution is almost unaffected. At longer distances x_2, ($\sigma_z(x_2) \gg h_i$), a point of homogeneous vertical concentration distribution is soon reached; further dilution of the concentration in the plume is possible only by horizontal spreading via the width $\sigma_y(x)$, thus increasing the concentration at ground level.

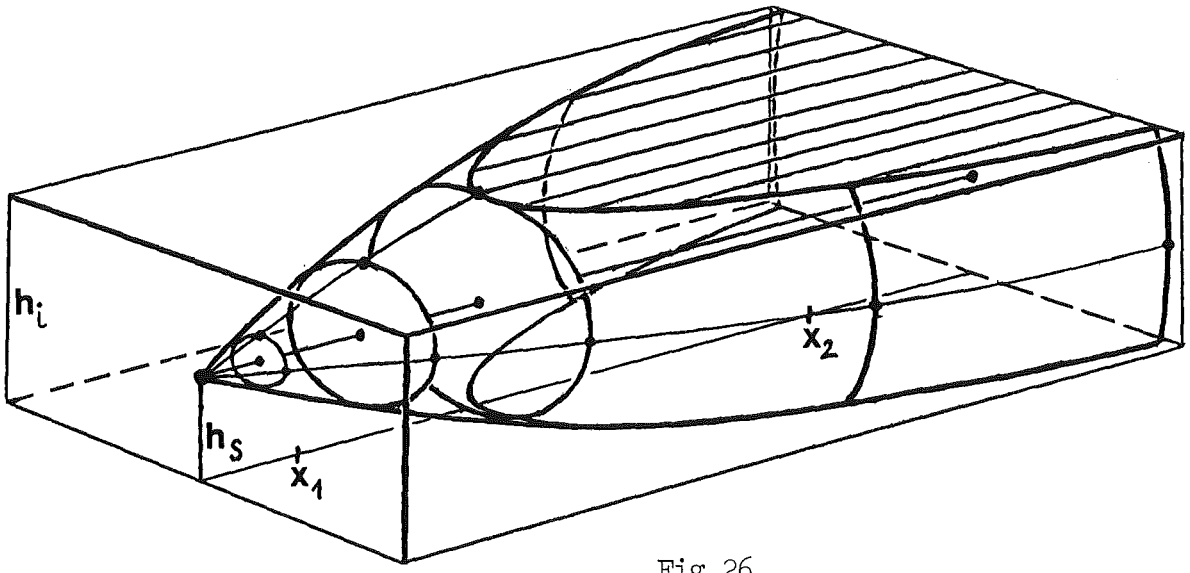

Fig.26

This effect can be well reproduced with Gaussian-type models; an example is given in Fig. 27 with the results of DOSI and MUSEMET.

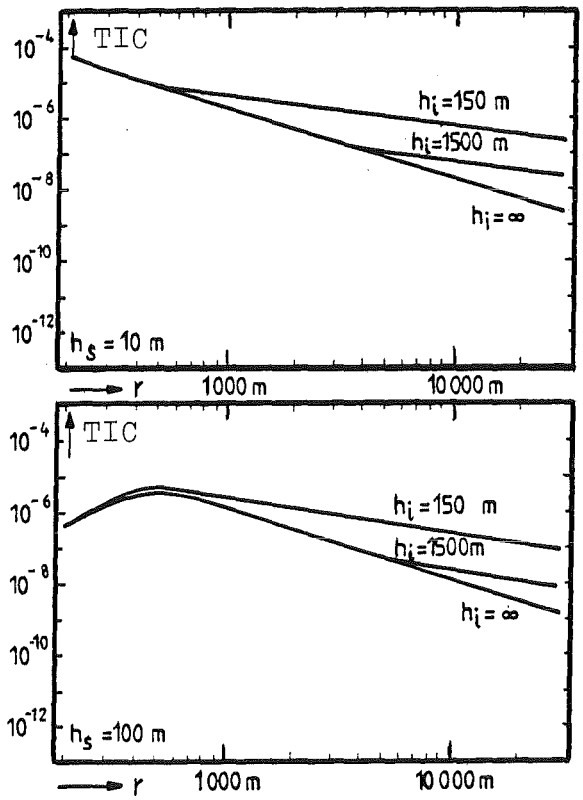

DOSI/MUSEMET, σ_{KJ}

Fig.27

With release heights of 10m and 100m and inversion layers at 150m and 1500m different Gaussian models calculate the same effect on the TIC as compared with the case of a mixing layer without upper boundaries ($h_i=\infty$).

With h_i=1500m, complete vertical mixing is achieved at r=4000m; with h_i=150m, this is the case already at r=1000m. As expected, the concentration values for h_i=1500m and h_i=150m differ by a factor 10 in the region of vertical mixing (the two heights of inversion have a ratio of 10 and the σ_y parameters are identical).

7.3.2.2. Numerical models:

a) Lagrangian model

Figs. 28a and b present the results of the Lagrangian model for release heights 10m and 100m, compared with the TIC without inversion effects. The results are quite close to those of the Gaussian models. No concentrations are calculated for an emission height of 200m, i.e. within the inversion layer. This behaviour of the model is explained by the total reflection of the particles at the lower edge of the inversion layer.

b) Models with a vertical profile of the diffusion constant $K_z(z)$ (FOG, TRANSLOC, Dunst model

These models have some common flaws and are therefore treated together. For example, FOG and TRANSLOC are unrealistic at release height 10m: TIC without inversion at a height of 150m are higher by a factor 5 to 10 than with an assumed inversion layer (Figs. 29,30). This case (h_s=10m) was not calculated by the Dunst model.

TRANSLOC:

The results obtained with TRANSLOC for a release height h_s=10m are not in accordance with physical laws: Without inversion (h_i=∞), the TICs are higher by a factor 4 than with inversion. (h_i=150m). Correct results were obtained at h_s=100m (TIC(h_i=∞)< TIC(h_i=150m)), but only for distances up to 2000m from the source. Already at 8000m, the calculated concentration for the case with inversion is again lower by a factor 2 than the TIC without inversion (Fig.29).

Further, in case of emissions within the stable stratified inversion layer (h_s=200m), which ought to delay (or reduce) transport to the ground, TRANSLOC calculates much higher concentrations at ground level (see Fig.29, bottom). Both observations suggest problems in the modelling of vertical diffusion.

FOG:

The results of FOG are similar in some respects:
At emission heights h_s=10m and 100m, i.e. below the inversion layer, FOG calculates slightly higher TICs near the source than without inversion. However, beyond a distance of x=10000m, the curves intersect (Fig.30), and the concentrations for the inversion case are smaller than the TICs without inversion. As in TRANSLOC, this is not in accordance with physical laws.

If the emission takes place in the inversion layer (h_s=200m) FOG calculates reduced TIC at ground level as compared to the case of an emission into a homogeneous atmosphere; this behaviour is qualitatively correct.

Dunst model:

The Dunst model has been applied only to the case h_s=100m, with and without inversion. Slightly higher concentrations at ground level are calculated for the inversion case (Fig.31).

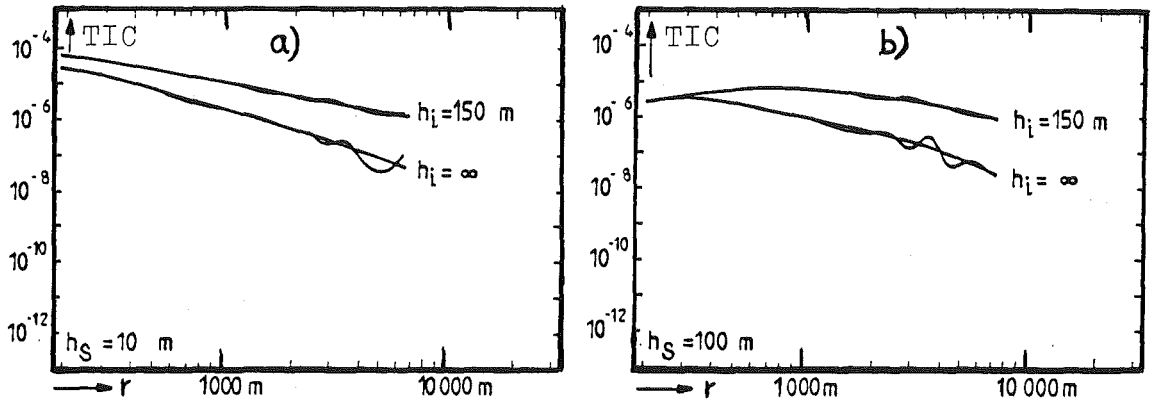

Fig.28 **Lagrange m.**

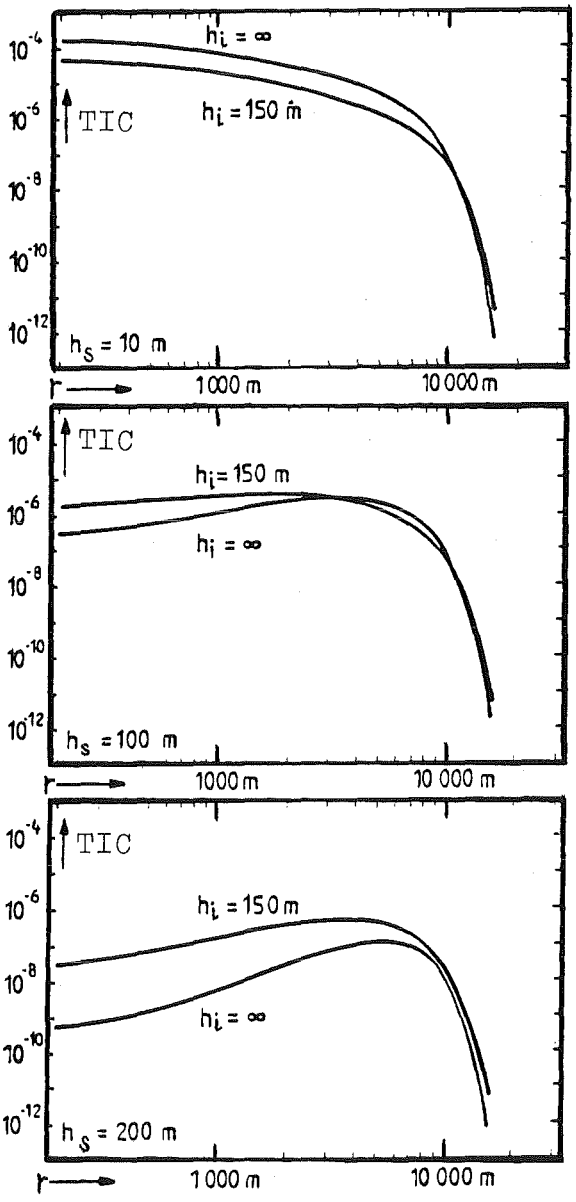

Fig.29 **TRANSLOC**

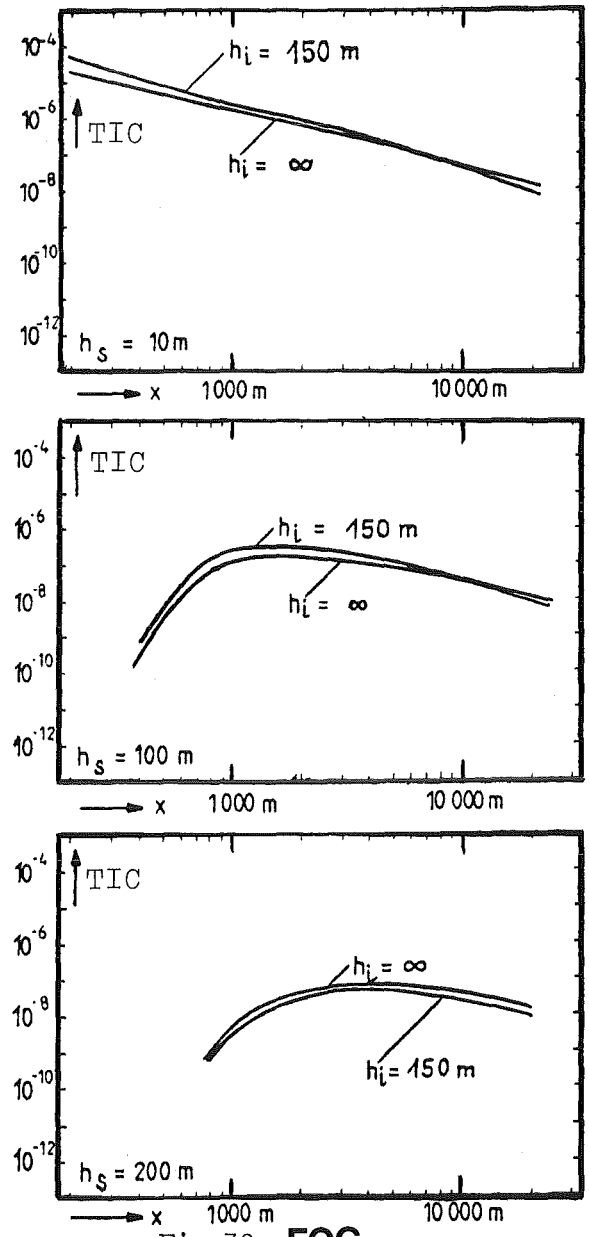

Fig.30 **FOG**

Inversion situation (problem II.2)

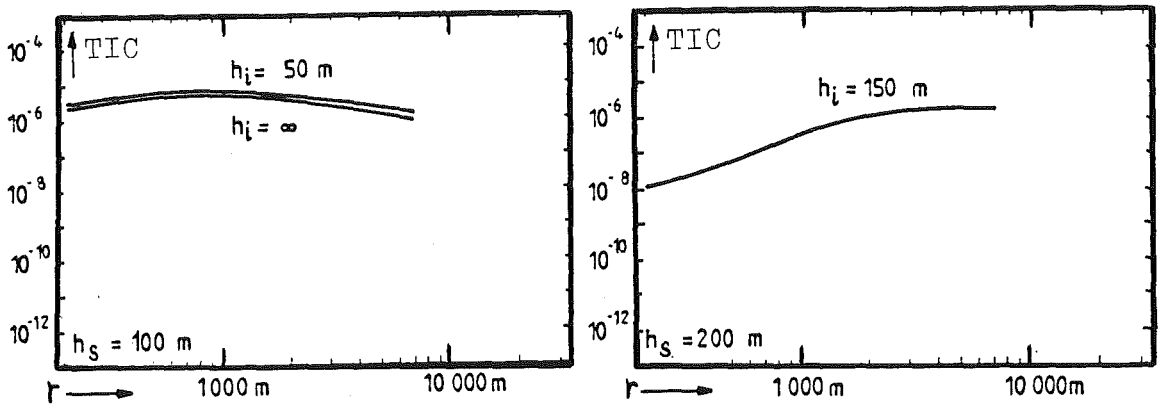

Fig.31 **Dunst's m.**

The results of the Gaussian-type models and the Lagrangian models differ clearly and in a characteristic manner from the results obtained for models with a K_z profile approach.

All in all, it can be stated that the inversion situation of problem II.2. is better modelled by the Gaussian-type and Lagrangian models than by the numerical models used in the present investigation, in spite of the simplifying assumption of total reflection at the lower edge of the inversion layer.

Part 2: Validation studies

8. The dispersion experiments

The validation problems III are based on four atmospheric dispersion experiments of different laboratories. To reduce the possibility of falsified results (i.e. results adapted to the concentration data measured in these experiments),a variety of KFA-Jülich, KfK, Cabauw, and Risø experiments was proposed by the AVVA working group, and one experiment of each laboratory was chosen among these. The meteorological data, release data and surface roughness data of these experiments were then used in problems E1 to E4. The original problems are presented in Annex 3.

The tracer emission rates $\dot{Q}$ were normalized, so that a unit source term was obtained for the sampling time. Further, the similarity theory quantities L (Monin-Obukhov length) and u_* (friction velocity) were calculated from the time-averaged wind and temperature profiles in consideration of the roughness length z_o and the height of zero displacement d. For this purpose, the wind velocity profiles (see annex) of the boundary layer at ground level, which are normally linear-logarithmic, as well as the corresponding temperature profiles of similarity theory were fitted to the measured values (the L and u_*values are derived from the best fit).

Table 9 gives a short survey of the main data of the four selected dispersion experiments E1 - KFA Jülich, E2 - KfK Karlsruhe, E3 - Cabauw, E4 - Risø. The concentration data of the experiments are presented in tables 1-4 in Annex 2.

9. Methods of evaluation

Validation calculations are to provide objective information on whether the models gave an accurate picture of the experimental results within the statistical variation.

Exp.:	E1	E2	E3	E4
Data:	KFA-Jülich, Exp.58 19.7.76	Karlsruhe, Exp.31 22.5.75	Cabauw, Exp.13 10.10.78	Risø 6.7.79
h_s m	100	60	80	115
d m	16	10	≈ 0	≈ 0
z_o m	1.2	1.2	0.2	0.6
$\overline{u}$(100m) m/s	7.5	6.5	6.3	9
$\overline{u}$(40m) m/s	3.3	5.0	4.0	4 ($\overline{u}_{40}$)
wind direction	WSW-W	NNE	ESE	WNW - NW
$\overline{\sigma_\theta}(z)$	2.6° (120m)	11.2° (100m)	5° (80m)	8.8° (115m)
$\overline{\sigma_\phi}(z)$	2.3° (120m)	9.4° (100m)	3° (80m)	4.7° (115m)
$\overline{\partial\theta/\partial z}$ K/100m	+1.6 (20-120m)	-0.7 (30-100m)	+0.5 (10-60m)	-0.4 (20-120m)
L m	+70	-100	+200	-70
u_* m/s	0.27	0.8	0.3	0.7
h_{mix} m	-	-	200	800
stab.-class	E	C	D - E	C - D
tracer	Ho 166	CF_2Br_2 and $CFCl_3$	SF_6	SF_6
$\dot{Q}$	0.28 TBq/h	7.8 g/s 11.8 g/s	1.42 g/s	3 g/s
release-time h	1	1	1	1
no. of sampling positions	21	30	18	39
sampling-time h	1 50'	0 30'	2x 30'	1 (3x 20')
distance-interval m	500 - 14000	100 - 1300	3300 - 4500	1800 - 5500
angle-interval	45°	90°	35°	35°

Table 9: Data of the tracer experiments used for the validation studies.

Formally, pairs of functional values $\varrho_M(r_i,\Theta_i)$ and $\varrho_R(r_i,\Theta_i)$ are compared, with ϱ_M and ϱ_R representing the standardized, measured concentrations and the calculated concentrations at ground level along the coordinates (r_i,Θ_i) of the measuring points i.

Such a purely numerical comparison of measured and calculated data in a limited number of points under consideration (r_i,Θ_i) may be inadequate in defining the quality of the model. For example, a deviation $\Delta\Theta$ between the measured and the calculated mean plume dispersion direction would, by a numerical comparison, result in large deviations between $\varrho_R(r_i,\Theta_i)$ and $\varrho_M(r_i,\Theta_i)$, even if the density distributions were identical except for the angular deviation: $\varrho_R(r_i,\Theta_i+\Delta\Theta) = \varrho_M(r_i,\Theta_i)$.

9.1. Isoline representation

In view the above problem, it was preferred to start by getting an idea of the location and shape of the distributions $\varrho(r,\Theta)$. This was done with the aid of isolines of concentrations at ground level, e.g. in steps of powers of ten. The isoline representations are shown in Figs. 32 - 35.

Simple characteristics, e.g. plume width and plume axis direction, can be derived directly from the isoline representation of the experimental and the theoretical distributions.

Errors in transport direction (= plume axis direction) are often not model-based but caused by wrong input data (e.g. a measured wind direction not representative of the region in which dispersion takes place).

continued on page 66

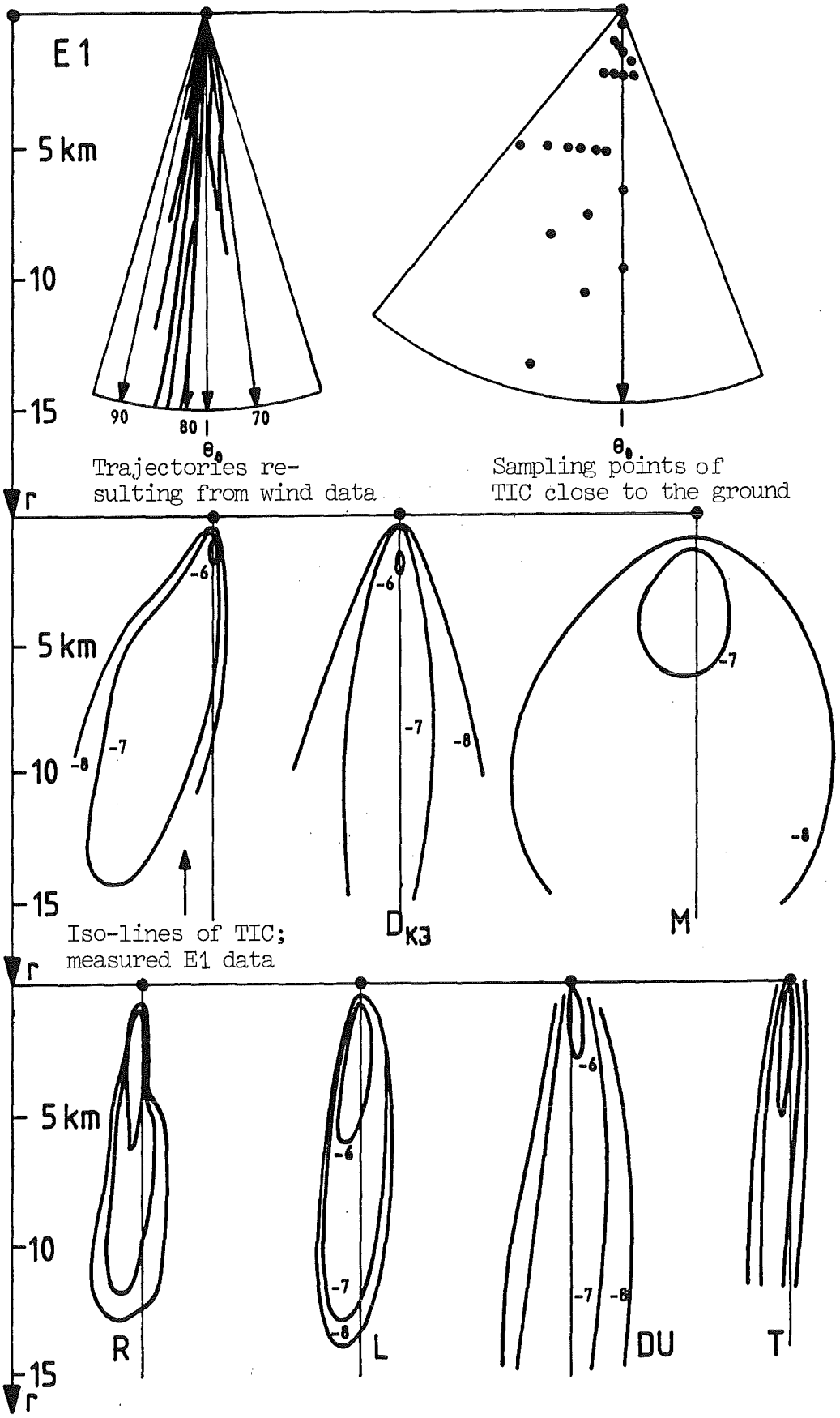

Fig.32: Iso-TIC-lines of E1 and computed results of models.

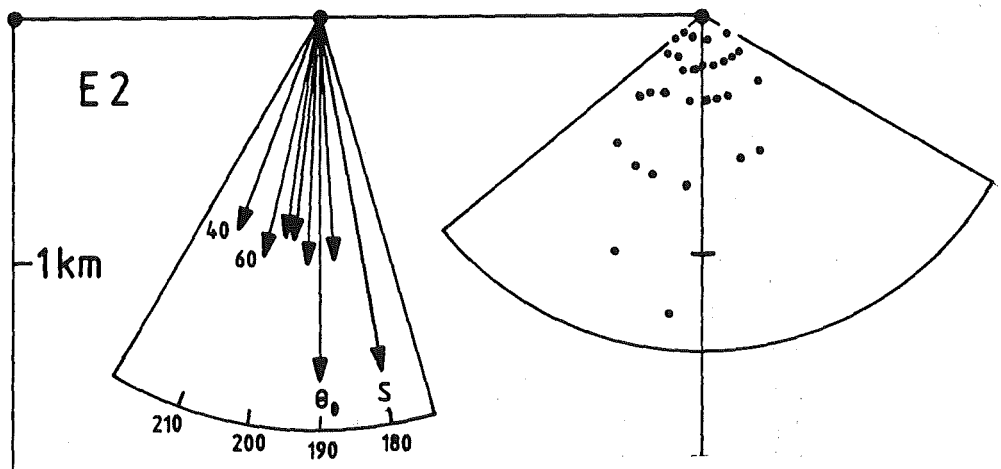

10 min average wind vector directions at z=40m and 60m.

Sampling points of TIC close to the ground.

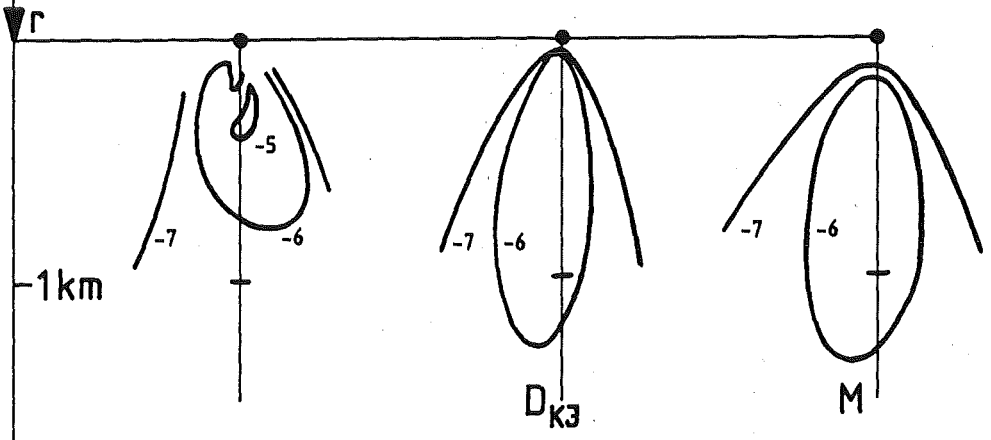

Iso-lines of TIC; measured E2 data.

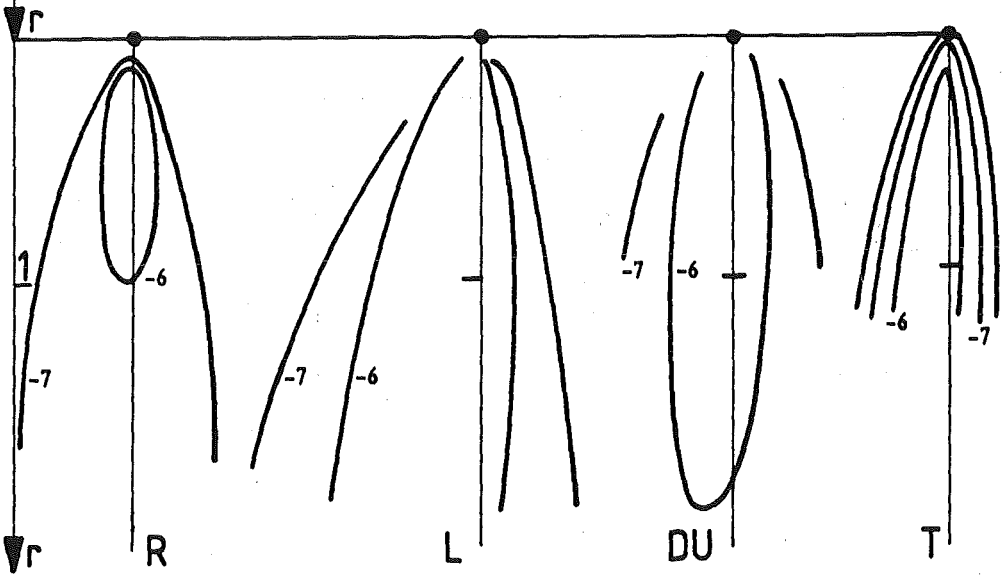

Fig.33: Iso-TIC-lines of E2 and computed results of models.

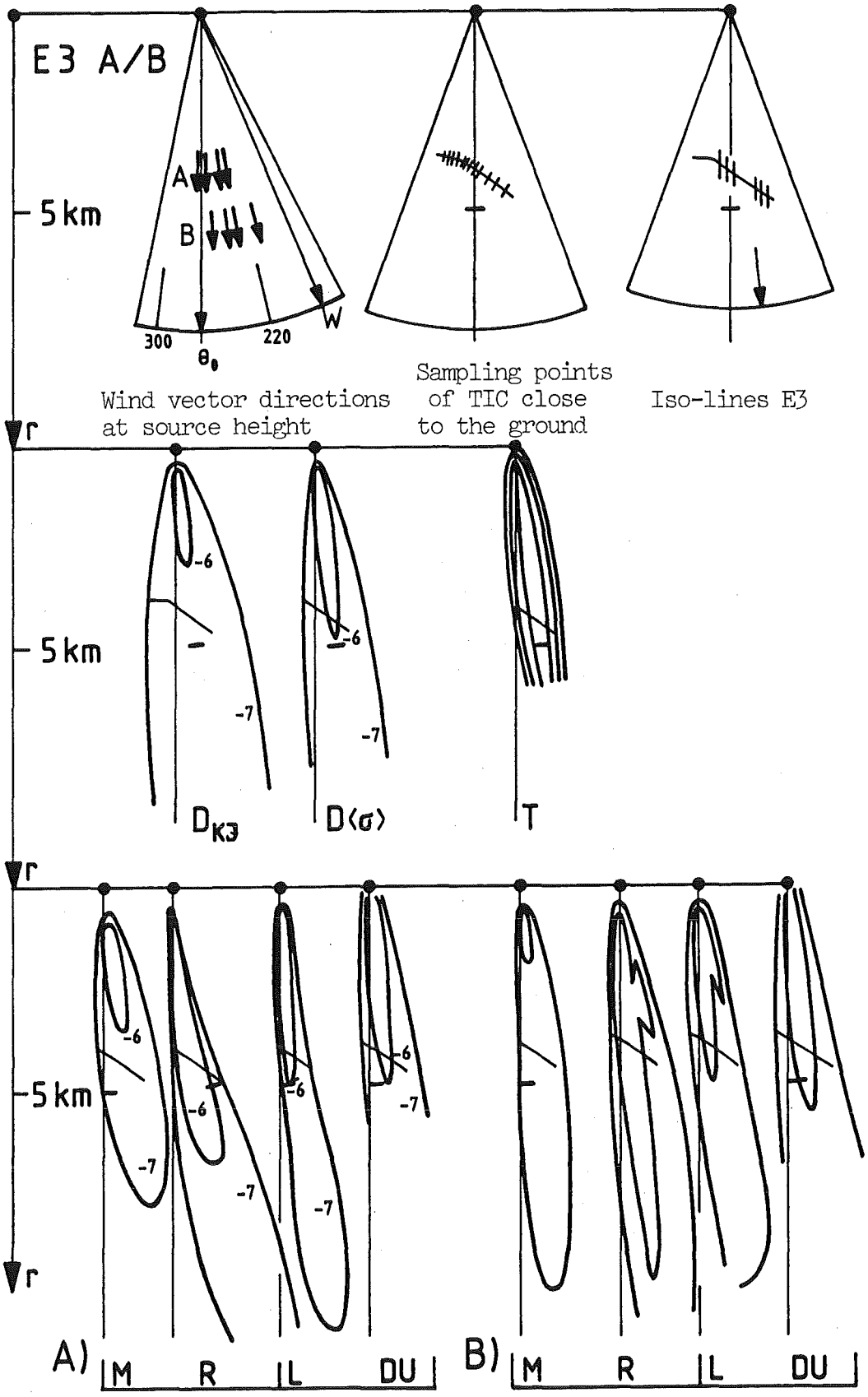

Fig.34: Iso-TIC-lines of E3 and computed results of models.

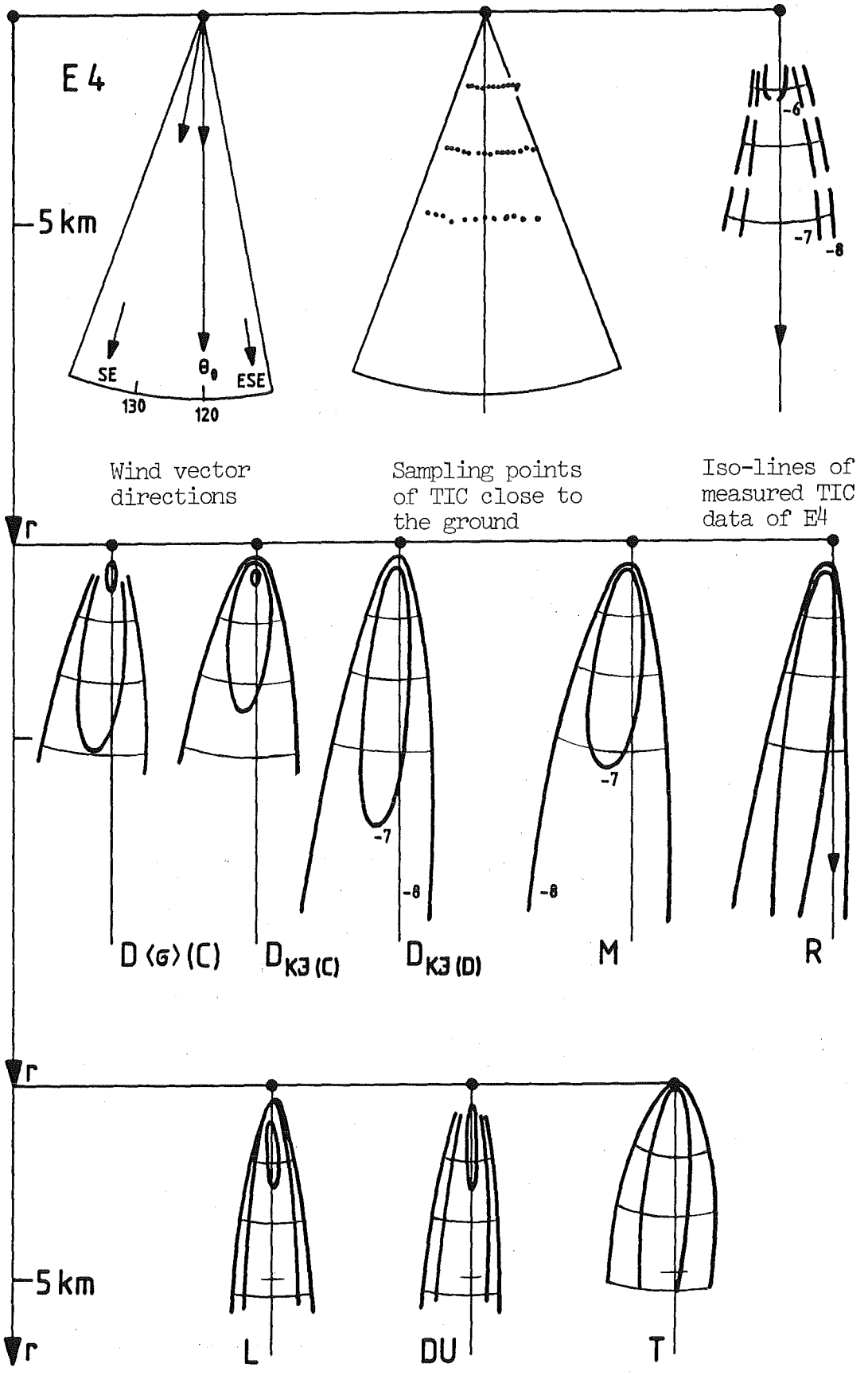

Fig.35: Iso-TIC-lines of E4 and computed results of models.

Model		E1	E2	E3		E4
DOSI	D	+8	-5	0	0	-5
MUSEMET	M	+8	-5	+3	0	-6
RIMPUFF	R	--	-2	-7	-9	-7
Lagrange	L	+10	-8	-3	0	0
Dunst	Du	+6	-4	+2	+2	-2
TRANSLOC	T	+8	-5	0	0	-5

Tab.10: Angular corrections of TIC distributions $\Delta\theta$ at ground level calculated by the different models for experiments E1 - E4.

Explanations of the angular corrections in Table 10

The $\Delta\theta$ values were determined as follows:

Figs. 32-35 present the experimental isoline representations of the TIC as well as the model results without angular corrections. The correction angles $\Delta\theta$ rotate the calculated concentration plumes around the source point into the position in which they best match the experimental concentration distributions. Systematic angular corrections were found to be necessary for the different experiments. The mean values are:

E1 : $\overline{\Delta\Theta} = +8°$
E2 : $\overline{\Delta\Theta} = -5°$
E3 : $\overline{\Delta\Theta} = 0°$
E4 : $\overline{\Delta\Theta} = -5°$

Exceptions are models L and Du, which hardly required corrections in Experiment E4, and R in Experiment E1. R requires stronger corrections in Experiment E3.

The corrections to be made for Experiment E1 show that the available wind data are not sufficiently representative of the dispersion process. The same applies to E2. In E4, the mean wind direction at source height (115 m) is displaced by about 5° with reference to the mean transport direction. Models L and Du have no angular errors since they take account of the 10m wind data.

To distinguish these errors from errors in plume shape modelling, angular corrections were carried out prior to the numerical evaluations. These corrections consisted in a shift of the "plume axes" of the calculated concentration distributions at ground level, to match with the axis of the measured concentration field. This procedure yields the angular deflections $\Delta\Theta$ (Table 10).

9.2. Further steps of evaluation

The angle-corrected concentration distributions are the basis for further evaluations, e.g. comparisons of the angular distributions of concentrations at ground level for a fixed distance from the source. Angular distribution in this context means the profile of the plume cross section in horizontal direction; in steady-state Gaussian models, this profile has the shape of a Gaussian curve. Figs. 36 - 39 show the angular distributions of experiments E1, E2, E3 A and B, E4 (fat curves) as compared with the model calculations.

The chosen distance r from the source was 2 - 3 times the distance of the concentration peak:

E1 : r = 5000 m
E2 : r = 600 m
E3 : r = 4000 - 4500 m
E4 : r = 3600 m

In analogy to the angular dependence, also the radius dependence of the concentration can be used for the comparison. In this case, concentrations "below the plume axis" are compared, i.e. concentration curves along the plume below the cross section peaks of the concentration distribution at ground level.

The matching of the concentration curves of model and experiment within the experimental error range is an essential element in the validation of a model. Figs. 40-43 present the calculated concentrations as compared with the experimental data obtained for the Batch III problems E1 - E4.

Another method of evaluation consists in plotting the measured and calculated data in "scatterplots". In this method, the measured data M_i are plotted against the calculated data R_i in a double-logarithmic representation, yielding "point clusters" (points $P_i=(M_i,R_i)$). The higher the agreement between model and experiment in the measuring range, the narrower and the closer to the 45° axis are the clusters. The number of scatterplots is quite large (number of models times number of experiments); they are presented in Figs. 44-47.

The double-logarithmic scatterplots give a good picture of the interdependence with the frequency distributions of the R/M ratio (calculated to measured value). The frequency distribution is obtained by projecting the points P onto an axis normal to the 45° line assuming different thresholds. Two different thresholds have been set in the frequency distributions in Figs. 48-51: 1. Consideration of points $P_i(M, R)$ with M and $R \geqslant 1 \cdot 10^{-9}$ m^{-3} (thin lines); 2. Consideration of points $P_i(M,R)$ with M and $R \geqslant 100 \cdot 10^{-9}$ m^{-3} (fat lines). This serves to show the contribution of the lower concentrations to the width of the frequency distributions.

Further, a purely numerical evaluation was carried out. The quantities χ^2, χ^2_{rel}, C_{corr}, and $\overline{Q}$ were calculated for each experiment and for each model. These quantities are defined as follows:

(continued on page 84)

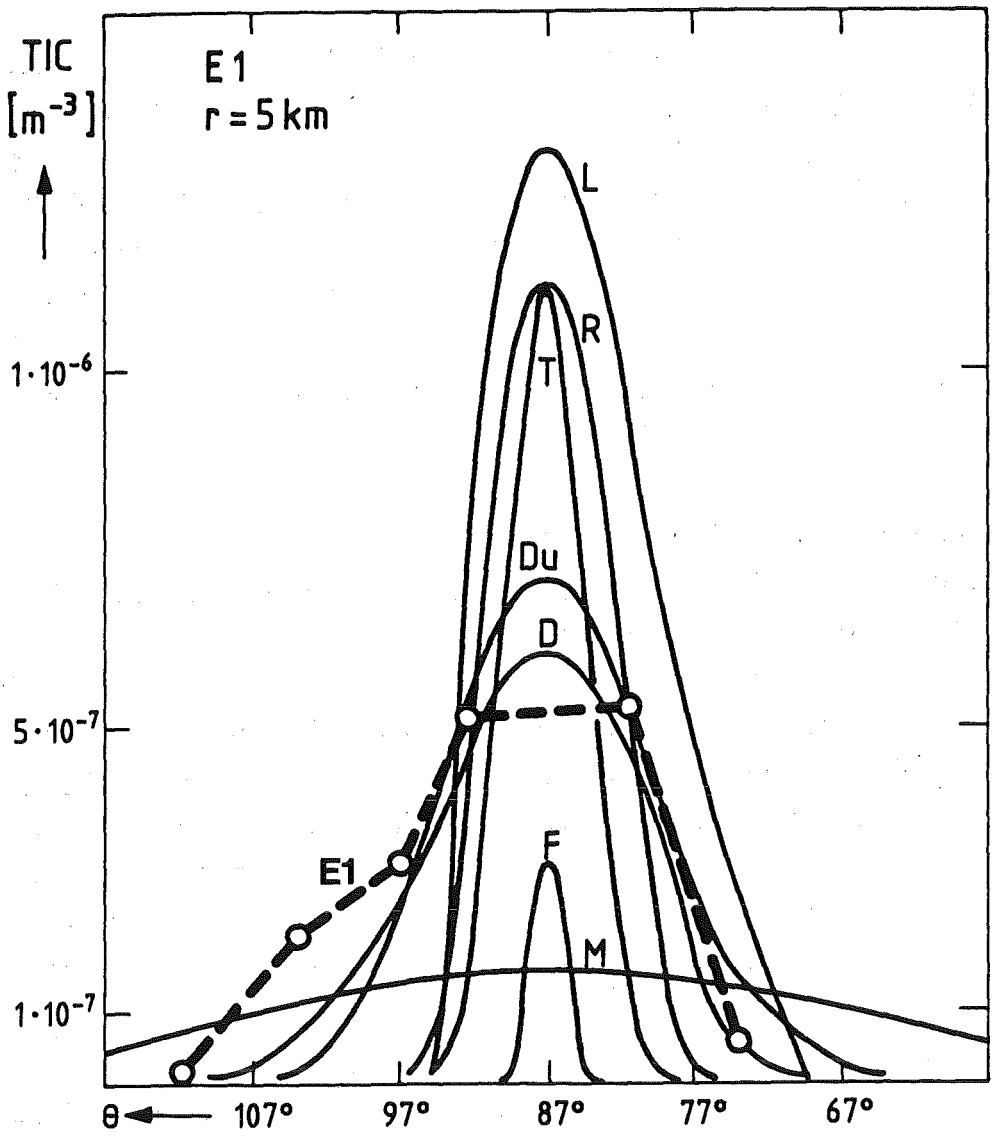

Fig.36: Angular distributions of TIC;
measured data of E1 compared with calculated
data of the models.
Source distance r = 5000m.

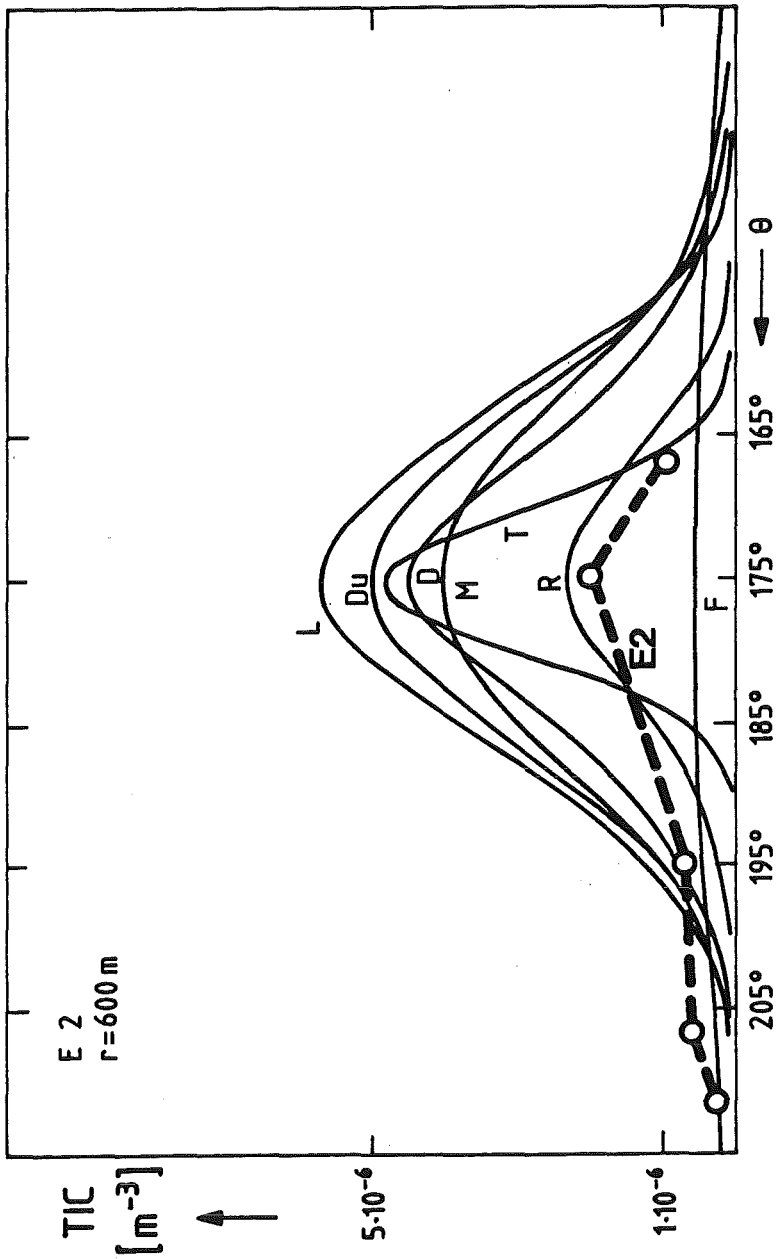

Fig.37: Angular distributions of TIC;
measured data of E2 compared with calculated
data of the models.
Source distance r = 600m.

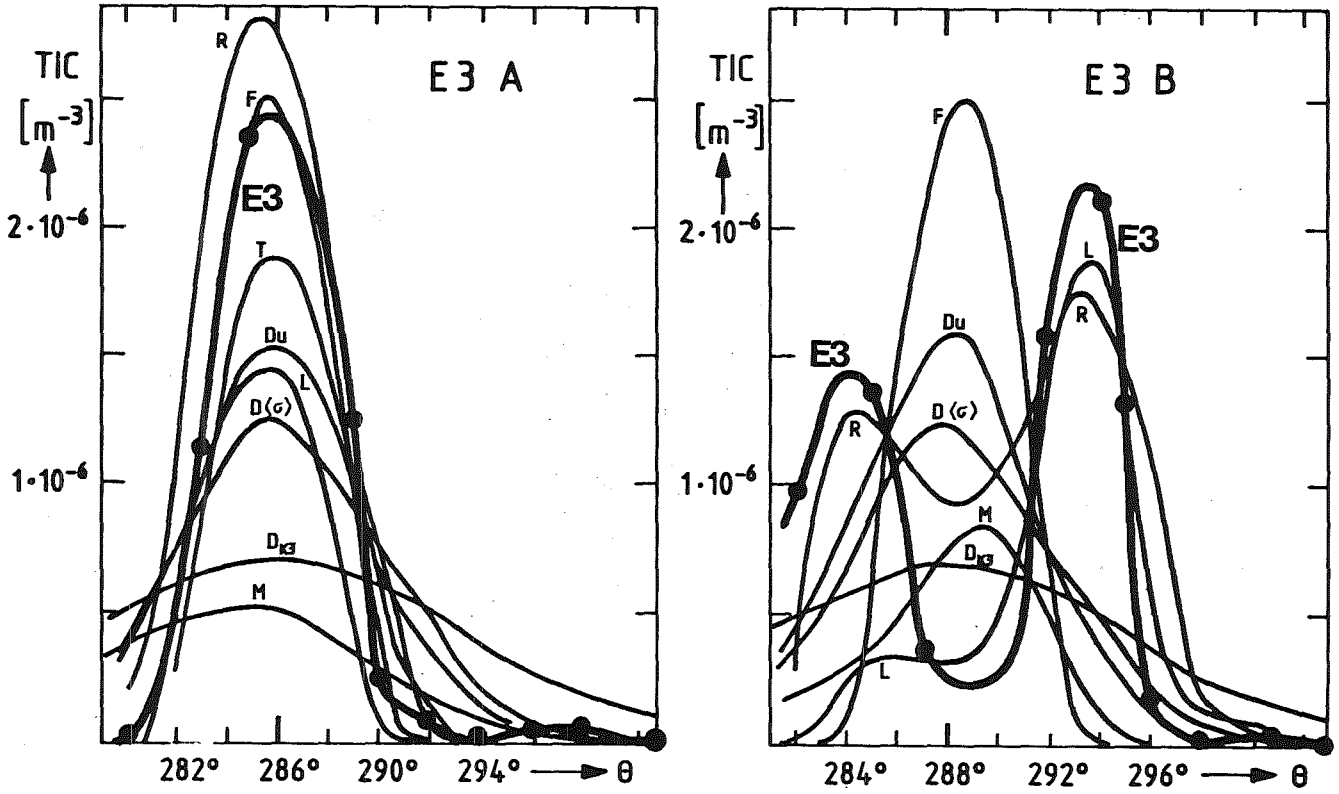

Fig.38: Angular distributions of TIC; measured data of E3/A and /B compared with calculated data of the models.
Source distance r = 3500 - 4500m

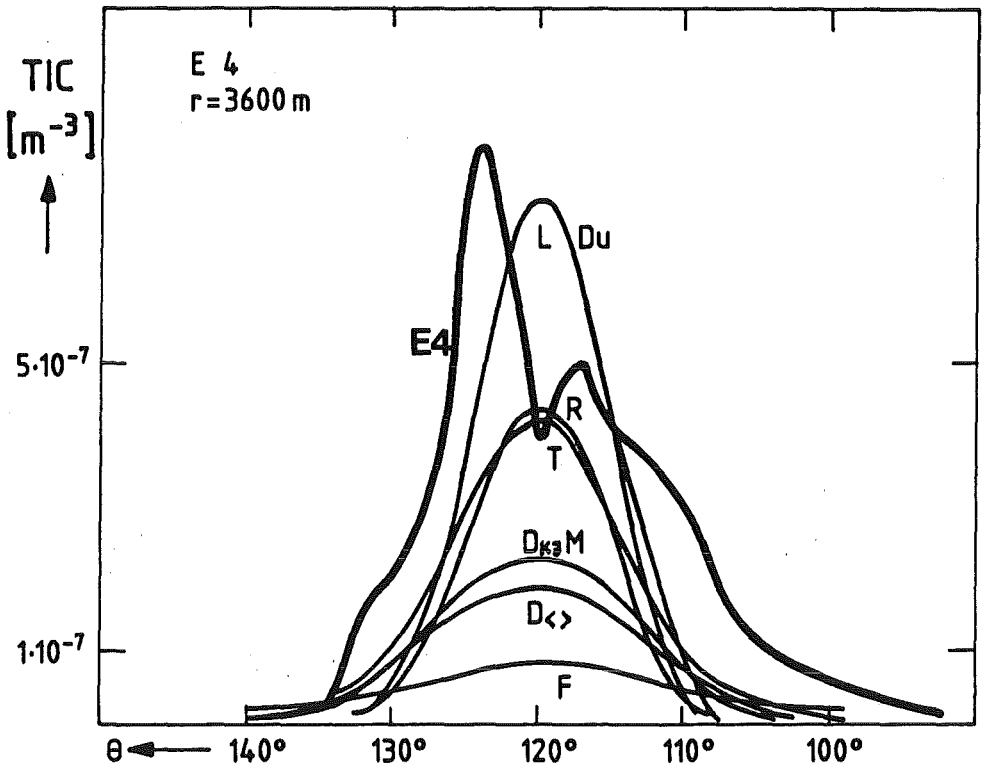

Fig.39: Angular distributions of TIC;
measured data of E4 compared with calculated
data of the models.
Source distance r = 3600m

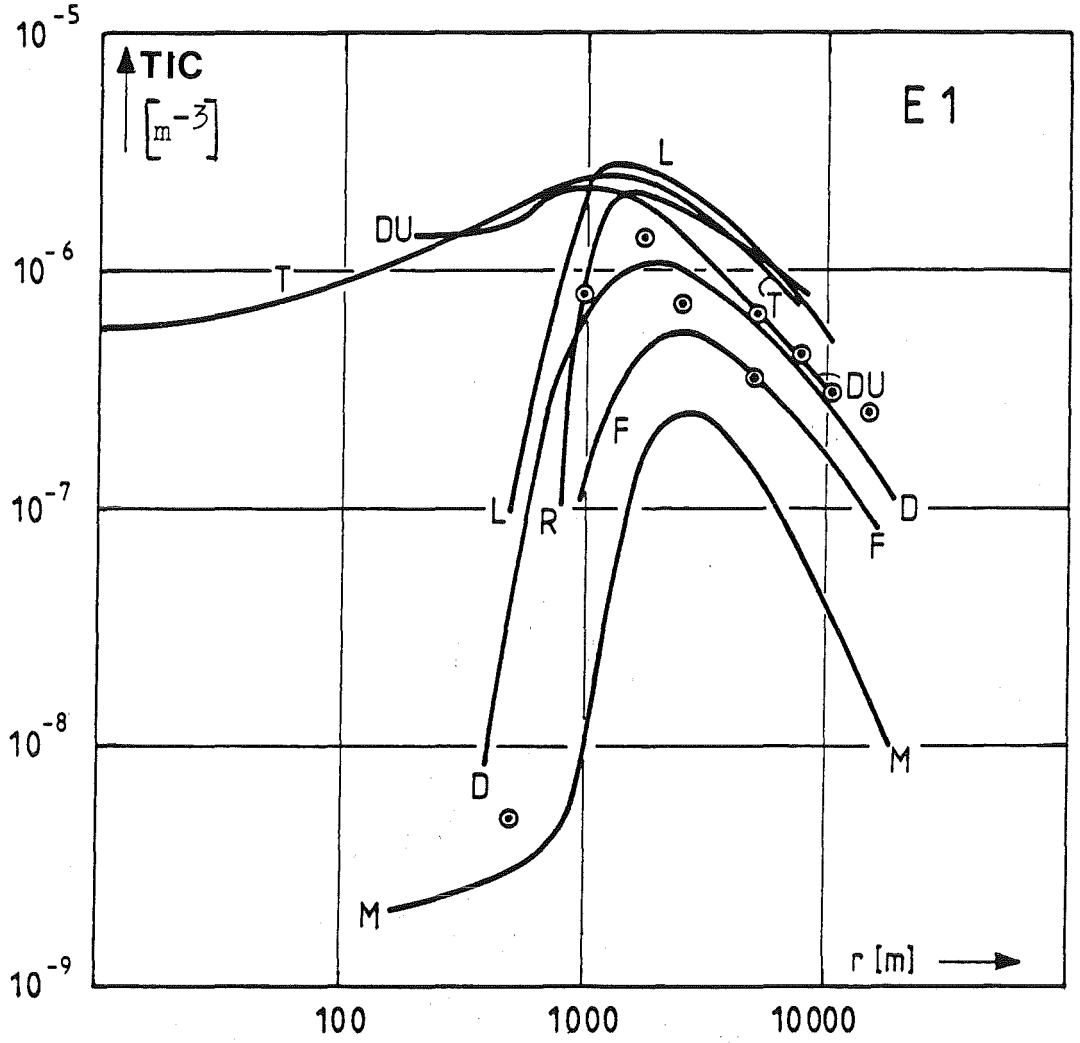

Fig.40: TIC below the plume axis versus source distance r; comparison of measured (⊙) and calculated (—) data.
Problem III, E1.

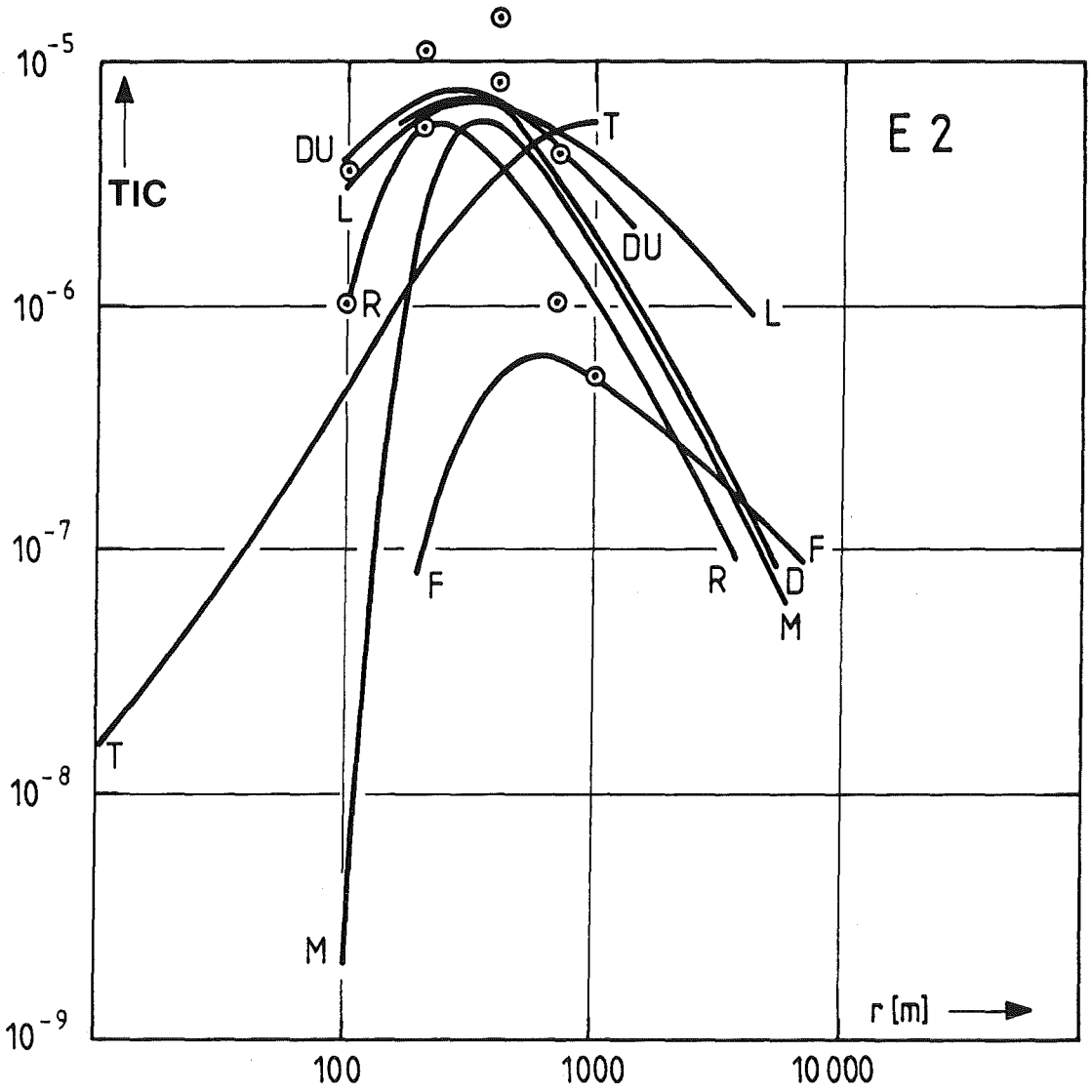

Fig.41: TIC below the plume axis versus source distance r; measured data (⊙), calculated data (—). Problem III, E2.

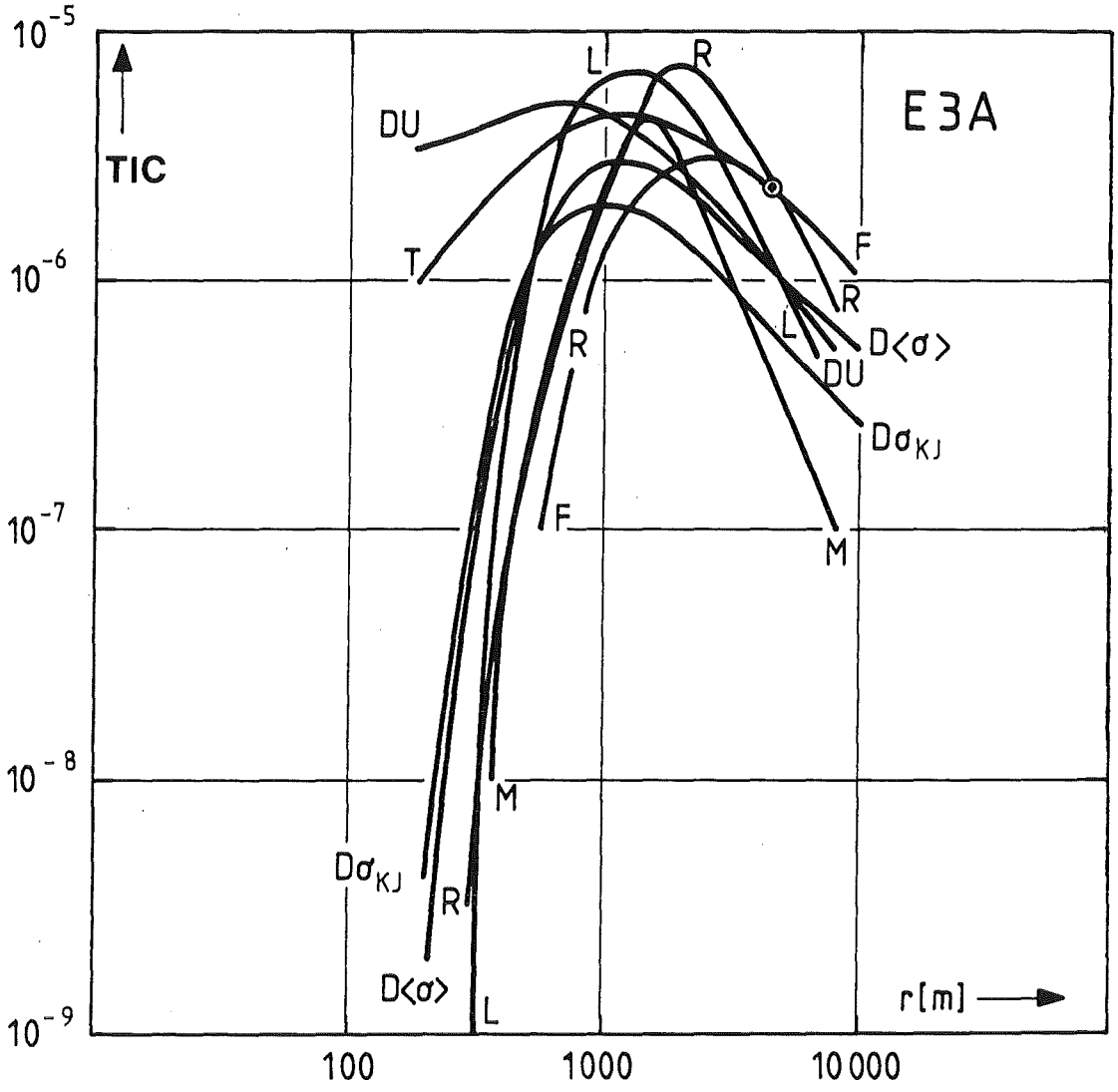

Fig.42: TIC below the plume axis versus source distance r; measured data (⊙), calculated data (—). Problem III, E3/A.

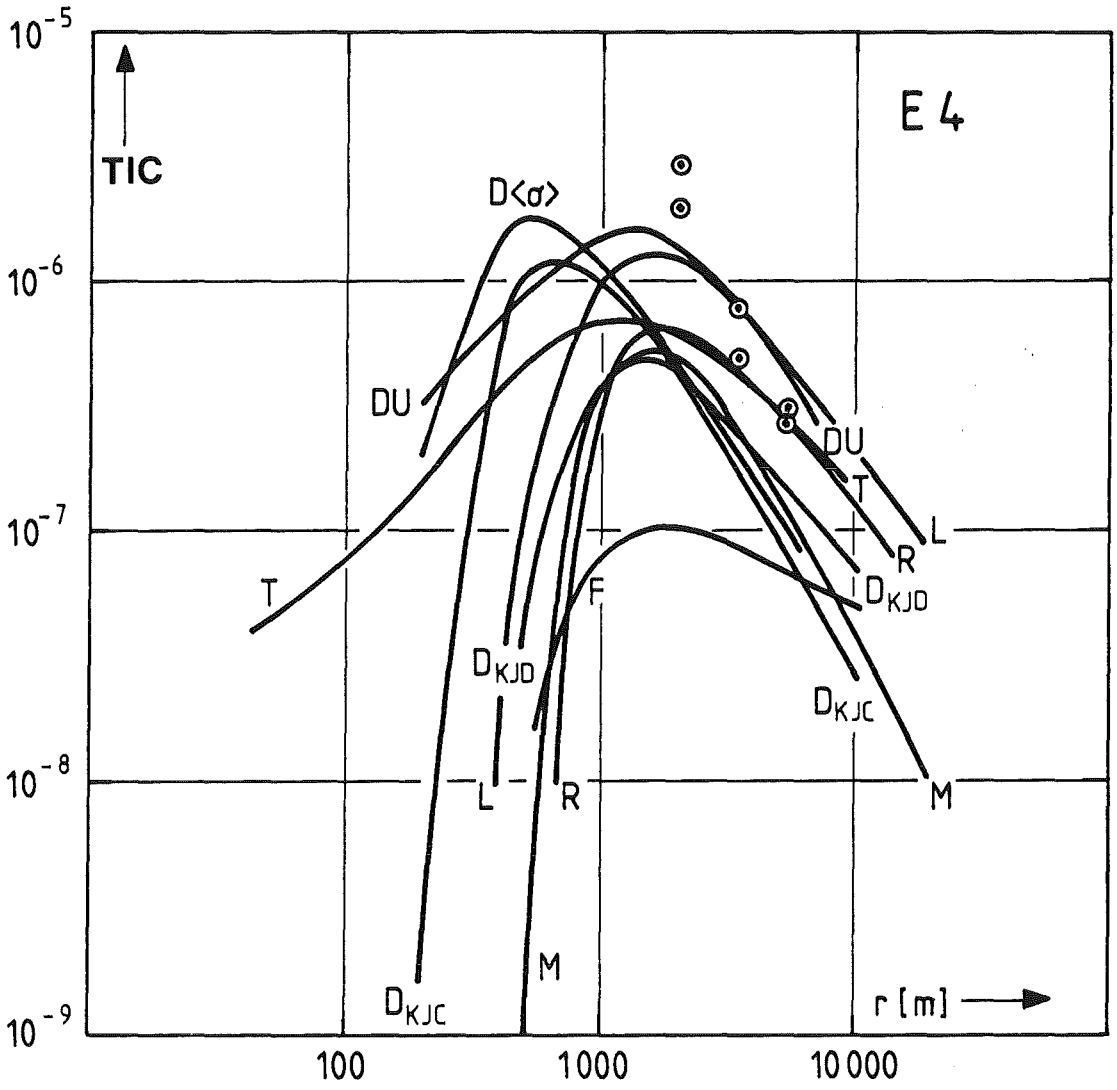

Fig.43: TIC below the plume axis versus source distance r; measured data (⊙), calculated data (—). Problem III, E4.

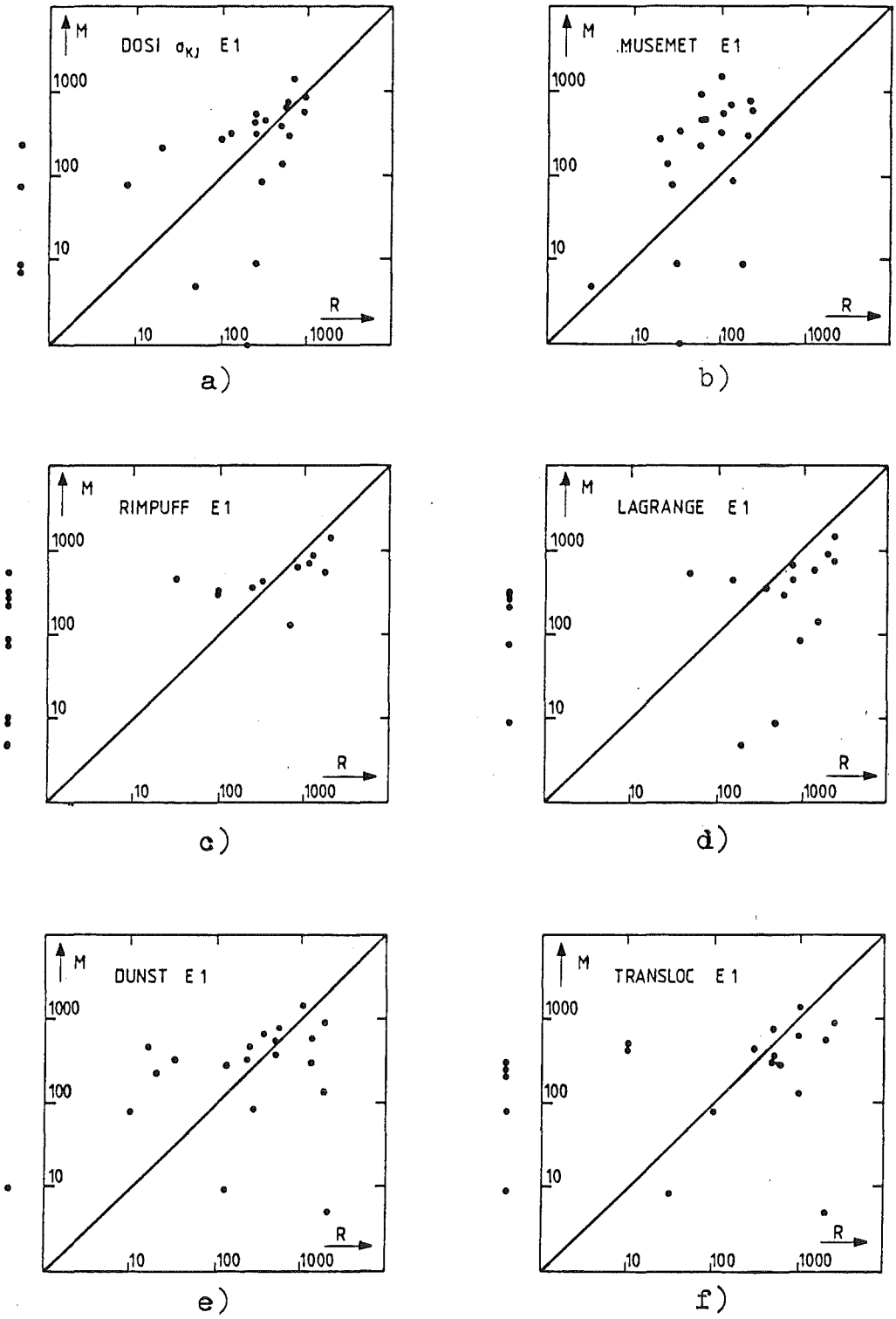

Fig.44: Logarithmic scatterplots of measured data (M) versus calculated data (R) of different models; Experiment E1.

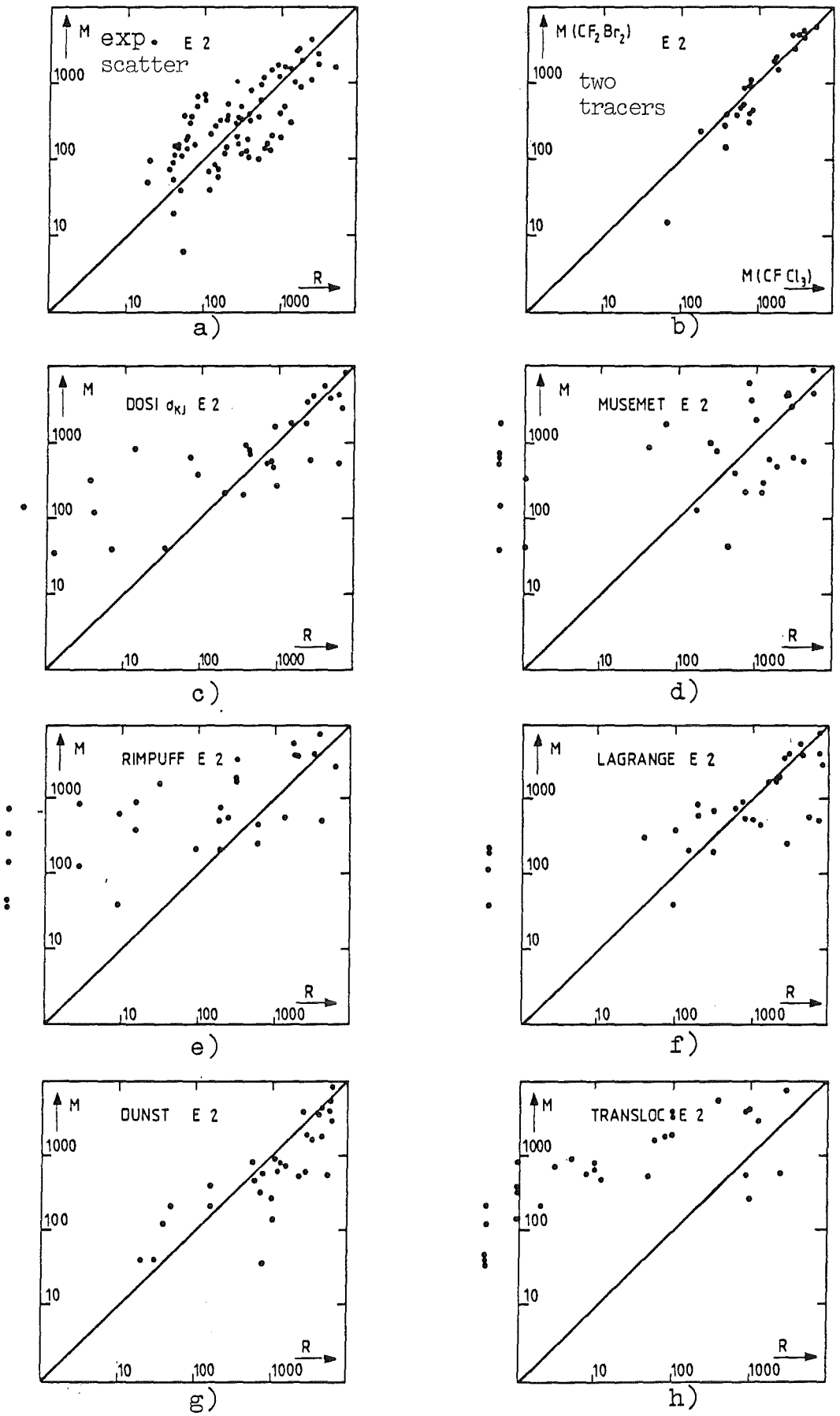

Fig.45: like Fig.44, but for Exp.E2.
a) estimated experimental scatter E2.
b) two tracers emitted during Exp.E2.

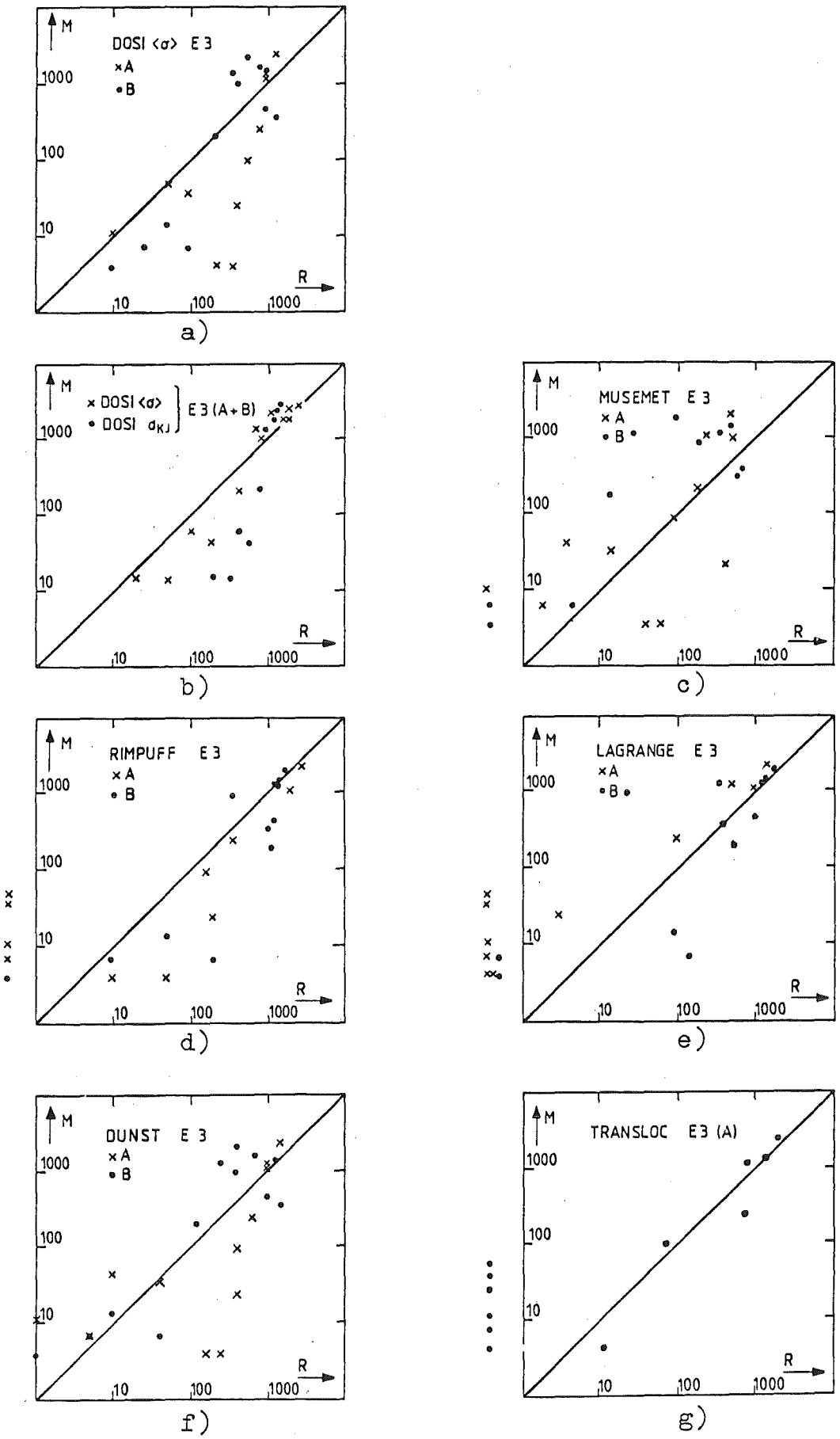

Fig.46: like Fig.44, but for Exp.E3/A and E3/B.

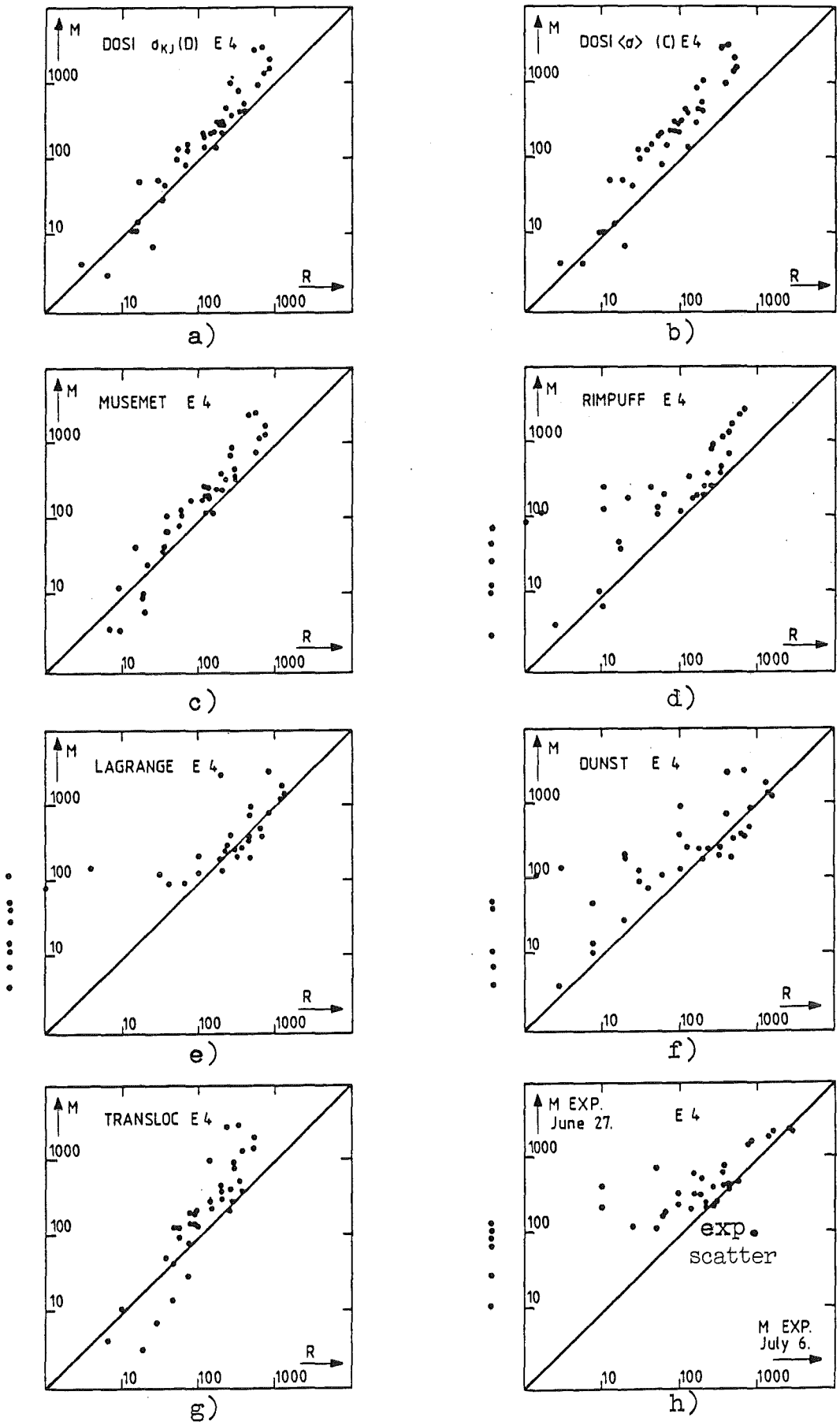

Fig.47: like Fig.44, but for Exp.E4
h) estimated experimental scatter E4.

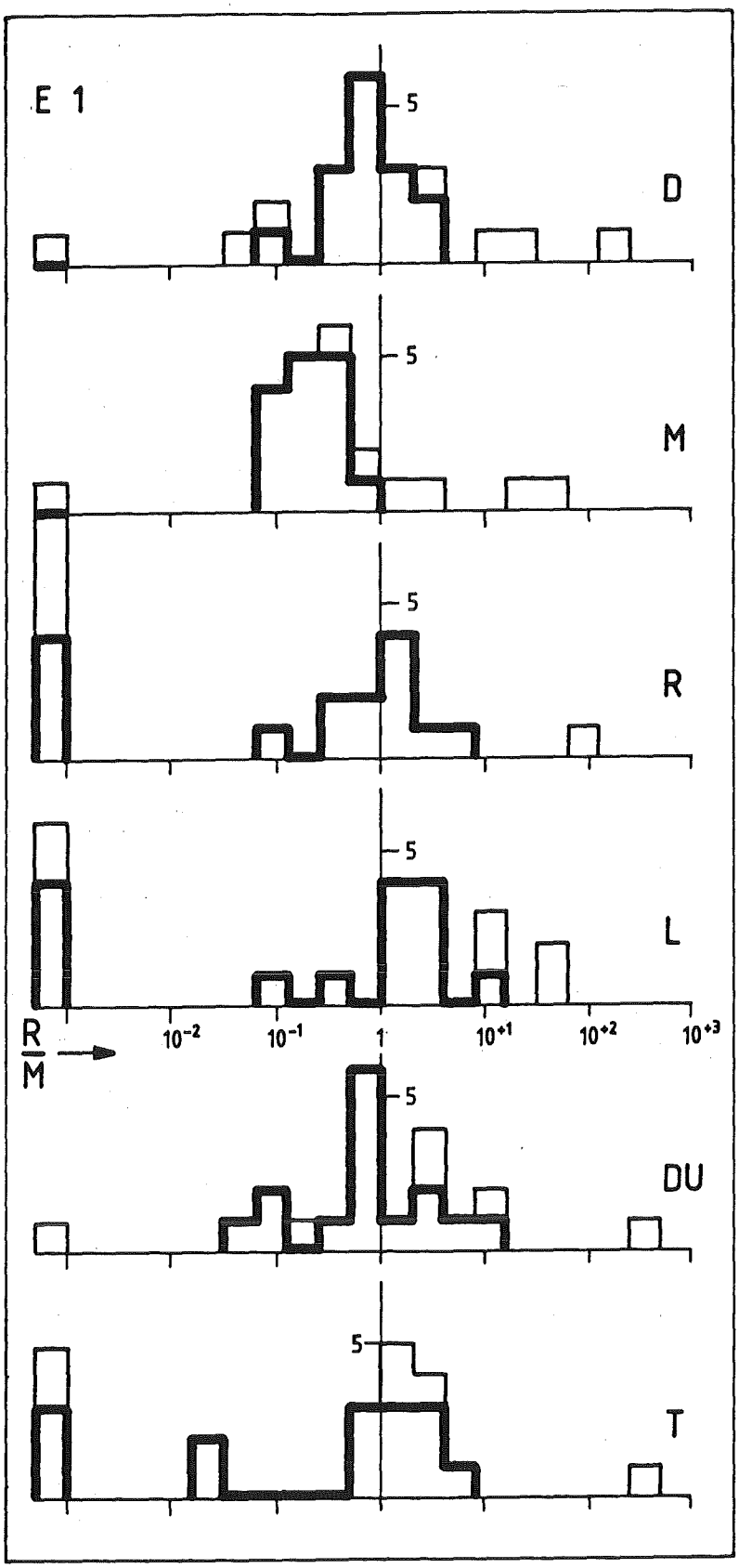

Fig.48: Frequency distributions of R/M (calculated/measured ratio); III, E1.

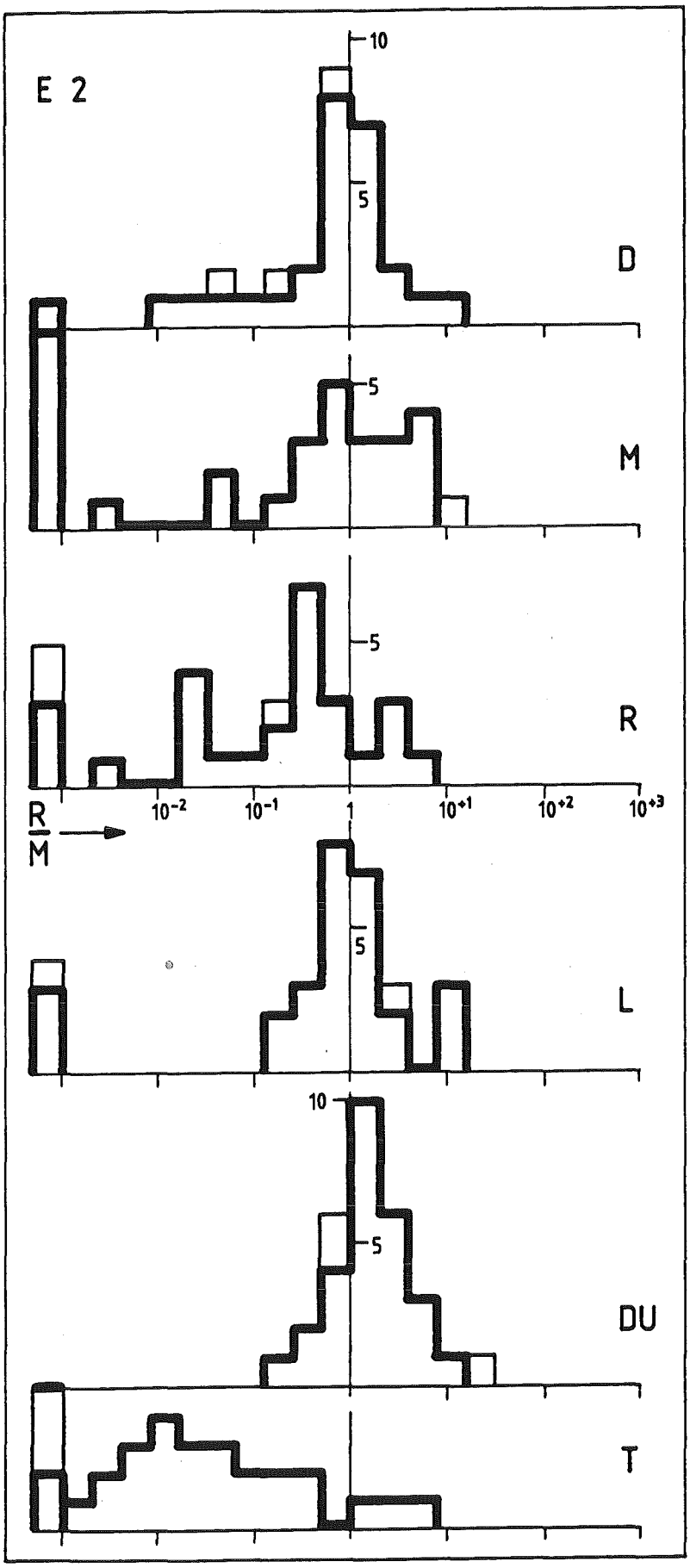

Fig.49: like Fig.48, but for E2.

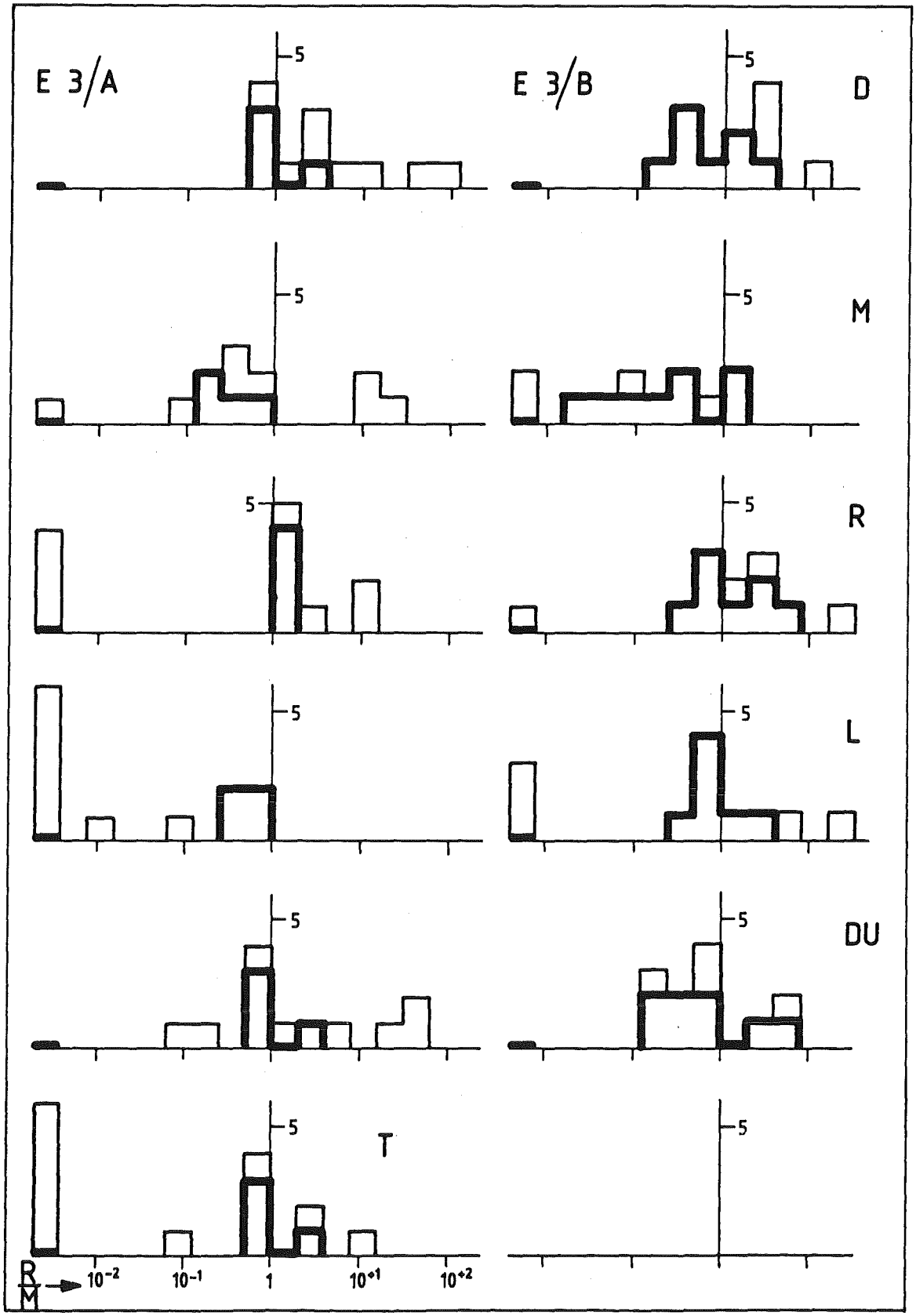

Fig.50: like Fig.48, but for E3/A and /B.

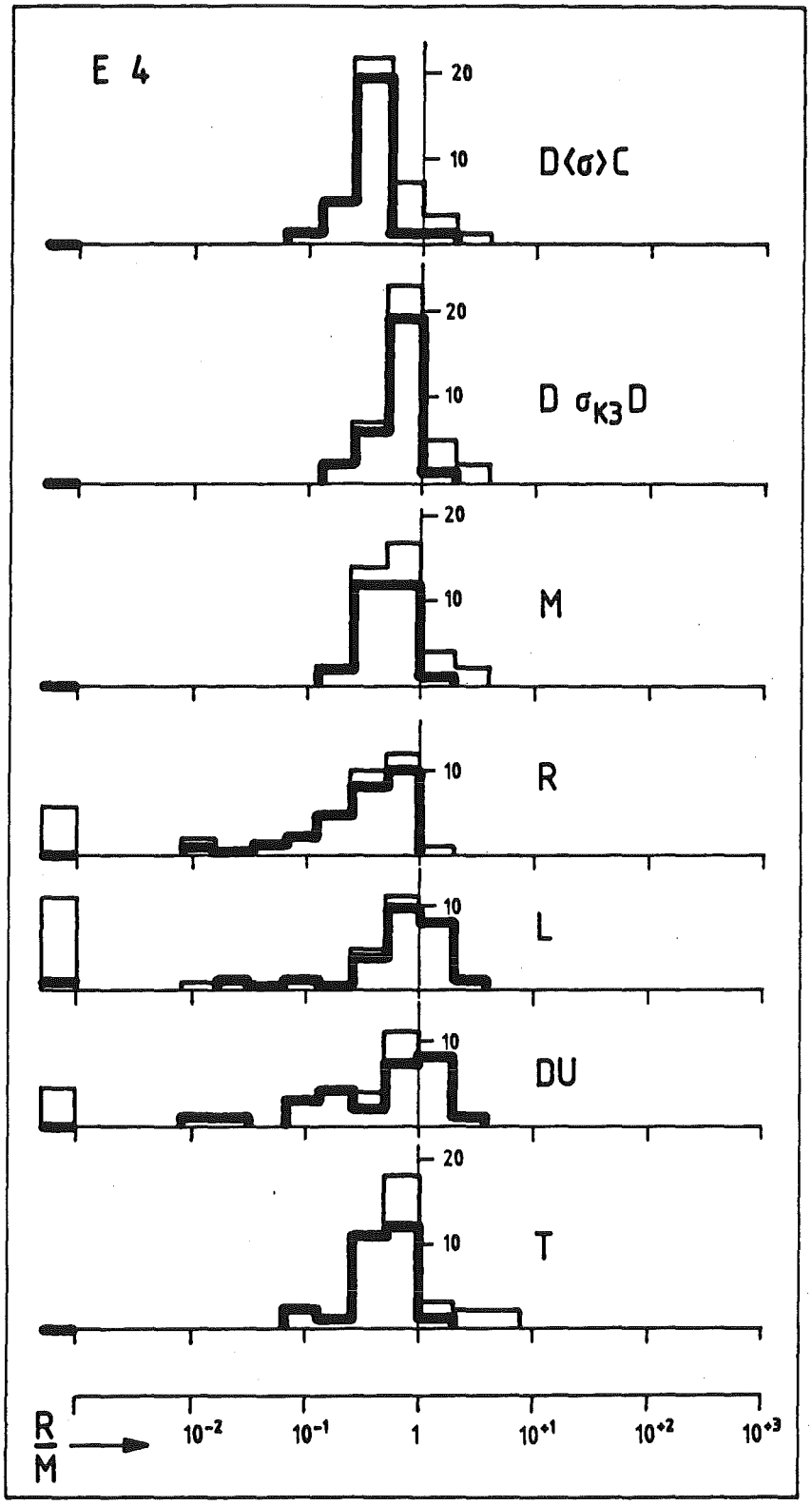

Fig.51: like Fig.48, but for E4.

Chi square:

$$\chi^2 = \frac{1}{N} \sum_{i=1}^{N} (M_i - R_i)^2$$

Relative chi square:

$$\chi^2_{rel} = \frac{1}{N} \sum_{i=1}^{N} \left(\frac{M_i - R_i}{M_i + R_i} \right)^2$$

Correlation coefficient:

$$C_{corr} = \frac{\sigma_{RM}}{\sigma_R \cdot \sigma_M}$$

$$= \frac{\frac{1}{N-1} \sum^{N} (R_i - \bar{R}) \cdot (M_i - \bar{M})}{\sqrt{\frac{1}{N-1} \sum_{i=1}^{N} (R_i - \bar{R})^2} \sqrt{\frac{1}{N-1} \sum_{i=1}^{N} (M_i - \bar{M})^2}}$$

Mean error factor:

$$\bar{Q} = \left(\prod_{i=1}^{N} Q_i \right)^{\frac{1}{N}}, \quad Q_i = \max\left(\frac{R_i}{M_i}, \frac{M_i}{R_i} \right) \geq 1$$

Chi square describes the mean square deviation between measured and calculated data. Identical differences are equally weighted, independent of whether they occur between large or small pairs of data. This flaw is remedied by the relative Chi square which weights the deviations $M_i - R_i$ by $1/(M_i + R_i)$, thus relating the deviations to the values except for $M_i \gg R_i$ or $M_i \ll R_i$. The values of χ^2_{rel} are between 0 and 1; small χ^2_{rel} means good agreement between theoretical and experimental data.

continued on page 91

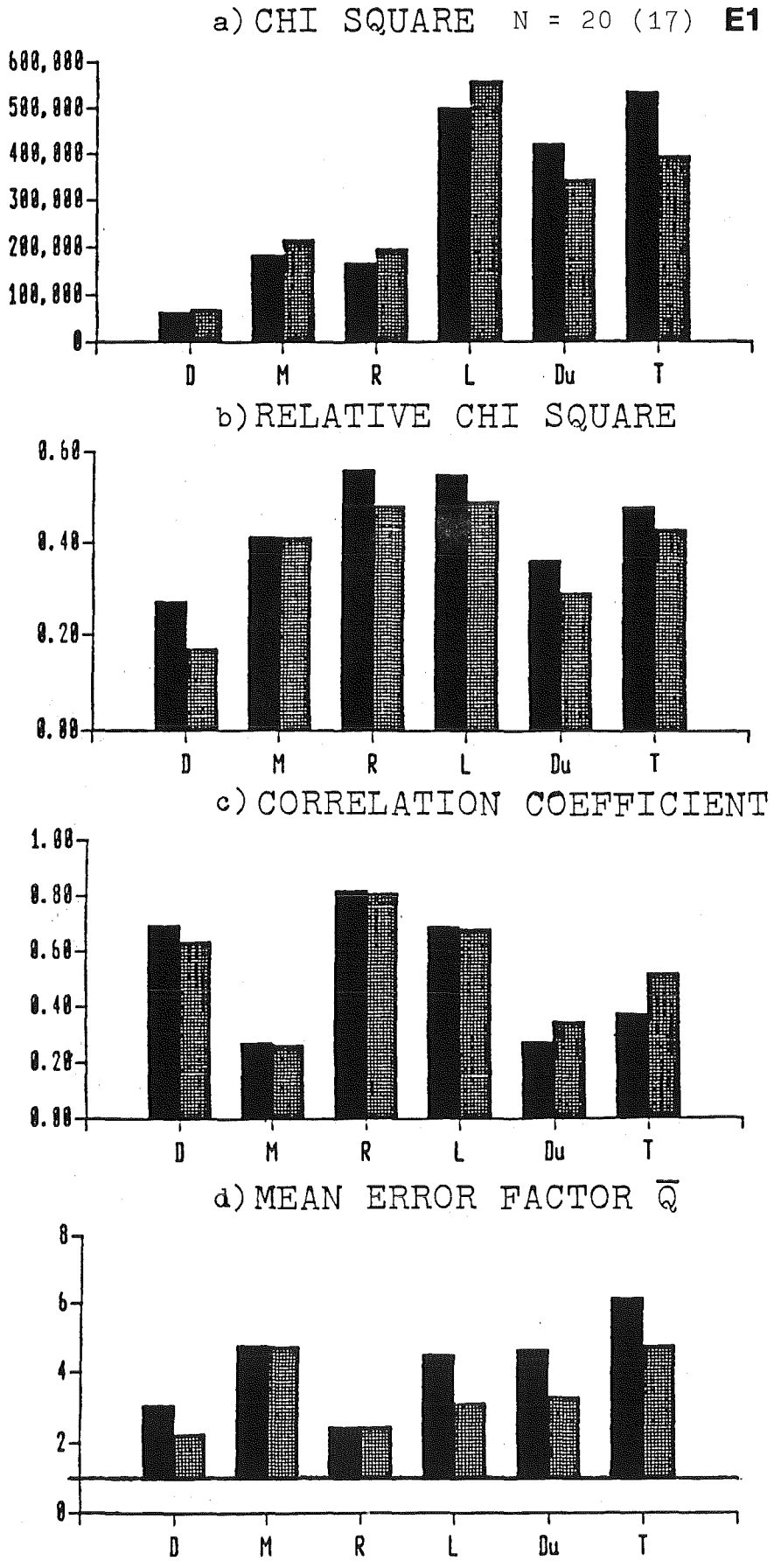

Fig.52: Results of the numerical analysis of E1 data; further information on page 90.

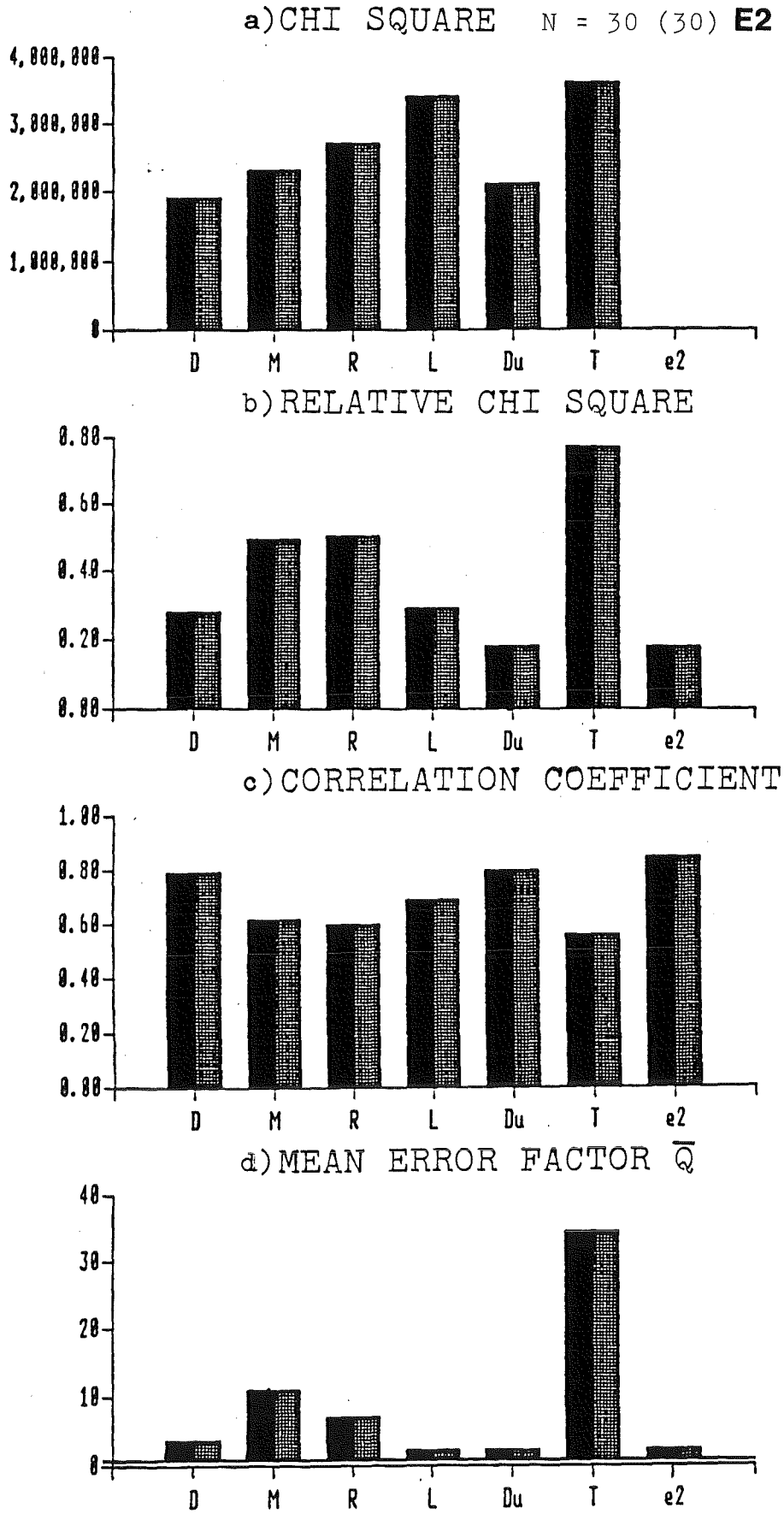

Fig.53: Results of the numerical analysis of E2 data; further information on page 90.

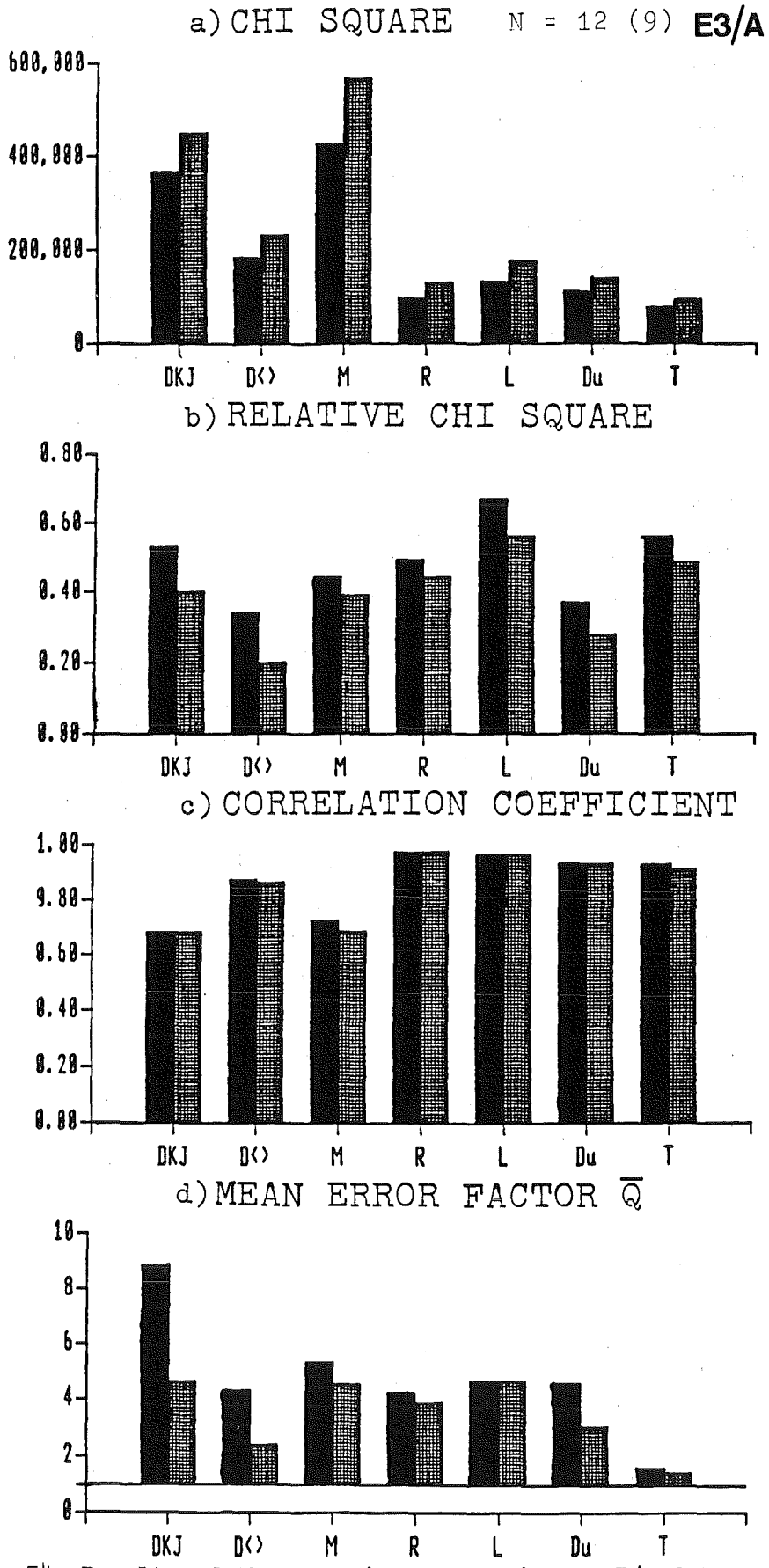

Fig.54: Results of the numerical analysis of E3/A data; further information on page 90.

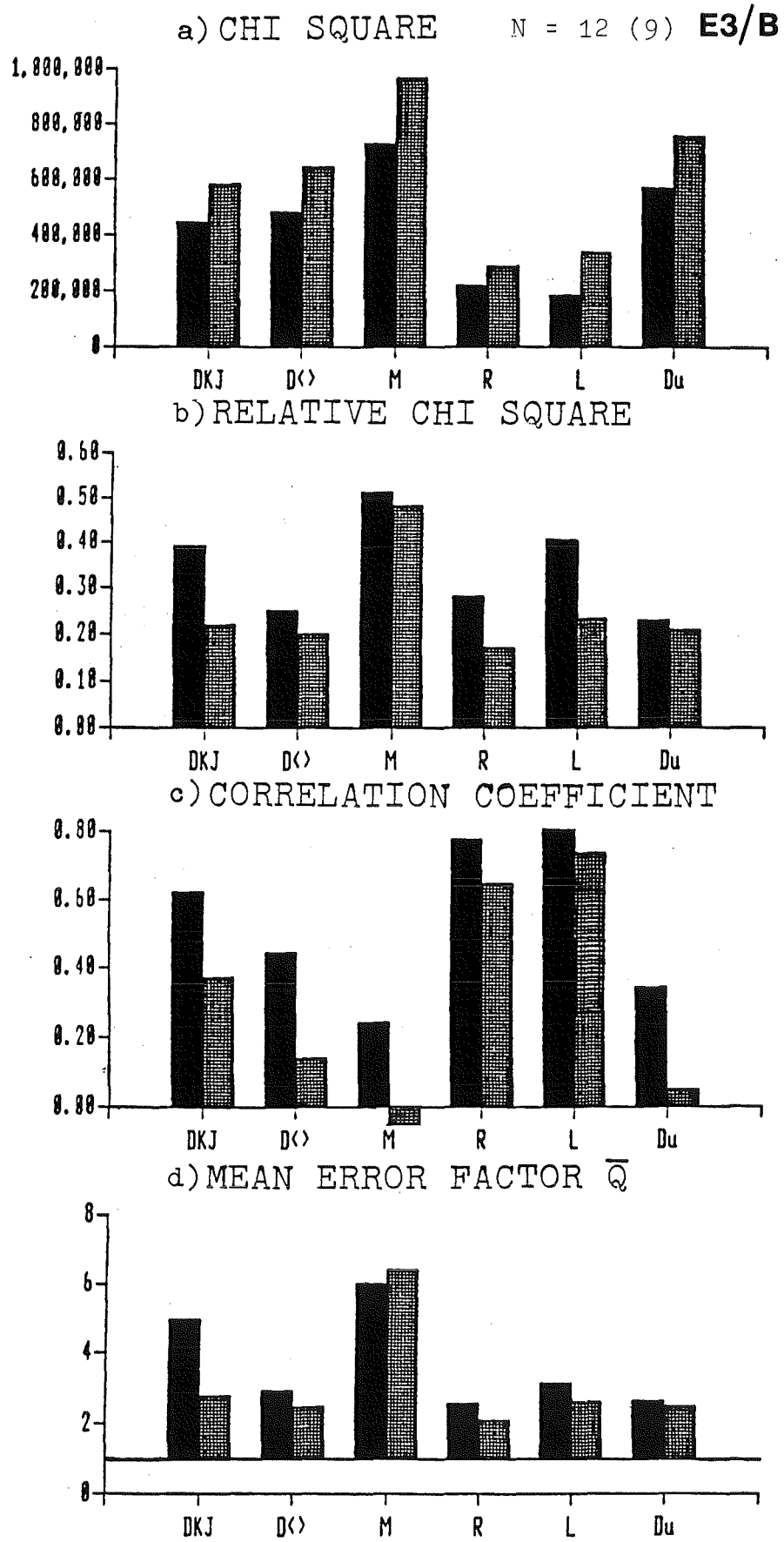

Fig.55: Results of the numerical analysis of E3/B data; further information on page 90.

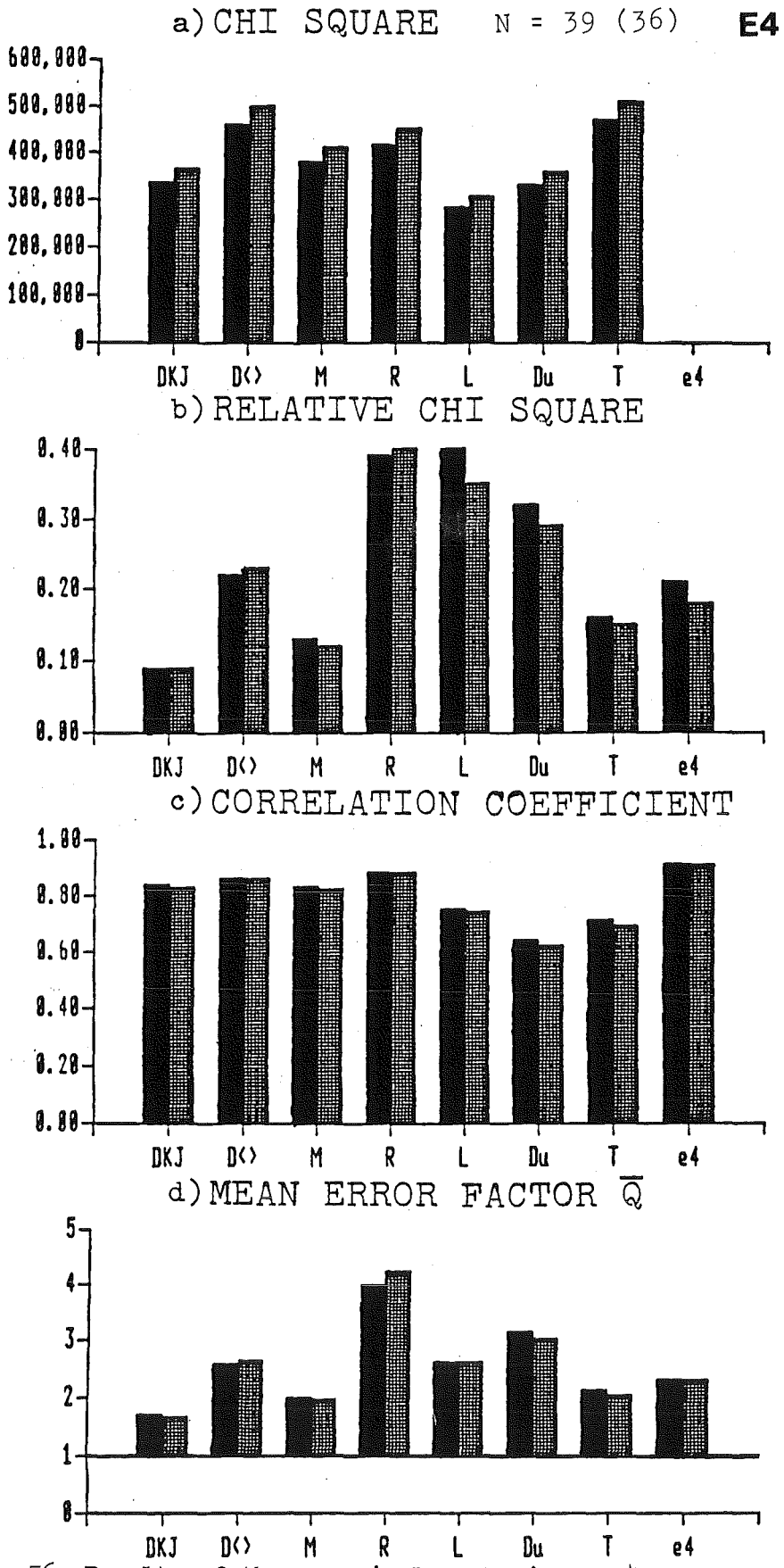

Fig.56: Results of the numerical analysis of E4 data; further information on page 90.

Explanation of Figs. 52-56:
(Results of the numerical evaluations)

The numerical evaluation of the measured and calulated data M_i and R_i was carried out with two different thresholds:

1) $M_i \geq 1 \cdot 10^{-9}$ m^{-3}: black
2) $M_i \geq 10 \cdot 10^{-9}$ m^{-3}: rastered

The data given for N on top of the figures also apply to these two thresholds. For example, N=20(17) means that 20 pairs of values (M_i, R_i) per model were evaluated for threshold 1, and 17 for threshold 2.

For the mean error factors $\overline{Q}$ (bottom of the figures), an additional joint threshold

$$(M_i, R_i) \geq 0.1 \cdot 10^{-9} \text{ m}^{-3}$$

had to be introduced because of the R_i/M_i (or M_i/R_i) ratio. With the above thresholds for M_i, this is merely an additional threshold for R_i. For N' evaluated pairs of values (M_i, R_i), $N' \leq N$ applies.

The correlation coefficient is a measure of the "proportionality" of two sets of data: If $R_i = a \cdot M_i$ for all i, a=const≠0), all values R_i will be completely correlated with M_i and $|C_{corr}| = 1$. If the linear relationship is superposed by statistical or systematic deviations, then $|C_{corr}| < 1$.

A large correlation coefficient together with a proportionality factor $a \approx 1$ means good agreement between calculated and measured data.

A further criterion for determining divergences between model and experiment is the mean error factor $\overline{Q}$. $\overline{Q}=1$ means negligible deviations while $\overline{Q}=2$ stands for error factors R_i/M_i = 2 and 1/2. The mean error factor is related to the frequency distributions of R/M: Symmetric and narrow distributions correspond to $\overline{Q}$ values of 1 and 2 while asymmetric or wide distributions have bigger $\overline{Q}$ values.

10. Estimation of typical variations in the dispersion experiments

Typical variations of the concentration field at ground level in tracer experiments with given wind and turbulence conditions at a given site are determined as follows:

Several experiments with identical source heights, integration times and similar stability, i.e. temperature gradient, wind profile, σ_θ and σ_ϕ are selected from a series of measurements made in one site.

The concentration data measured in these experiments are standardized using a factor $\overline{u}(h_s)/\dot{Q}$ in order to be independent of the mean wind velocity and emission rate.

The resulting data sets have the remaining statistical variations resulting from the variability of the turbulent dispersion processes and the limited resolution power in stability determination.

10.1 Experiment E2

Experiment E2 was carried out at Karlsruhe (Exp.31/1). Five further experiments with similar dispersion conditions were made in this campaigne: Exp. 28/1, 28/2, 31/2, 32/1, 32/2. The time-averaged dispersion data of these experiments are:

KfK-experiment no.	$\overline{\partial T / \partial z}\Big|_{30m}^{100m}$	stabil. class	$\overline{u_{60}}\ [\frac{m}{s}]$	$\overline{\sigma_\theta}(z=40m)$	$\overline{\sigma_\phi}(z=40m)$
28/1	- 1.2	C	3	20^0	13^0
/2	- 1.1	C	3	20^0	13^0
31/1 (E2)	- 1.7	C	6	15^0	10^0
/2	- 1.6	C	6	15^0	10^0
32/1	- 1.5	C	5	15^0	12^0
/2	- 1.5	C	5.5	16^0	12^0

Tab.11: Meteorological data of experiments similar to experiment E2.

From these experiments, the angular distributions of the concentration at r=500m, 1000m, and 1500m were measured along with their range of variations, and two sets of random data were

generated within these angular distribution bands. The two synthesized data sets were compared using the method of evaluation described. The results of the synthetic E2 data are presented in Figs. 45a, 57b, and 53b, c, and d.

10.2 Experiment E4:

This experiment was made at Risø (exp. of 6-7-79(1)). There was only one similar experiment in this campaign, i.e. the experiment of 27-6-79(2).

Risø; date of experiment	$\overline{\partial\theta/\partial z}$	stabil. class	$\overline{u_{100}}\ [\frac{m}{s}]$	$\overline{\sigma_\theta}$(z= 115m)	$\overline{\sigma_\phi}$(z= 115m)
1) 6.7.79 E4	- 0.4	C - D	9	8.8	4.7
2) 27.6.79	- 0.7	C - D	7.6	11.8	7.0

Tab.12: Experiment similar to E4

The data in $\overline{\partial\theta/\partial z}$ and $\overline{\sigma_\phi}$ do not agree too well; the deviations between concentration fields at ground level seem to be somewhat higher than the typical experimental variations. In order to eliminate at least the effect of the major horizontal changes of wind direction, Experiment E4/2 was corrected by adapting the width of the angular distributions to that of E4/1 by multiplying with $\overline{\sigma_\theta(1)}/\overline{\sigma_\theta(2)}$; at the same time, the height of distribution was corrected by an inverse factor to achieve mass conservation. Corrections of the concentrations at ground level with regard to σ_ϕ are not possible.

The data of E4/1 and E4/2 are presented as scatterplot in Fig. 47h, as frequency distribution of the ratio C_1/C_2 in Fig.57c, and as numerical evaluation in Figs. 56b,c, and d.

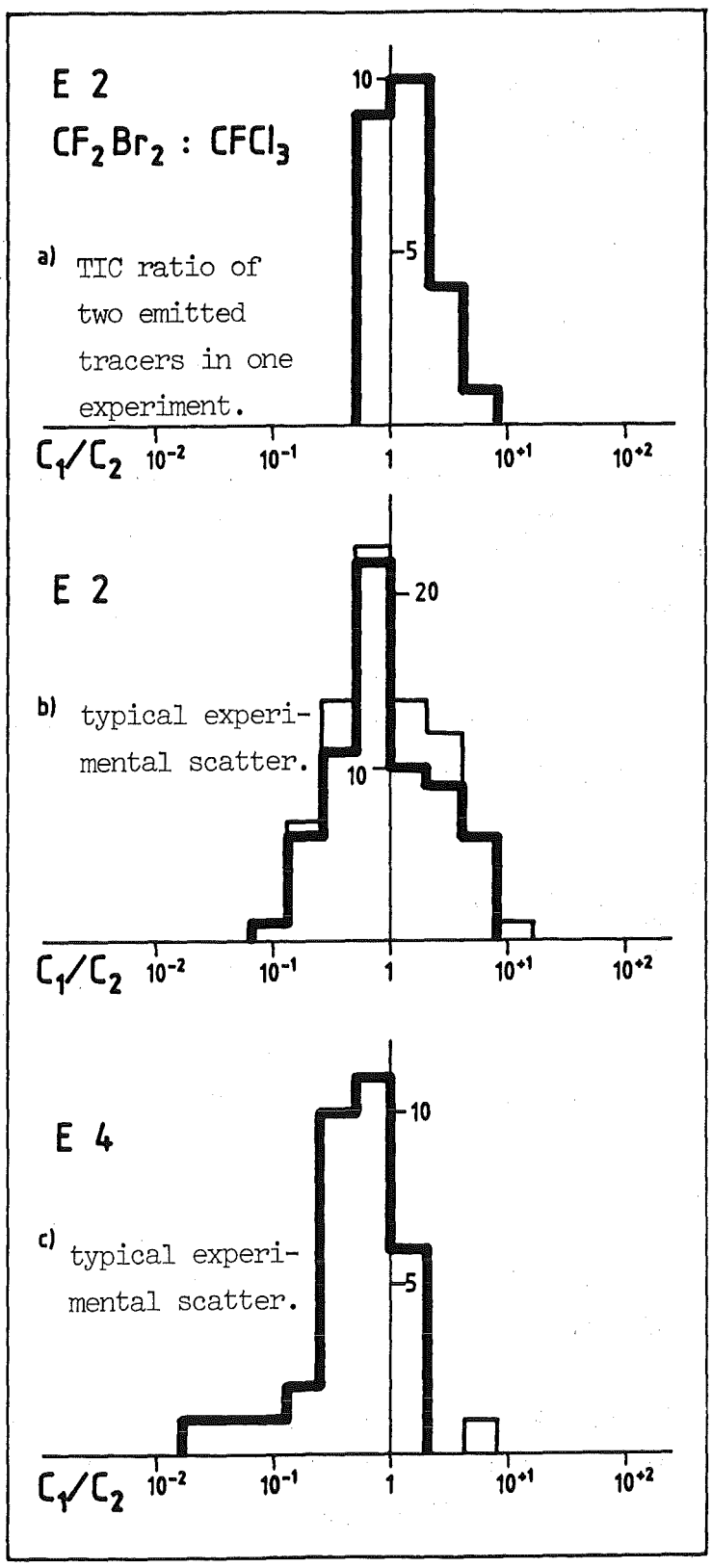

Fig.57: Experimental scatter E2 and E4.

11. Efficiencies of the models in validation problems III. E1 - E4

The above methods of evaluation provide information on the efficiency of the models in solving the problems posed in our investigation. The large number of evaluation methods is to keep the subjective factor at a minimum. In two of the problems E2 and E4, a "quality standard" is set: no model is expected to provide better results than the typical experimental variations. In the two other problems, only relative efficiencies can be determined.

The methods of evaluation were applied in the following order:

1. Visual comparison of iso concentration line representations of models and experiments (see Figs. 32-35).

2. Visual comparison of angular distributions (horizontal concentration profiles) for fixed distances from the source (see Figs. 36-39)

3. Comparison of time-integrated concentrations at ground level below the plume axis (see p.66).

4. Comparison of measured and calculated data by logarithmic plotting (see p.67). Visual evaluation of point clusters.

5. Comparison of frequency distributions of the R/M ratio (see p.67). Visual evaluation of width and location.

6. Comparison of the values of Chi square, relative Chi square, the correlation coefficient C_{corr}, and the mean error factors $\overline{Q}$ (see p.84).

This procedure was applied to all problems E1, E2, E3/A, E3/B and E4 for the models DOSI(D), MUSEMET(M), RIMPUFF(R), the Lagrangian model(L), the Dunst model(Du), TRANSLOC(T) and, to a certain extent, FOG(F).

Since the amount of data to be valuated is quite large and complex, an attempt was made to make a summary valuation of the model efficiencies with regard to the various problems.

11.1 Summary valuation of model calculations

For each of the problems E1-4 and for each model, one obtains a set of results for the above methods of evaluation. If a problem is considered to be solved "well" by a model according to a method of evaluation, a positive mark ("+") is assigned. Calculations with low agreement with the experiment get a negative mark ("-"). In the case of "fair" agreement between model and experiment, the model is marked "neutral" ("0").

Before carrying out the summary valuation, the criteria of valuation were defined for the graphical methods of evaluation (1-5) and thresholds for assigning "+", "-", and "0" were defined for the numerical method (6).

11.2 Criteria and thresholds of valuation

Method 1 (visual comparison of isoconcentration line images)
Criterion of valuation: Width, length of the isoline image, shape of lines (see Figs. 32-35)

Method 2 (Visual comparison of angular distributions) Criterion of valuation: Width, height, shape of distribution (see Figs. 36-39)

Method 3 (Comparison of TIC below the plume axis with experimental data) Criterion of valuation: Factor deviation, shape deviation as related to the experimental variation (see Figs. 40-43)

Method 4 (Scatterplots of measured and calculated data) Criterion of valuation: position of the point clusters relative to the 45° axis, width, underflow (see Figs. 44-47)

Method 5 (Frequency distribution of R/M) Criterion of valuation: peak location, width of distribution, underflow (see Figs. 48-51)

Method 6 (numerical evaluation) (see Figs. 52-56, bar charts).

a) CHI square

Here, the models can only be evaluated relative to each other. If χ^2 values differ clearly, the models with the small (large) values are given a positive (negative) mark; if the differences are small, they are marked neutral.

b) Relative CHI square

Here, fixed threshold values have been used:

$$0 \leq \chi^2_{rel} < 0.3 \quad . \; . \; . \quad "+"$$

$$0.3 \leq \chi^2_{rel} < 0.45 \quad . \; . \; . \quad "0"$$

$$0.45 \leq \chi^2_{rel} < 1 \quad . \; . \; . \quad "-"$$

In accordance with the equation

$$\chi^2_{rel} = \left(\frac{\bar{Q}-1}{\bar{Q}+1}\right)^2$$

which is valid in the case of $Q=R_i/M_i$ independent of i,

the above χ^2_{rel} threshold values have been chosen so as to match the $\overline{Q}$ threshold values given below.

c) Correlation coefficient C_{corr}

Threshold values:

$$1 \geq C_{corr} \geq 0.67 \quad . \; . \; . \; "+"$$
$$0.67 > C_{corr} \geq 0.4 \quad . \; . \; . \; "0"$$
$$0.4 > C_{corr} \quad . \; . \; . \; "-"$$

d) Mean error factor $\overline{Q}$

Threshold values:

$$1 \leq \overline{Q} < 3 \quad . \; . \; . \; "+"$$
$$3 \leq \overline{Q} < 5 \quad . \; . \; . \; "0"$$
$$5 \leq \overline{Q} \quad . \; . \; . \; "-"$$

11.3 Valuation of the models in problem E1

Problem E1 is used to illustrate the method of evaluation.

In the first step, isoline representations (Fig.32) are compared. Models D,R, and L are quite compatible with the measurements; D has the highest similarity. M has an excessive plume width, Du does not calculate a sufficiently fast decrease with longer distances, and T is too narrow. F is even narrower. The result is

Model	D	M	R	L	Du	T	F
Mark	+	-	0	0	-	-	-

The comparison of angular concentration distributions (Fig.36) results in:

M is too low and wide, F is much too narrow and low. D and Du are quite compatible with the measured data. R and T are slightly too narrow and too high. L is accurate with regard to the width of the distribution but too high by a factor of about 2.

The result is:

Model	D	M	R	L	Du	T	F
Mark	+	-	0	0	+	0	-

The comparison of concentrations below the plume axis (Fig.40) has the following results: D is best compatible with the measurements; R,L, and F diverge by a factor 2, Du and T are at least two orders of magnitude too high in the $x < 1000m$ range, M is generally too low. The result is:

Model	D	M	R	L	Du	T	F
Mark	+	-	0	0	-	-	0

This is followed by a comparison of the scatterplots of measured and calculated data (Fig.44).

Here, D is close to the 45°axis at high values, while there are only few low values outside the represented range (underflow). Du has higher scatter but less underflow. R has little scatter at high values but much underflow. L is similar to R but with higher scatter. T has very high scatter but exhibits aggregation near the axis at high values. M has a strongly scattered, asymmetric aggregation of points. The result is:

Model	D	M	R	L	Du	T
Mark	+	-	0	0	+	0

Comparison of frequency distributions of the R/M ratio (Fig. 48):

D and Du are central, with slight scatter and little underflow. R and L have higher scatter and much underflow. The distribution of M is displaced. T has high scatter and much underflow. The result is:

Model	D	M	R	L	Du	T
Mark	+	-	0	0	+	-

Results of the numerical evaluation (see Fig. 52 and definition of thresholds on p.97):

MODEL:	D	M	R	L	DU	T	F	
CHI-SQUARE	+	0	0	-	-	-		
REL.CHI-SQ.	+	0	-	-	0	-		E1
CORR.-COEF.	+	-	+	+	-	-		
ERROR FACT.	+	0	+	0	0	-		

Tab.13 is completed by the above valuation results:

ISO-LINES	+	-	0	0	-	-		
ANGUL.DISTR.	+	-	0	0	+	0	-	
PLUME AXIS	+	-	0	0	-	-	0	E1
SCATTERPLOT	+	-	0	0	+	0		
R/M-DISTR.	+	-	0	0	+	-		
TOTAL E 1:	+	-	0	0	0	-	-	

The comprehensive table shows that model D is quite successful in modelling the experimental data of E1 while models M, T and F diverge grossly. F was not completely evaluated but the results would have been similar to T.

Models R, L, and Du yield average results.

11.4 Interpreation of the results obtained for problem E1

The good results of the Gaussian model (DOSI) after an angular correction of the direction of the plume axis by $+8^{\circ}$ are based on two factors:

1. The dispersion conditions of experiment E1 are not too complex; the topographic and meteorological conditions are homogeneous and steady, and the source is not located at ground level but at a height of 100m.

2. The model uses the Karlsruhe-Jülich σ parameters; these are based on measuring compaigns which comprise Experiment E1, i.e. the σ parameters are optimally chosen for the purpose.

The poor results of the Gaussian volume source model M (MUSEMET), according to its authors, result from a nonadequate conversion of the measured σ_θ data of the vector wind vane at a height of 120m. The resulting plume is far too wide and has too low maximum concentration. This is not a general failure of the model but a parameter error in plume width modelling.

The results of R (RIMPUFF), L (Lagrangian), and Du (Dunst) are compatible with the measurements as far as the plume width is concerned. Differences occur in the concentrations at ground level. The divergence from the experimental values results from the modelling of vertical turbulent transport. With other

parameters, RIMPUFF (Gaussian puff model) would have yielded comparable or even more accurate results than DOSI. The same applies to models L and Du.

T (TRANSLOC) yields generally too high and too narrow concentration distributions for problem E1. Both horizontal and vertical turbulence are not modelled in accordance with the situation of the experiments were entered only indirectly in TRANSLOC, which caused an axially symmetric plume.

F (FOG) results in too low and very narrow distributions, as can be seen from the angular distributions (Fig.36). For an explanation of this behaviour, see comments on the solutions to the Batch I problems (p.42).

11.5 Valuation of the models in problem E2

The data of experiment E2 are best modelled by the models D (DOSI), Du (Dunst), and L (Lagrangian). This results not only from the general valuation in Table 14 but also from the scatterplots (Fig. 45). Only the point clusters of models D, L and Du correspond to the typical experimental scatter (Fig.45a) with regard to their location and shape. This is clearly indicated also by the R/M ratio (Figs. 49 and 57b).

The results of the numerical evaluation (Fig.53) confirm these observations.

Tab.14: valuation table E2

MODEL:	D	M	R	L	DU	T	F	
ISO-LINES	+	+	0	-	0	-		
ANGUL.DISTR.	0	0	-	+	+	-	-	
PLUME AXIS	+	0	+	+	+	-	-	
SCATTERPLOT	+	0	0	+	+	-		
R/M-DISTR.	+	0	0	+	+	-		**E2**
CHI-SQUARE	+	0	0	-	+	-		
REL.CHI-QU.	+	-	-	+	+	-		
CORR.-COEF.	+	0	0	+	+	0		
ERROR FACT.	+	-	-	+	+	-		
TOTAL E 2:	+	0	0	+	+	-	-	

In DOSI, the Karlsruhe-Jülich σ parameters were used again. As in problem E1, these parameters were derived from measuring campaigns comprising Experiment E2. This explains the good results of DOSI.

In the case of L and Du, one should note that the measured and calculated values agree only near the source in the range $r \leq 600$m, where most of the measuring points are located. If the isoline representations of the two models are compared with those of Experiment E2 (Fig.33). The concentrations have a wider radial range with L and Du.

With regard to this criterion, M (MUSEMET) and R (RIMPUFF) have better results than L and Du.

T (TRANSLOC) and F(FOG) do not give an accurate representation of the concentration distribution of Experiment E2. T calculates a plume too narrow (see isolines and angular distributions E2, Figs. 33 and 37) and a strongly divergent curve for the concentrations below the plume axis (Fig.41). Similar results are achieved by the scatterplot (Fig.45h), the frequency distribution of R/M (Fig.49), and the numerical evaluation (Fig.53a-d).

F calculates a plume which is too wide (Fig.37), leading to much too low concentrations at ground level.

In F and in T, the problems result from the modelling of vertical and horizontal diffusion, as has already been shwon in Batch I.

11.6 Valuation of the models in the problems E3

The data of Experiment E3, A and B, differ from those of the other experiments in that they were obtained from a single measured angular distribution at a distance r=3700-4500m from the source, so that radial dependences and plume shapes cannot be compared.

The main criterion of valuation therefore is the degree of correspondence between the calculated and the measured angular distributions (Figs. 38a,b).

11.6.1 Problem E3/A

As can be seen in Fig.38a, the distributions calculated by R, T, and F match best with the distribution measured in Experiment E3/A.

D(KJ) and M calculate much too wide and low distributions.

The results of D⟨σ⟩, L and Du show average agreement with the measured data.

The result is:

Model	D(KJ)	D⟨σ⟩	M	R	L	Du	T	F
Mark	-	0	-	+	0	0	+	+

If the other methods of evaluation are considered as well (without isolines and concentrations below the plume axis), the following valuation table is obtained for problem E3/A:

MODEL:	DKJ	D<>	M	R	L	DU	T	F	
ISO-LINES									
ANGUL.DISTR.	-	0	-	+	0	0	+	+	
PLUME AXIS									
SCATTERPLOT	-	0	-	0	-	0	0		
R/M-DISTR.		0	0	0	-	+	0		**E3/A**
CHI-SQUARE	-	0	-	+	+	+	+		
REL.CHI-SQ.	-	0	0	-	-	0	-		
CORR.-COEF.	+	+	+	+	+	+	+		
ERROR FACT.	-	0	-	0	0	0	+		
TOTAL E3A:	-	0	-	+	0	+	+	+	

Tab.15

The overall evaluation of this table differs hardly from the evaluation based on angular distributions.

11.6.2 Interpretation of the results obtained for problem E3/A

Owing to the short roughness length z_o=0.2m, the Gaussian model D with Karlsruhe-Jülich σ parameters calculates too wide angular distributions. If the concentration distributions of the two half-hour experiments E3/A and E3/B are superposed and the result is compared with the distribution of D$\langle\sigma\rangle$ (Scatterplot Fig. 46b), the calculations are found to be in good agreement with the measurements.

The good results of T and F in this case are partly explained by the fact that models T and F always calculate very narrow distributions for near-neutral conditions (see Fig.12c). Experiment E3/A is the only experiment with a narrow plume.

11.6.3 Problem E3/B

This part of Problem E3 clearly illustrates the advantage of dispersion models taking account of the changes of wind direction with time during the dispersion process. In principle, models M,R,L,Du and T should be capable of doing this, but only models R and L were successful. Fig.38a clearly shows that the double peak of the measured distribution was modelled only by these two models.

M uses too large σ_θ values, so that the influence of changes in wind direction is hidden. Du and T use too rough spatial and time averages so that the structure of the angular distribution cannot be resolved.

The valuation on the basis of angular distributions is:

Model	D(KJ)	D⟨σ⟩	M	R	L	Du	T	F
Mark	-	-	-	+	+	-	-	-

The overall valuation considering all methods of evaluation (again without isolines and concentrations below the plume axis), is:

MODEL:	DKJ	D<>	M	R	L	DU	T	F	
ISO-LINES									
ANGUL.DISTR.	-	-	-	+	+	-	-	-	
PLUME AXIS									
SCATTERPLOT	-	0	-	+	+	0			
R/M-DISTR.		+	-	+	+	0			**E3/B**
CHI-SQUARE	0	0	-	+	+	0			
REL.CHI-SQ.	0	+	-	+	0	+			
CORR.-COEF.	0	0	-	+	+	0			
ERROR FACT.	0	+	-	+	0	+			
TOTAL E3B:	-	0	-	+	+	0	-	-	

Tab.16

The only change is for models D and Du, which are now marked "O" instead of "-". The two models are satisfactory "on average" for the measured angular distributions (see Fig.38b).

11.7 Valuation of the models in problem E4

With this problem, the scatter of calculation results was less than with the other problems. This is due to the given meteorological conditions: Stability is near neutral, the wind velocity is high, changes of wind direction and height-dependent directional shear are low. Further, there are no measuring points before the concentration peak (other than in E1 and E2). The sensitivity of the models for $\sigma_z(x)$ (vertical diffusion) is less pronounced at long distances than at short distances ahead of the concentration peak (see Section 6.3).

11.7.1 Valuation results E4

Good results are obtained with D(KJ), M, and L. D(KJ) and M are optimal as can be seen by a comparison of scatterplots (Figs. 47a,c,h, R/M distributions (Figs.51 and 57c) and χ^2_{rel} and $\overline{Q}$ data (Figs. 56b,d).

Average agreement with the experiment was obtained with models D<σ>, R, Du, and T.

The results of F are quite divergent and much too low (see Figs. 39,43). The behaviour is the same as in Problem I (Figs. 18,19).

The valuation table for problem E4 is as follows (Tab.17):

MODEL:	DKJ	D<>	M	R	L	DU	T	F	
ISO-LINES	+		+	0	0	0	0		
ANGUL.DISTR.	-	-	-	0	+	+	0	-	
PLUME AXIS	0	0	0	0	+	+	0	-	
SCATTERPLOT	+	0	+	0	0	0	+		
R/M-DISTR.	+	0	+	0	0	0	+		**E4**
CHI-SQUARE	0	-	0	0	+	+	-		
REL.CHI-SQ.	+	+	+	0	0	0	+		
CORR.-COEF.	+	+	+	+	+	0	+		
ERROR FACT.	+	+	+	0	+	0	+		
TOTAL E 4:	+	0	+	0	+	0	0	-	

12. Summary of the results of the validation studies

The valuation results can be summarized as follows (Tab.18):

	D(KJ)	D<σ>	M	R	L	DU	T	F
E1	+		-	0	0	0	-	-
E2	+		0	0	+	+	-	-
E3/A	-	0	-	+	0	0	+	+
E3/B	-	0	-	+	+	0	-	-
E4	+	0	+	0	+	0	0	-

With the exception of problem E3, good results were obtained with the Gaussian model DOSI with the Karlsruhe-Jülich σ parameters. With $\langle\sigma\rangle$ parameters, average results are achieved for problems E3 and E4.

The results of MUSEMET, RIMPUFF, Lagrange model, and Dunst model are average, with R, L and Du having some advantage over M. One should keep in mind, however, that the Gaussian-type models R and M may be brought to at least the standard of D(KJ) in cases of "neutral" or "negative" performance by choosing more appropriate σ-parameters.

The deviations from experimental data of TRANSLOC, which are quite marked in some cases, are due to undifferentiated input of time-dependent wind data, to problems in the modelling of vertical diffusion (at ground level), and to excessive mesh widths near the source. In principle, TRANSLOC should perform similar to the Dunst model.

The strata model FOG has problems in modelling horizontal and vertical diffusion which have already been discussed in Batch I, Section 6.3.

The following general extrapolations can be made from the results of the validation studies concerning the modelling of atmospheric dispersion processes at a distance $r \leq 20$ km:

- The mean error factor $\overline{Q}$ (see Section 9.2 p.83) will always be higher than 2-3.
- The minimum achievable value for χ^2_{rel} is 0.2

These figures apply to dispersion experiments similar to those described in the present study, with relatively accurate measurement of meteorological data. Further, the systematic errors in wind direction/transport direction $\Delta\theta$ (Table 10) have already been eliminated. The models use suitable σ parameters or diffusion models.

If these optimum conditions are not met, $\overline{Q}$ may easily reach values of 10 while χ^2_{rel} converges to 0.6-0.8.

In dispersion situations with strongly time-dependent wind vectors or with wind fields variable in space, with slight wind, or orographic effects, models like MUSEMET, RIMPUFF, the Lagrangian model, the Dunst model, and TRANSLOC may be applied if the wind field data are available. In this case, however, the above minimum values for $\overline{Q}$ and χ^2_{rel} will be clearly exceeded not only because of errors in the calculated wind field but also because of additional inaccuracies in the modelling of turbulence.

Better assessment of model efficiencies in case of more complex dispersion situations can only be reached after further validation studies.

The working group (AVVA) ought to continue its activities , if necessary with some other members, in order to get results on the more complex problems mentioned above.

References

Bu73 Businger, J.A. (1973): Turbulent transfer in the atmospheric surface layer; Workshop on Micrometeorology; Ann. Met. Soc., 67-100.

Cl79 Clarke, R.H. (1979): A Model for Short and Medium Range Dispersion of Radionuclides Released to the Atmosphere; NRPB-R91-Report, Harwell, Didcot, U.K.

Du84 Dunst, Hinrichsen, Fischer, Fehmer: "Untersuchung der Ausbreitung von Luftverunreinigungen bei Störfällen." Umweltbundesamt Report 104 09 203, Juli 1984.

Dy74 Dyer, A.J.: A Review of Flux-Profile Relationships; Boundary-Layer Meteorology 7 (1974), 363-372.

Ga81 Gassmann, F.: Schwadensimulationsmodell FOG; EIR Report, Sept. 1981 (unpublished).

Ge81 Geiß, Nester, Thomas, Vogt: In der Bundesrepublik Deutschland experimentell ermittelte Ausbreitungs-Parameter für 100m Emissionshöhe. Jül-1707/KfK-3095, Feb.1981.

Gi76 Gifford, F.A.: Turbulent Diffusion Typing Schemes: A Review; Nucl. Safety 17 (1) 71, (1976).

Ha80 Hartwig,S.,Schnatz,G.:"Transloc,ein numerisches Modell zur Simulation von Dispersionsvorgängen in der Atmosphäre und seine Anwendung für die Ausbreitung radioaktiver Substanzen bei einem Reaktorstörfall." Proc. Eur. Seminar on Radioactive Releases,Vol.2,p.555, Risø 1980.

Ha82 Hanna,S.R.:"Applications in Air Pollution Modeling", "Atmospheric Turbulence and Air Pollution Modeling", F.T.M.Nieuwstadt and H.van Dop, D.Reidel Publ.Comp., Dordrecht,Holland, 1982, p.275-286.

Hi84 Hinrichsen, K.: Bodennahe Ausbreitung in vertikal geschichteter Atmosphäre.-Ein neues Ausbreitungsmodell und seine Verifikation. Staub-Reinhaltung der Luft 44 (1984) No. 11, p. 488-491.

Ir79 Irwin, J.S.: A theoretical variation of the wind profile power-law exponent as a function of surface roughness and stability.(Technical Note), Atm. Env.13, 1979, p.191-194.

Jo82 Jones, J.A.:"Conclusions of a U.K.Working Group on a Model for Atmospheric Dispersion Calculations". Proc. of the Sympos. on Intermediate Range Atmospheric Transport Processes and Technology Assessment, Gatlinburg, Tenn. Oct. 1-3, 1980, p.335.

Mi82 Mikkelsen, T.: "A Parametric Description of A skewed Puff in the Diabatic Surface Layer." Risø - R - 476, Oct. 1982

Mi84 Mikkelsen, Larsen, Thykier-Nielsen: Description of the Risø Puff Diffusion Model. Nucl. Safety, Vol. 67, Oct. 1984, p. 56.

Mo58 Monin, A.S. and Obukhov, A.M.: "Fundamentale Gesetzmäßigkeiten der turbulenten Vermischung in der bodennahen Schicht der Atmosphäre." Sammelband zur statistischen Theorie der Turbulenz. Akademie-Verlag, Berlin 1958.

St81 Straka, Geiß, Vogt (KFA-Jülich): "Diffusion of Waste Air Puffs and Plumes under Changing Weather Conditions." Contrib. to Atm. Phys., Vol. 54, No.2, May 1981, p.207.

Sch84 Schorling, M.: "Application of A Lagrangian Dispersion Model to Short Term Releases of Pollutants." Air Pollution Control Association, San Francisco, 1984

Th81 Thomas, P. and Nester, K.: Experimental Determination of the Atmospheric Dispersion Parameters at the Karlsruhe Nuclear Research Center for 60 m and 100 m Emission Heights. Part 2: Evaluation of Measurements. KfK3091 (1981).

ANNEX 1

Transformation of wind-, temperature-, and turbulence-data of the tasks and experiments into the corresponding quantities of atmospheric similarity theory, L and u_*.

The Monin-Obukhov-length L can be taken as a measure of the atmospheric stability. It is defined as

$$L = - \frac{\varrho_a c_p \cdot u_*^3}{k \cdot g/T \cdot H} \qquad (1)$$

u_*	=	friction velocity	[m/s]
H	=	net radiation flux	[Watt/m^2]
ϱa	=	density of air	[kg/m^3]
Cp	=	specific heat of air	[Joule/kg/°K]
T	=	air temperature	[°K]
k	=	v. Karman's constant (0.4)	
g	=	gravitational acceleration = 9.81	[m/S^2]

Vertical profiles of the wind-velocity in the Prandtl-layer can be characterised by a friction velocity u_* that is nearly a constant. The vertical gradient of the wind velocity can be written like

$$\frac{\partial u}{\partial z} = \frac{u_*}{k \cdot z} \cdot \phi_M(z, L) \qquad (2)$$

The functions ϕ_M depend on stability /Dy74/, /Bu73/:

$$\text{unstable: } \phi_M = (1 - 15 \cdot \frac{z}{L})^{-\frac{1}{4}} \qquad (3)$$

$$\text{neutral : } \phi_M = 1 \qquad (4)$$

$$\text{stable : } \phi_M = 1 + 5 \frac{z}{L} \qquad (5)$$

Integration of (2) gives:

unstable:

$$u(z) = \frac{u_*}{k}\left\{\ln\frac{z}{z_0} - \ln\left(\frac{1}{2}\left(1+\frac{1}{\phi_M}\right)\right) - \ln\left(\frac{1}{2}\left(1+\frac{1}{\phi_M^2}\right)\right) - \frac{\pi}{2}\right\} \qquad (6)$$

neutral:

$$u(z) = \frac{u_*}{k}\ln\frac{z}{z_0} \qquad (7)$$

stable:

$$u(z) = \frac{u_*}{k}\left(\ln\frac{z}{z_0} + 5\cdot\frac{z}{L}\right) \qquad (8)$$

By fitting these wind-profile functions to the given wind-profiles considering stability and roughness-length u_* and L can be obtained.

In the case of additional information about the temperature lapse rate this is considered during the determination of L and u_*. From the definition of L (1) follows by insertion of

$$H = -\rho_a c_p \cdot \frac{k\cdot z\cdot u_*}{\phi_H(z,L)}\cdot\frac{\partial\theta}{\partial z} \qquad (9)$$

a relation between L, u_*, and $\partial\theta/\partial z$, the potential temperature lapse rate:

$$u_*^2 = L\cdot\frac{g}{T}k^2\frac{1}{\phi_H(z,L)}\cdot z\cdot\frac{\partial\theta}{\partial z} \qquad (10);$$

the functions ϕ_H are /Dy74/, /Bu73/:

$$\text{unstable: } \phi_H = 0.74\left(1-9\,\frac{z}{L}\right)^{-\frac{1}{2}} \qquad (11)$$

$$\text{stable : } \phi_H = 0.74 + 5\,\frac{z}{L} \qquad (12)$$

Then the proceeding is as follows:

I) an approximate value of L is taken.

II) with temperature lapse rate data and eq. (10) u_* is calculated.

III) with L, u_*, and equations (6,7,8) the wind-profiles are calculated.

IV) comparison of the calculated wind-profiles and the wind-profile data of the experiment or the task by chi-square. Variation of L (then go to II, etc.) until minimum chi-square is obtained.

The values of L and u_* for the comparative - and validation - tasks were calculated in this way.

The wind-and temperature-profiles used in II and IV are temporal average values of the experimental data and are valid during the whole sampling time.

When calculating vertical profiles the local zero-displacement d was considered by changing the variable z into z-d.

Determination of the Richardson-number Ri either follows from definition and measured gradients

$$Ri(z) = \frac{g/\theta \cdot \frac{\partial \theta}{\partial z}}{\left(\partial u/\partial z\right)^2} \qquad (13)$$

or from

$$Ri(z) = \frac{z}{L} \cdot \frac{\phi_H(z,L)}{\phi_M^2(z,L)} \qquad (14).$$

coordinates		measured TIC data E1	10^{-9} m^{-3}	calculated TIC data of different models **E1**				
r_i[m]	Θ_i[°]	M_i	D(KJ)	M	R	L	Du	T
1840	70	82	300	130	0.03	1000	270	100
1570	77	1381	700	102	2000	2350	1000	1000
2410	77	725	600	216	1120	2350	525	500
1340	84.5	860	950	56	1260	2000	1800	2500
2420	84.5	556	950	227	1780	1400	1260	2000
1180	91.5	134	500	24	708	1580	1800	1000
2560	92	287	600	212	100	630	1260	600
7300	77.5	436	250	67	320	790	16	10
5300	84.5	639	580	134	800	790	363	1000
5325	86.5	357	500	132	250	400	500	500
5565	94.5	525	250	109	0	50	468	10
7680	87.5	440	320	61	32	160	240	300
10900	84.5	312	250	33	100	0.02	32	480
5475	99.1	307	120	98	0	0.003	224	0.5
6110	107	215	20	56	0	0	20	0
8880	107	76	8	27	0	0	10	0
13435	91.5	266	100	19	0	0	125	0
6375	114.3	8.9	0.5	32	0	0	1	0
10500	77	0.9	200	33	70	10	2	1
560	84	4.8	50	3	0	100	1600	2000
2410	69.5	8.5	250	180	0	700	100	30

Normalized values of TIC close to the ground;
measured and calculated data.

coordinates		measured TIC data E2	10^{-9} m^{-3} calculated TIC data of different models **E2**					
r_i[m]	Θ_i[°]	M_i	D(KJ)	M	R	L	Du	T
135	141	137	0.5	0	0	0	1000	1
100	175	1745	2200	0.1	320	2000	4400	80
110	215	524	670	0.7	200	1000	2200	50
125	225	627	70	0.7	10	200	1200	10
145	223	322	3.5	1.1	0.4	40	700	1
215	145	36	1.2	0.03	0	0	750	0
215	153	698	410	0.5	0	320	1470	3
215	165	1615	870	62	32	1580	3400	60
215	176	5420	3750	830	1740	3980	5650	400
215	187	2870	6400	2840	6000	7080	6000	1300
225	197	531	5800	4030	4270	7000	5400	900
240	208	3830	2600	2500	1900	2820	2500	100
200	219	768	400	300	200	630	1260	10
200	230	819	13	40	3	200	560	1
360	150	40	32	0.9	0	100	20	0
360	172	3385	2300	880	320	2510	4000	100
360	179	3885	4500	2470	1860	4260	5700	900
360	189	7485	7700	5240	3700	7000	6000	3000
355	197	4125	5700	5500	3200	7000	4500	1000
355	215	553	770	1440	250	800	750	8
385	223	382	85	540	16	100	160	1
420	227	122	4	158	3	0	40	0
620	167	898	370	250	16	710	1100	5
635	175	1865	1350	1000	320	2140	2800	100
710	195	585	2550	3040	1380	5250	2800	2500
700	207	459	850	1790	630	1260	600	12
695	212	209	350	1160	200	320	160	2
545	223	39	6.8	450	10	0	30	0
1245	196	261	930	1170	630	2820	1000	1000
1045	210	212	200	735	100	150	50	0.1

Normalized values of TIC close to the ground;
measured and calculated data.

coordinates		measured TIC data E3/A	10^{-9} m^{-3} calculated TIC data of different models **E3**						
r_i [m]	Θ_i [°]	M_i	D(KJ)	D⟨θ⟩	M	R	L	Du	T
4720	282	25	500	390	440	200	3	400	0
4490	285	1127	650	890	517	2000	1000	1000	750
4275	287	2358	690	1220	488	2800	1400	1480	1800
4065	291	1267	650	900	247	1260	500	1000	1250
3975	292	245	600	750	192	630	100	630	850
3905	294	97	535	525	96	160	1	400	70
3830	295	4	450	335	65	50	0	250	10
3770	296	4	375	210	42	10	0	160	0
3695	298	36	275	90	15	0.2	0	40	0
3635	300	47	210	50	4	0	0	10	0
3615	301	7	160	25	2	0	0	5	0
3545	303	11	100	10	0.5	0	0	1	0
		E3/B							
4720	282	986	500	390	200	350	20	400	0
4490	285	1372	650	890	380	1250	350	1260	750
4275	287	360	690	1220	620	1050	350	1480	1800
4065	291	457	650	900	700	1220	800	1000	1250
3975	292	1584	600	750	500	1400	1400	700	850
3905	294	2113	535	525	100	1700	1800	400	70
3830	295	1339	450	335	30	1380	1200	250	10
3770	296	205	375	210	15	1150	500	126	0
3695	298	7	275	90	5	200	160	40	0
3635	300	14	210	50	1.5	50	100	10	0
3615	301	7	160	25	0.5	10	0	5	0
3545	303	4	100	10	0	0	0	1	0

Normalized values of TIC close to the ground;
measured and calculated data.

coordinates		measured TIC data E4	10^{-9} m^{-3} calculated TIC data of different models **E4**						
r_i [m]	θ_i [°]	EM_i	D(KJ)	D⟨6⟩	M	R	L	Du	T
2100	100	14	16	14	10	0	0	8	50
1965	102	29	35	34	20	0	0	20	75
1940	104	79	69	61	40	0.1	1	40	80
1895	108	270	208	160	200	10	220	180	150
1870	114	918	600	380	570	25	790	760	300
1790	116	1350	730	471	620	340	1120	1500	400
1820	119	1490	845	514	750	400	1260	1410	550
1855	121	2010	845	502	750	450	1150	1260	550
1840	125	2930	660	423	550	630	790	630	350
1870	127	2720	530	343	450	560	600	400	250
1855	131	990	260	199	270	250	180	100	150
1915	133	133	168	128	160	100	100	30	100
3810	102	5	6.5	5.4	10	0	0	3	20
3675	104	50	17	13	15	0	0	8	40
3685	107	94	52	32	57	1	40	30	60
3660	110	140	118	66	130	10	200	100	90
3645	112	274	182	96	177	40	295	235	150
3625	114	367	260	128	230	125	440	500	200
3595	117	421	350	170	300	220	630	630	270
3515	119	515	390	191	310	330	630	790	350
3515	121	400	390	191	300	360	450	690	370
3530	124	792	325	163	250	400	450	400	300
3535	127	436	220	118	200	320	250	100	200
3555	129	216	150	84	140	160	100	20	100
3600	132	144	72	43	60	50	4	3	80
3615	134	43	36	25	35	16	0	0.7	50
3500	135	7	26	20	20	10	0	0.2	30
5600	106	11	14	9	20	0.05	0	8	10
5630	110	126	55	29	60	1.6	32	60	50
5455	113	198	117	57	110	20	180	200	80
5325	115	223	156	78	120	60	320	330	150
5300	118	216	202	100	140	200	450	480	270
5360	121	288	208	102	140	230	370	350	280
5380	124	295	175	85	120	200	230	125	200
5480	127	194	117	56	80	135	63	20	90
5500	129	122	72	38	40	50	0.5	1.5	60
5410	132	50	30	18	37	16	0	0.08	40
5400	134	11	14	10	20	9	0	0	10
5385	137	4	3	3	7	2.5	0	0	7

Normalized values of TIC close to the ground;
measured and calculated data.

ANNEX 3

Tasks I, II
(Comparative calculations)

Coordinate system for computation of concentrations

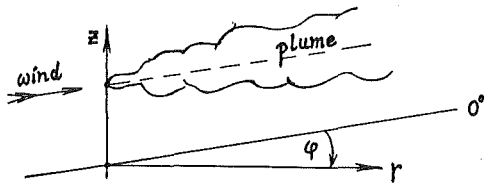

Cylinder-coordinates or plain polar coordinates.

$$\text{grid}: (r, \varphi, z) \longrightarrow (r_i, \varphi_j, z_k)$$

r_i, i=1,20 (if computer-time has to be saved you can choose an $i_{max} < 20$!)

{200,400,800,1200,1600,2000,2400,3000,3600,4400,5400,6600, 8000,10000,12000,14000,16000,20000,24000,30000} [m]

φ_j : constant 5°-steps (for narrow plumes 2.5°-steps). If concentrations C(r,φ,1m) become smaller than 10^{-3}· C(r,0°,1m) 10°-steps can be used or cut off.

z_k, k=1,11

{1,30,60,90,....300} [m]

This height variation is only important if vertical profiles of concentration shall be computed.

wind-profile u(z):

$$u(z) = u_{10} \cdot \left(\frac{z}{10m}\right)^{p(S, z_o)}$$

p(S, z_o): stability, Roughness-length

u(z > 200m) = u(z=200m)

wind-profile exponent p(S,z_o):

S	z_o = 0.1 m	z_o = 1.0 m
A	0.08	0.16
B	0.08	0.17
C	0.10	0.20
D	0.15	0.27
E	0.30	0.38
F	0.50	0.60

The σ-parameters, temperature lapse rates, wind-profiles, Richardson numbers, Monin-Obukhov-lengths, friction velocities, etc., used to compute the tasks should be sent to Karlsruhe together with the results.

To achieve higher precision the meterological situations of task I & II were also formulated with equations of the atmospheric similarity theory. The resulting numbers and tables were sent to all participants. These data can be found in the main part of this report.

Task I (simple atmospheric conditions) — Batch I

Release- and diffusion-conditions:

stationary release, sampling time 1h (for stationary Gaussian models)
constant release for 1h, sampl. time 1h (for time dependent models)
unit release rate: 1 unit/h
stationary dispersion conditions
wind direction: 180°
plain, uniform topography
mixing height h_{mix}="∞" (i.e. influences of the capping inversion shall be neglected)

The following different cases shall be computed:

source-heights: h_s = 10 m, 100 m, 200 m,
each with the roughness-lengths: z_o = 0.1 m and 1.0 m;
atmospheric stabilities and wind velocities are (*):

	B	D	F
u_{10} = 2 m/s	*	*	*
u_{10} = 8 m/s	–	*	–

The corresponding potential temperature lapse rates $\partial\theta/\partial z$ [°/100m] depending on height are:

u_{10} = 2 m/s	z ≤ 50m: −0.5	+0.3	z ≤ 100m: +2.3
	50–150m: 0.0		100–300m: +1.0
	z > 150m: +0.3		z > 300m: +0.3
u_{10} = 8 m/s	–	+0.3	–

Task II (wind-shear and inversion) — Batch II

Release- and diffusion-conditions:

constant release for 1h, sampl. time 1h
unit release rate: 1 unit/h
stationary dispersion conditions
plain, uniform topography

The following different cases shall be computed:

source-heights: h_s = 10 m, 100 m, 200 m,
each with the roughness-lengths: z_o = 0.1 m and 1.0 m,
and the wind velocities: u_{10} = 2 m/s and 4 m/s.

Task II.1)

Wind-direction shear dependent on height

The wind-direction close to the ground is 180° according to a plume transport direction of 0°. At a height of 200 m this direction has turned to +45°:

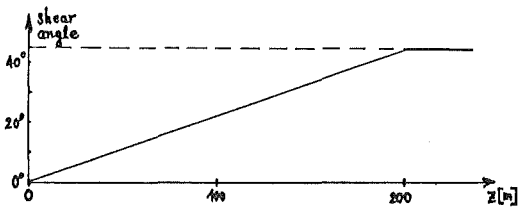

no shear above the height of 200 m.

The absolute value of the wind velocity $u(z) = |\vec{u}(z)|$ has the same height-dependence like in task I.

Task II.1 shall only be computed for a stable stratification (stability class F).

Again the influence of the inversion above the mixed layer shall be neglected.

Task II.2)

stationary inversion situation

Inversion with $\partial\theta/\partial z = +2\left[{}^{\circ}K/100\right]$
lower edge : $z_l = 150$ m
upper edge : $z_u = 350$ m

temperature lapse rate below the inversion layer according to stability class B

$$\partial\theta/\partial z = -0.5\left[{}^{\circ}K/100m\right]$$

wind direction: 180°

wind velocity profile: like task I

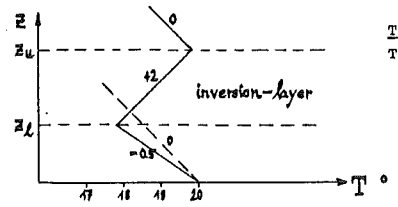

Task II.2:
Temperatureprofile

desired output (task I and II)

1. time-integrated concentrations close to the ground
   $C_{TIC}(r, \varphi, 1\text{ m})$
2. if possible, compute also dry deposition
   $C_{DEP}(r, \varphi)$; $V_{DEP} = 1\left[\frac{cm}{s}\right]$.
3. time dependent concentrations in the air:
   vertical profiles of concentration
   $C(r_i, 0^{\circ}, z_k; t)$* ($z_k$, k=1,11 → coordinates)
   r_i = 1200 m, 2000 m, 5400 m; t = 1 h.
4. time dependent concentrations close to the ground
   $C(r_i, \varphi_j, 1\text{ m}; t_l)$ (φ_j → coordinates)
   t_l = 15 min, 30 min, 60 min
   r_i = 1200 m, 2000 m, 5400 m.

*) only task II.1:
also compute $C(r_i, 20^{\circ}, z_k; t)$.

Structure of output data:

Storing of the angle-dependent concentrations:

1) positive angles:
   C(0°), C(2.5°),...., C(42.5°), (2.5°-steps)
   C(45°),C(55°) ,...., C(175°), (10° -steps)

2) negative angles:

   same as positive angles: C(0°), C(-2.5°),...,C(-45°),...,
   C(-175°)
   Finally the value at the angle 180o is stored.
   The 10°-steps are optional.

Comments on the output-FORTRAN-program:

IFLAG = 0: only 2.5°-steps are stored.
IFLAG = 1: also 10°- steps are stored.

CINT1F (IR,IPHI,IPM): TIC close to the ground (z=1m)
CINTBF (IR,IPHI,IPM): at the radius r_{IR} and angle φ_{IPHI}.
↘ Concentration deposited on the ground.

$r_{IR} \in \{200,400,800,1200,1600,2000,2400,3000,3600,4400,5400,6600,8000,10000,12000,14000,16000,20000,24000,30000\}$ [m]

$14 \leq IRMAX \leq 20$

IPM = 1 means $\varphi_{IPHI} \in \{0^{\circ},2.5^{\circ},...,42.5^{\circ}\}$
IPM = 2 means $\varphi_{IPHI} \in \{0^{\circ},-2.5^{\circ},...,-42.5^{\circ}\}$

CINT1G (IR,IPHI,IPM): like CINT1F, but: ...
CINTBG (IR,IPHI,IPM): like CINTBF, but:....

...if IPM = 1 : $\varphi_{IPHI} \in \{+45^{\circ},...,+165^{\circ}\}$
...if IPM = 2 : $\varphi_{IPHI} \in \{-45^{\circ},...,-165^{\circ}\}$

C1200 (IPHI,IZ): TICs in air at the height z_{iz}
C2000 (IPHI,IZ): at the radii 1200 m, 2000 m, and 5400 m.
C5400 (IPHI, IZ): $z_{iz} \in \{1,30,60,90,...,300\}$ [m]
IPHI = 1 : $\varphi = 0^{\circ}$
IPHI = 2 : $\varphi = 20^{\circ}$

C15F (IR,IPHI,IPM): time dependent (not time-integrated)
C30F (IR,IPHI,IPM): concentrations in air at different
C60F (IR,IPHI,IPM): times and radii:

{15 min, 30 min, 60 min}
IR = 1,3 : 1200 m, 2000 m, 5400 m.
$|\varphi_{IPHI}| \in \{0^{\circ},2.5^{\circ},...42.5^{\circ}\}$

C15G (IR,IPHI,IPM): like C15F, etc., but
C30G (IR,IPHI,IPM): $|\varphi_{IPHI}| \in \{45^{\circ},.....165^{\circ}\}$.
C60G (IR,IPHI,IPM):

FORTRAN output scheme

```
      WRITE (1,100) IFLAG, IRMAX
      DO 10 IR = 1,IRMAX
        DO 20 IPM = 1,2
          DO 30 IPHI = 1,18
             WRITE (1,200) CINT1F (IR,IPHI,IPM), CINTBF (IR,IPHI,
                  IPM)
 30     CONTINUE
        IF (IFLAG . EQ.0) GOTO 20
        DO 40 IPHI = 1,13
           WRITE (1,200) CINT1G (IR,IPHI,IPM),CINTBG (IR,IPHI,IPM)
 40     CONTINUE
 20   CONTINUE
        If (IFLAG.EQ.0) GOTO 10
        WRITE(1,200) CINT1G(IR,14,1), CINTBG (IR,14,1)
 10   CONTINUE

        DO 50 IZ = 1,11
          DO 60 IPHI = 1,2
             WRITE(1,300) C1200(IPHI,IZ), C2000(IPHI,IZ),C5400
                  (IPHI,IZ)
 60     CONTINUE
 50   CONTINUE

        DO 95 IR = 1,3
          DO 70 IPM = 1,2
            DO 80 IPHI = 1,18
              WRITE(1,300) C15F (IR,IPHI,IPM),C30F(IR,IPHI,IPM),
                   C60F(IR,IPHI,IPM)
 80     CONTINUE
        IF(IFLAG.EQ.0) GOTO 70
        DO 90 IPHI = 1,13
           WRITE(1,300)C15G( IR,IPHI,IPM),C30G(IR,IPHI,IPM),C60G
                (IR,IPHI,IPM)
 90      CONTINUE
 70   CONTINUE
      IF( IFLAG.EQ.0) GOTO 95
      WRITE( 1,300) C15G(IR,14,1),C30(IR,14,1),C60(IR,14,1)
 95   CONTINUE
100   FORMAT (I1,I3)
200   FORMAT (2E14.4)
300   FORMAT (3E14.4)
```

III. Validation Problems

E1/1

Experiment 1 E1

constant emission (source-term) for 1 h
source height: h_s = 100 m
source term: $\dot{Q}$ = 1 unit/h
total diffusion- and sampling time: 1h 50 min
maximum distance of sampling devices
downwind of the source: ~14000 m

The time-integrated concentrations in the air close to the ground surface (at a height of 1 m) shall be calculated at given points downwind of the source. In the experiment the whole plume has crossed all the sampler positions.

The sampling-(integration-) time is 1h 50' for time dependent numerical models which consider windshear and σ_x-diffusion.

The sampling-time is 1h for simple Gaussian models; (1h-segment of a stationary Gaussian plume).

Topography

Roughness-length z_0 = 1.2 m
Zero displacement d = 16 m

Uniform flat terrain with buildings and forest.

E1/2

Stability and wind-profile

The Pasquill-category E was derived from synoptical data, the temperature lapse rate, radiation, and $\sigma_\theta - \sigma_\phi$ -measurements; (night-time experiment).

Temperature lapse rate: $\frac{\Delta T}{100m} = 0.6°/100m$

$\Rightarrow \frac{\partial \theta}{\partial z}(20\text{–}120m) = +0.016 \left[\frac{°K}{m}\right]$

net radiation flux:	- 14	Watt/m²
cloud amount:	3/8	
horizontal and vertical wind fluctuations;		
σ_θ (= σ_A), z=120m:	2.6°	mean values calculated from
σ_ϕ (= σ_E), "	2.3°	11 10-min-average data.

Monin-Obukhov length L and friction velocity u_* are derived from the time-averaged wind-profile:

z	2	10	20	30	50	80	100	120	[m]
u(z)	0.3	0.5	1.0	2.3	3.8	5.8	6.7	7.2	[m/s]

Wind-profile according to similarity theory, stable case:

$$u(z) = \frac{u_*}{k}\left[\ln\left(\frac{z-d}{z_0}\right) + \frac{(z-d)\cdot 5}{L}\right] \qquad d = 16m,\ z_0 = 1.2m$$

The values for u_* and L come from a least-squares fit of this function to the wind-profile data with z' = z - d > 0 m.

E1/3

L = 70 m (± 10 m)

$u_* = 0.265 (\pm\ 0.015)$ m/s

These results are in good agreement with the similarity theory as indicated by the temperature lapse rate:

$$\frac{\partial\theta}{\partial z}(z'=50\text{m}) = \frac{T}{g}\cdot\frac{u_*^2}{0.16}\cdot\frac{0.74 + \frac{5\cdot 50}{L}}{50\cdot L} = 0.0161\ \left[\frac{°K}{m}\right];$$

the measured value $\overline{\frac{\partial\theta}{\partial z}}(20\text{–}120\text{m})$ is $0.016\ \left[\frac{°K}{m}\right]$

Richardson number, Ri(z)(z') :

$$\frac{\partial u}{\partial z}(z=50\text{m})(z'=34\text{m}) = 0.07\ \left[\frac{m/s}{m}\right] \qquad \frac{\partial\theta}{\partial z} = 0.0174\ \left[\frac{°K}{m}\right]$$

$$\frac{\partial u}{\partial z}(z=100\text{m})(z'=84\text{m}) = 0.035\ \left[\frac{m/s}{m}\right] \qquad \frac{\partial\theta}{\partial z} = 0.0134\ \left[\frac{°K}{m}\right]$$

Ri(z=50m)(z'=34m)=0.119
Ri(z=100m)(z'=84m)=0.366.

E1/4

Profiles of the wind vector $\vec{u}$ (10-min-average values)
upper part: $|\vec{u}|(z)$; lower part: wind directions (*)

z[m]	10 min	20 min	30	40	50	60	70	80	90	100	110 min
2	0.2	0.2	0.5	0.2	0.3	0.3	0.9	0.3	0.1	0.1	0.1
10	0.5	0.4	0.6	0.3	0.5	0.4	1.6	0.6	0.3	0.1	0.2
20	1.0	0.7	1.3	0.7	1.2	1.0	2.0	1.1	0.9	0.4	0.6
30	2.5	2.1	2.7	2.5	2.7	2.2	2.9	2.0	1.9	1.5	2.3
50	4.4	3.6	4.5	4.1	4.4	3.7	3.6	3.4	3.3	2.8	4.0
80	6.3	5.8	6.9	6.5	6.6	6.0	4.6	5.7	5.1	4.7	5.6
100	7.4	6.7	7.9	7.7	7.7	7.1	4.8	6.7	5.8	5.4	6.2
120	8.1	7.3	8.4	8.5	8.6	7.6	5.1	7.0	6.2	5.8	6.6
30	250	255	260	255	250	245	250	240	235	220	220
50	255	260	260	255	255	250	270	245	240	230	230
120	268	265	265	261	260	259	275	258	255	250	248

(*) the angles given in the last three lines accord to the meteorological wind directions.

E1/5

desired output

The time-integrated air-concentrations close to the ground shall be calculated at the points of intersection of a polar-coordinate grid:

$$C^o_{TI}(r_i, \varphi_j);$$

the values of r are

r_i = {200, 400, 600, 800, 1000, 1200, 1600, 2000, 2400, 3000, 2600, 4400, 5400, 6600, 8000, 10000, 12000, 14000, 16000, 20000} [m] (i=1,20);

the values of φ are given by

$$\varphi_j = \varphi'_j + \varphi_0 ,$$

Where φ_0 is an "average dispersion direction" with "geographic" angle definition (north=0°).

for experiment E1 : $\varphi_0 = 77°$

φ'_j = {-45°, -42.5°, ... , 0°, +2.5°, ... +45°} (2.5° - steps).

The calculated concentration values $C_{TI}(r_i, \varphi_j)$ together with the coordinates r_i and φ'_j shall be written on a magnetic tape (→ p.E1/6).

E1/6

Writing on mag-tape

IEXP	experiment-no.: (here=1)
IPHA	run-no.: (here only =1)
IR	index of radius IR=1, IRMAX=2Ø r_i takes the values given on page E1/5
JPHI	index of angle JPHI=1, JPHIX=37 φ'_j takes the values given on page E1/5
CINT	time-integrated concentration close to the ground.

Writing sheme

```
      WRITE(1,1ØØ)IEXP,IPHA,IRMAX,JLHIMX
      DO1Ø IR=1,IRMAX
      DO2Ø JPHI=1,JPHIMX
      WRITE(1,2ØØ) CINT(IR,JPHI)
   2Ø CONTINUE
   1Ø CONTINUE
  1ØØ FORMAT(I2,I2,I3,I3)
  2ØØ FORMAT(E14.4)
```

9 track-tape, 1600 BPI, NOLABEL

E2/1

Experiment 2 **E2**

constant emission (source term) for ~1h
source height: h_s=60 m
source-term: $\dot{Q}$ = 2 units/h
beginning of release: t_o= 0 min
start of sampling: t_1=20 min
end of sampling: t_2=50 min
maximum downwind distance of sampling devices: ~1300 m.

The time-integrated concentrations in the air close to the ground (at a height of 1m) shall be calculated at given points downwind of the source.

The sampling-(integration-) time interval is
$\Delta t = t_2 - t_1 = 30$ min

Topography

Roughness-length z_o=1.2 m
Zero displacement d=10 m

Uniform flat terrain with buildings and forest.

E2/2

Stability and wind-profile

The Pasquill-category C was derived from synoptical data, the temperature lapse rate, radiation, and σ_θ, σ_ϕ-measurements.

Temperature lapse rate: $\frac{\Delta T}{100m} = -1.7 \left[\frac{°K}{100m}\right]$

$\frac{\partial \theta}{\partial z}(30\text{–}100m) = -0.007 \left[\frac{°K}{m}\right]$

net radiation flux $\approx$ + 300 Watt/m^2

horizontal and
vertical wind fluctuations

σ_θ	(z=40 m) :	18.0°
	(100 m) :	11.2°
σ_ϕ	(z=40 m) :	10.8°
	(100 m) :	9.4°

Monin-Obukhov length L and friction velocity u_* are derived from the temperature lapse rate.

wind-profile :

z	40	60	80	100	150	[m]
u(z)	5.3	6.0	6.3	6.5	7.0	[m/s]

wind-profile from similarity theory

$$u(z) = \frac{u_*}{k}\left[\ln\frac{z-d}{z_o} - 2\ln\left(\frac{1}{2}+\frac{1}{2}\phi_m\right) - \ln\left(\frac{1}{2}+\frac{1}{2}\phi_m^2\right) + 2\arctan\left(\frac{1}{\phi_m}\right) - \frac{\pi}{2}\right]; \quad \phi_m = \left(1+15\frac{z}{|L|}\right)^{-\frac{1}{4}}$$

E2/3

Temperature lapse rate

$$\left|\frac{\partial\theta}{\partial z}\right| = \frac{T}{g}\cdot\frac{u_*^2}{k^2}\cdot\frac{\phi_H}{z/|L|}; \quad \phi_H = 0.74\left(1+9\cdot\frac{z}{|L|}\right)^{-\frac{1}{2}}$$

wind-profile gradient

$$\frac{\partial u}{\partial z} = \frac{u_*}{k(z-d)}\phi_m$$

The values of L and u_* fitting both lapse rate and windprofile are:

L = -100 m (± 20 m)
U_*= 0.8 m/s (±0.1 m/s);

from this one obtains the time-averaged gradient $\partial\theta/\partial z$:

$$\frac{\partial\theta}{\partial z}(z=50m, z'=40m) = -0.01\left[\frac{°K}{m}\right]$$

$$\frac{\partial\theta}{\partial z}(z=100m, z'=90m) = -0.0033\left[\frac{°K}{m}\right]$$

together with average wind gradients the Richardson numbers can be calculated:

Ri(z= 50, z'=40m)=-0.30
Ri(z=100, z'=90m)=-0.88

E2/4

Time-dependent wind-, temperature-, and turbulence-data

z[m]	t [min]	Wind-velocity [m/s]							Wind-direction [°]							$\sigma_{\theta L}$ [°]							σ_ϕ [°]						
40	40–0	5.7	5.2	5.3	6.0	5.0	5.3	5.6	12	13	19	17	31	19	18	13.3	19.3	16.6	16.7	20.9	14.4	12.8	11.1	11.8	10.5	9.7	10.8	11.0	10.4
60	0–10	6.6	5.4	6.1	6.7	5.6	5.9	6.4	7	8	15	7	23	13	12														
100	10–20	7.0	6.4	6.2	7.0	6.1	6.2	6.8	4	11	16	9	19	12	11	10.2	12.6	11.3	10.1	11.9	11.5	9.8	9.3	9.3	9.6	9.0	10.0	9.2	8.9
160	20–30	8.2	7.2	6.9	7.8	7.1	7.0	7.4	1	12	14	6	13	12	10														
200	30–40	8.2	7.4	6.8	7.7	7.3	7.2	7.4	9	18	20	11	17	17	13														
40	40–50								12	13	19	17	31	19	18														
60	50–60								7	8	15	7	23	13	12														
100									4	11	16	9	19	12	11														
160									1	12	14	6	13	12	10														
200									9	18	20	11	17	17	13														

t_o = 0 min: beginning of tracer-emission
t_1 = 20 min: start sampling
t_2 = 50 min: stop sampling

E3/3

During the experiment also quantities like $|\overline{u'w'}|$ and $|\overline{w'T'}|$ were evaluted, however precision was not high.

According to $u_* = \sqrt{|\overline{u'w'}|}$ and $L = -\frac{T}{k \cdot g} \cdot \frac{u_*^3}{\overline{w'T'}}$,

or $L = \frac{5 \cdot z}{\frac{kz}{u_*}\frac{\partial u}{\partial z} - 1}$ u_* and L can be calculated:

first: $u_* = \sqrt{|\overline{u'w'}|}$ and $L = 5z/(\frac{kz}{u_*}\frac{\partial u}{\partial z} - 1)$:

t [min]	$\lvert\overline{u'w'}\rvert$ 20m-40m	u_* [m/s]	L [m]
0-30	0.12	0.34	220m
30-60	0.105	0.32	190m
60-90	0.09	0.30	190m
90-120	0.155	0.39	140m

second: L calculated from $\overline{u'w'}$ - and $\overline{w'T'}$:

	$\overline{w'T'}$	$\Rightarrow$ L
0-30	-0.01 ± 0.005	+293 m
30-60	-0.01 ± 0.005	+245 m
60-90	-0.01 ± 0.005	+202 m
90-120	+0.01 ± 0.005	-443 m

It is proposed to use the values of the first method:

t	0-30	30-60	60-90	90-120	[min]
u_*	0.34	0.32	0.30	0.39	[m/s]
L	+220	+190	+190	+140	[m]

E3/4

wind-and turbulence-profils (10 min-averages)

σ_α [°] azimuthal fluctuation of direction
σ_ε [°] elevation
u [m/s] windspeed
α [°] met.wind-direction
σ_u [%] fluctuation of speed $\bar{u}$

t [min]:		z=[m]: 40	80	120	160	200
10	u	3.70	5.52	6.71	7.96	7.86
	α	111.2	107.26	109.24	110.53	113.33
	σ_α	7.43	4.45	3.15	2.18	1.57
	σ_ε	1.40	1.35	1.10	1.31	1.19
	σ_u	0.26	0.60	0.32	0.36	0.23
20	u	4.52	5.94	6.63	7.49	8.61
	α	114.33	111.64	111.24	111.78	113.24
	σ_α	3.31	3.45	3.13	3.49	1.66
	σ_ε	1.67	1.12	1.32	1.70	1.41
	σ_u	0.28	0.39	0.29	0.37	0.24
30	u	4.58	5.84	6.03	7.56	6.53
	α	114.28	113.25	112.51	114.34	115.16
	σ_α	3.24	3.22	1.42	2.66	1.63
	σ_ε	2.83	3.16	3.03	2.24	1.10
	σ_u	0.25	0.32	0.24	0.27	0.22
40	u	3.96	5.62	6.57	7.18	7.15
	α	107.03	110.24	110.28	110.96	112.64
	σ_α	2.69	4.55	3.34	2.23	1.23
	σ_ε	2.42	2.86	2.08	1.34	0.84
	σ_u	0.22	0.34	0.30	0.31	0.27
50	u	3.51	5.43	6.25	7.36	7.41
	α	111.42	107.65	111.90	112.10	110.57
	σ_α	2.52	4.26	4.82	4.36	1.01
	σ_ε	2.18	3.14	1.46	0.93	0.17
	σ_u	0.66	0.53	0.22	0.29	0.21
60	u	3.24	4.71	5.92	7.06	7.25
	α	103.52	105.05	103.78	104.24	110.71
	σ_α	2.48	3.66	2.62	1.94	0.75
	σ_ε	2.62	3.03	2.02	1.28	0.48
	σ_u	0.48	0.36	0.31	0.22	0.19

E3/5

t [min]:		z = [m]: 40	80	120	160	200
70	u	3.49	4.26	6.08	7.22	7.45
	α	111.42	107.89	111.92	110.22	116.37
	σ_α	2.91	3.68	2.23	1.64	1.06
	σ_ε	1.80	1.20	1.83	1.24	0.47
	σ_u	0.22	0.32	0.29	0.25	0.13
80	u	3.70	4.59	5.94	7.09	7.43
	α	106.60	98.04	104.83	109.42	122.53
	σ_α	4.52	3.83	4.29	3.01	2.33
	σ_ε	2.43	1.52	3.00	2.30	1.47
	σ_u	0.29	0.24	0.27	0.24	0.37
90	u	4.28	5.80	6.49	7.31	7.44
	α	103.31	103.04	110.45	110.44	115.83
	σ_α	2.21	4.23	3.33	2.69	2.33
	σ_ε	2.65	1.38	2.40	1.81	0.95
	σ_u	0.26	0.32	0.28	0.24	0.25
100	u	4.53	5.84	6.86	7.43	6.43
	α	109.94	109.24	106.11	114.98	119.94
	σ_α	1.83	4.92	2.32	2.04	1.88
	σ_ε	2.61	4.94	4.35	4.05	2.71
	σ_u	0.24	0.28	0.42	0.27	0.20
110	u	4.89	5.66	7.00	8.96	7.90
	α	109.56	111.12	111.06	115.42	122.47
	σ_α	3.48	2.17	1.60	1.44	1.07
	σ_ε	4.63	4.55	4.16	4.44	0.85
	σ_u	0.24	0.33	0.24	0.23	0.22

E3/6

Temperature profiles (1/2 h average values) in [°C]

t [min]	z [m] 10	20	40	80	120	160	200
0-30	19.7	19.6	19.5	19.3	19.2	19.2	19.5
30-60	19.9	19.8	19.8	19.6	19.4	19.4	19.8
60-90	20.0	20.0	19.8	19.7	19.4	19.3	19.4
90-120	19.7	19.7	19.6	19.5	19.2	19.0	18.8

Geostrophic wind (hourly) :

t [min]	Ug	αg
-60	8.6 m/s	141°
0	8.4 m/s	131°
60	7.9 m/s	140°
120	8.0 m/s	148°

E2/5

desired output

The time-integrated air-concentrations close to the ground shall be calculated at the points of intersection of a polar-coordinate grid:

$$c^{o}_{TI}(r_i, \varphi_j) \ ;$$

the values of r are

r_i= {100, 200, 300, 400, 600, 800, 1000, 1200, 1600, 2000, 2400, 3000, 3600, 4400, 5400} [m] (i=1,15);

the values of φ are given by

$$\varphi_j = \varphi'_j + \varphi_0$$

Where φ_0 is an "average dispersion direction" with "geographic" angle definition (north=0°).

for experiment E2 $\varphi_0 = 190°$

= {-45°, -42.5°, ..., 0°, +2.5°, ... +45°}
(2.5° - steps).

The calculated concentration values $c^{o}_{TI}(r_i, \varphi_j)$ together with the coordinates r_i and φ'_j shall be written on a magnetic tape (→ p.E1/6).

E2/6

Writing on mag-tape

IEXP	experiment-no.: (here=2)
IPHA	run-no.: (here only =1)
IR	index of radius IR=1, IRMAX=15 r_i takes the values given on page E2/5
JPHI	index of angle JPHI=1, JPHIMX=37 φ'_j takes the values given on page E2/5
CINT	time-integrated concentration close to the ground.

Writing scheme

```
      WRITE(1,1ØØ)IEXP,IPHA,IRMAX,JPHIMX
      DO1Ø IR=1,IRMAX
      DO2Ø JPHI=1,JPHIMX
      WRITE(1,2ØØ) CINT(IR,JPHI)
   2Ø CONTINUE
   1Ø CONTINUE
  1ØØ FORMAT(I2,I2,I3,I3)
  2ØØ FORMAT(E14.4)
```

9 track-tape, 1600 BPI, NOLABEL

E3/1

Experiment 3 **E3**

constant emission (source-term) for 2h
source height: h_s=80 m
source term: $\dot{Q}$=2 units/h
beginning of release: t_o = 0 min
start sampling, run 1: t_{11}= 45 min
stop sampling, run 1: t_{21}= 75 min
start sampling, run 2: t_{12}= 75 min
stop sampling, run 2: t_{22}=105 min
maximum downwind distance of sampling devices: ~5000 m

The time-integrated concentrations in the air close to the ground (at a height of 1m) shall be calculated at given points downwind of the source.

The sampling-(integration-) time intervals of the two runs are $\Delta t_1 = t_{21} - t_{11}$ and $\Delta t_2 = t_{22} - t_{12}$.

Topography

Roughness-length: z_o = 0.2 m
Zero displacement: d = 0 m

Uniform, flat rural terrain.

E3/2

Stability and wind-profile

Near neutral, slightly stable stratification; Pasquill-category D-E.

time-averaged temperature lapse rate: $\frac{\Delta T}{100m} = -0.5\left[\frac{°K}{100m}\right]$

$$\Rightarrow \overline{\frac{\partial \theta}{\partial z}}(10-60m) = +0.005\left[\frac{°K}{m}\right]$$

T= 20°C, cloud amount: 100%, at noon.
Mixing-height h_m = 200 m.

Complete data for wind-profile, temperature-profile, and σ_a, σ_b, σ_u are given on page E3/4 and 5.

Monin-Obukhov length L and friction velocity u_*:

From z_o=0.2 m and $\overline{\frac{\partial \theta}{\partial z}}$ =+0.005$\left[\frac{°K}{m}\right]$ follows:
L=+200(±50)m.

By using $\frac{\partial u}{\partial z} = \frac{u_*}{k \cdot z}(1+\frac{5z}{L})$ and $\frac{\partial u}{\partial z}(z=25\ m)=0.05\left[\frac{m/s}{m}\right]$
the friction velocity can be calculated:

$u_* \approx 0.3$ m/s

More precise half-hour average values are given on the following page.

E3/7

desired output

The time-integrated air concentrations close to the ground shall be calculated at the points of intersection of a polar-coordinate grid:

$$c^{o}_{TI}(r_i, \varphi_j) \ ;$$

Both runs (E3/A and E3/B) shall be calculated separately.

the values of r are

r_i = (200, 400, 800, 1200, 1600, 2000, 2400, 3000, 3600, 4400, 5400, 6600, 8000, 10000) [m] (i=1,14)

the values of φ are

$\varphi_j = \varphi'_j + \varphi_0$, where φ_0 is an "average dispersion direction" with "geographic" angle definition (north=0°).

for experiment E3 : $\varphi_0 = 292°$

φ'_j = (-30°, -27.5°, ... , 0°, +2.5°, ... +30°)
(2.5 - degree steps).

The calculated concentration values $c^{o}_{TI}(r_i, \varphi_j)$ together with the coordinates r_i and φ'_j shall be written on a magnetic tape (→ p.E3/8).

E3/8

Writing on mag-tape

IEXP	experiment-no.: (here=3)
IPHA	run-no.: (here=1,2)
IR	index of radius IR=1, IRMAX=14 r_i takes the values given on page E3/7
JPHI	index of angle JPHI=1, JPHIMX=25 φ'_j takes the values given on page E3/7
CINT	time-integrated concentration close to the ground.

Writing scheme

```
      DO 1 IPHA=1,2
      WRITE(1,1ØØ)IEXP,IPHA,IRMAX,JPHIMX
      DO 1Ø IR=1,IRMAX
      DO 2Ø JPHI=1,JPHIMX
      WRITE(1,2ØØ)CINT(IR,JPHI)
   2Ø CONTINUE
   1Ø CONTINUE
    1 CONTINUE
  1ØØ FORMAT(I2,I2,I3,I3)
  2ØØ FORMAT(E14.4)
```

9-track tape, 1600 BPI, NOLABEL

E4/1

Experiment 4 **E4**

constant emission (source-term) for 1h 30'
source height: h_s = 115 m
source-term: $\dot{Q}$ = 1 unit/h
beginning of release: t_o = 0 min
start of sampling: t_1 =30 min
end of sampling: t_2 =90 min
maximum distance of sampling devices downwind of source: ~5000 m.

The time-integrated concentrations in the air close to the ground surface (at a height of 1 m) shall be calculated at given points downwind of the source.

The sampling-(integration-) time intervall is $\Delta t = t_2 - t_1$ =60 min.

Topography:

Roughness-length z_o = 0.6 m
Zero displacement d = 0 m

flat country with houses and trees.

E4/2

Stability and wind-profile

The wind-profile does not fit very well to similarity theory profiles, and therefore stability- and Monin-Obukhov length-determination was carried out by calculation of the bulk-Richardson number.

L = -70 [m] (from bulk-Richardson number)

u_* = 0.7 [m/s] (from wind-profile z=0-30 m)

these numbers correspond to a Pasquill-category B-C.

the mixing-height was measured: h_m = 800 m.

The high wind-speed at a height of z = 60 m, however, makes a lower unstability (C-D instead of B-C) more probable.

Standard deviation of wind-vector

at a height of 115 m:

$\overline{\sigma_v}$ = 1.35 [m/s] $\quad$ $\overline{\sigma_\theta}$ = 8.8°

$\overline{\sigma_w}$ = 0.72 [m/s] $\quad$ $\overline{\sigma_\phi}$ = 4.7°

E4/3

Wind- and temperature-data of the experiment E4

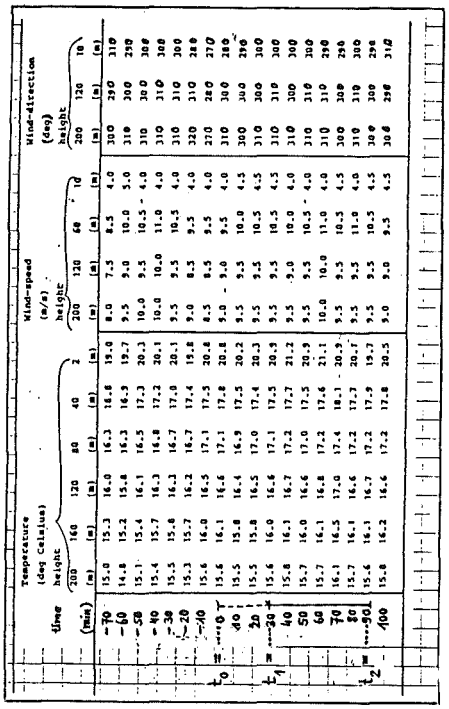

E4/4

desired output

The time-integrated air concentrations close to the ground shall be calculated at the points of intersection of a polar-coordinate grid:

$$c^{\circ}_{TI}(r_i, \varphi_j) \ ,$$

the values of r are

r_i= (200, 400, 600, 800, 1000, 1200, 1600, 2000, 2400, 3000, 3600, 440, 5400, 6600, 8000, 10000, 12000, 14000, 16000, 20000) /m/ (i = 1,20)

the values of φ are

$\varphi_j = \varphi_j' + \varphi_0$, where φ_0 is an "average dispersion direction" with geographic angle definition (north = 0°.).

for experiment E4 : $\varphi_0 = 120°$

φ_j' = (-30°, -27.5°, ... , 0°, +2.5°, ... + 30°)
(2.5 - degree-steps).

The calculated concentration values $C_{TI}(r_i, \varphi_j)$ together with the coordinates r_i and φ_j' shall be written on a magnetic tape (+ p. E4/5).

E4/5

Writing on magnetic tape

IEXP	experiment-no. (here=4)
IPHA	run-no. (here only=1)
IR	index of radius: IR=1, IRMAX=2Ø r_i takes the values given on page E4/4
JPHI	index of angle: JPHI=1, JPHIMX=25 φ_j takes the values given on page E4/4
CINT	time-integrated concentration close to the ground

Writing scheme

```
      WRITE (1,1ØØ) IEXP,IPHA,IRMAX,IPHIMX
      DO 1Ø IR=1,IRMAX
      DO 2Ø JPHI=1,JPHIMX
      WRITE (1,2ØØ) CINT (IR,JPHI)
   2Ø CONTINUE
   1Ø CONTINUE
  1ØØ FORMAT (I2,I2,I3,I3)
  2ØØ FORMAT (E14.4)
```

9-track tape, 1600 BPI, NOLABEL